2012

Mechanisms of urban influence on precipitation in the southeastern United States: precipitation enhancement, storm bifurcation, and synoptic characteristics

Anna Marie Trevino
Louisiana State University and Agricultural and Mechanical College, annamarietrevino@gmail.com

MECHANISMS OF URBAN INFLUENCE ON PRECIPITATION IN THE SOUTHEASTERN UNITED STATES: PRECIPITATION ENHANCEMENT, STORM BIFURCATION, AND SYNOPTIC CHARACTERISTICS

A Dissertation

Submitted to the Graduate Faculty of the
Louisiana State University and
Agricultural and Mechanical College
in partial fulfillment of the
requirements for the degree of
Doctor of Philosophy

in

The Department of Geography and Anthropology

by
Anna Marie Treviño
B.S., Texas A&M University, 2006
M.S., Texas A&M University, 2008
May 2012

ACKNOWLEDGMENTS

I would very much like to thank the Southern Climate Impacts Planning Program (SCIPP) for providing me with the funding to pursue this research project. I am also very thankful to Louisiana State University for awarding me with the Graduate School Dissertation Year Fellowship that allowed me to complete my research.

The guidance and advice given to me by my committee members, Robert Rohli, David Brown, Barry Keim, Lynne Carter, and Richard Bengtson, has been very valuable. The contributions of Luigi Romolo through the Synoptic Typer program, were also very significant to Study 3. Without their direction, I would not have been able to finish my dissertation. I am also very thankful to the climate students in our department. They have been very helpful through the sharing of their skills, many of which I was able to obtain over the last few years.

Finally, I would like to thank my husband, my family, and close friends who have given me their support throughout my time as a student. Obtaining this degree would not have been possible without them.

TABLE OF CONTENTS

LIST OF TABLES

LIST OF FIGURES

ABSTRACT

The continual growth of urban areas increasingly affects the environment on various spatial scales. Land cover changes, combined with decreasing vegetative cover and addition of atmospheric aerosols, potentially lead to growing urban heat islands that alter local moisture fluxes, which play a role in precipitation initiation and development. Some studies suggest a region of enhanced rainfall exists downwind of the main urban area and that frontal systems decelerate as they reach areas of high urban development.

Six urban areas within the southeastern United States were examined for urban precipitation enhancement: Atlanta, Birmingham, Dallas/Fort Worth, Houston, Memphis, and Tulsa. Three tests were employed to detect the existence of urban-enhanced precipitation: (1) "downwind *vs*. upwind" test, (2) temporal analysis, and (3) the "contour" test. Houston, Memphis, and Tulsa exhibited potential for urban influence, while Birmingham showed some urban influence. Dallas/Fort Worth likely experienced urban influence while Atlanta showed little evidence of urban influence.

A thorough, case study-based analysis of storm bifurcation occurrence in two urban areas (Atlanta and Dallas/Fort Worth) and one control site (Columbus, MS) was conducted using radar-derived precipitation estimates of heavy precipitation days ($\geq$ 25 mm). This threshold was selected based upon evidence of urban influence seen in previous studies. Bifurcation likely occurred in Atlanta, but little evidence was seen for Dallas/Fort Worth, unless opposing factors masked the effects of bifurcation. Little evidence for bifurcation was found for Columbus.

Finally, the degree of synoptic control over the heavy precipitation events and cases of bifurcation were assessed. The first circulation-to-environment approach, a principal

components analysis based method showed trough-to-ridge circulation regimes and steep geopotential height gradients as the dominating circulation types. The second circulation-to-environment approach, the Spatial Synoptic Classification scheme, was inconclusive as it revealed no significant link between heavy precipitation bifurcation events and synoptic pattern. Finally, composite 500 and 700 hPa geopotential heights during bifurcation days confirmed that trough-to-ridge flow patterns were most common among bifurcation days for Atlanta and Columbus. Dallas/Fort Worth exhibited a zonal flow, thereby displaying less upper-level support for surface frontal activity. These results will contribute to seasonal forecasting efforts and inform regional climate models.

CHAPTER 1. INTRODUCTION

1.1 Overview

As cities around the world grow at a rapid rate, the need to understand their influence on the local and regional climate becomes more necessary. It is known that urban areas have an influence on their local climate (Arnfield 2003, Shepherd 2005), as changes in land use and land cover continuously alter energy and moisture fields as well as circulation patterns above urban environments. The anthropogenic features of urban climates include expansion of urban heat islands (UHIs), increases in surface roughness, and the contribution of pollution increasing the number of cloud condensation nuclei over urban regions, with a complex series of feedbacks to cloud formation and precipitation (Shem and Shepherd 2009, Ntelekos et al. 2007, Changnon 1976, Diem and Mote 2005, Lacke et al. 2009).

Collectively, urban climate research suggests three primary mechanisms of urban-enhanced precipitation: (1) UHI-induced convection zones (Lacke et al. 2009), (2) enhanced aerosol concentrations (e.g., Shem and Shepherd 2009), and (3) increased surface convergence caused by surface roughness (Dixon and Mote 2003, 2005). A robust climatological understanding of precipitation processes over urban regions, driven primarily in the warm season by convergence and convection, is essential for a range of environmental and socioeconomic applications. This is especially true in the southeastern United States, where abundant precipitation that is highly variable across space and time is accompanied by rapidly-growing cities.

One facet of urban precipitation that remains particularly poorly understood is the impact of storm bifurcation. Bornstein and Lin (2000) have shown that when regional winds are strong,

surface diffluence occurs around city centers as a result of increasing surface roughness. Bornstein and LeRoy (1990) termed this diffluence the "building-barrier effect", a phenomenon also known as storm bifurcation. The process of storm bifurcation tends to produce precipitation maxima on the periphery and downwind edges of the urban region, and lesser precipitation amounts in the city center (Dixon & Mote 2003). Even though the dynamics associated with storm bifurcation have been shown to influence rainfall in several regions (Loose & Bornstein 1977, Bornstein & Lin 2000, Dixon & Mote 2003), no studies have examined storm bifurcation near urban areas in the southeastern United States. Furthermore, a broad understanding of urban-precipitation relationships across this region remains incomplete, including a comparative analysis of precipitation influences in different southeastern urban centers, as well as a synoptic-scale assessment of large-scale circulation conditions that may promote local and regional urban mechanisms.

1.2 Study Area

The study area consists of an eleven-state region in the southeastern United States (Figure 1.1) similar to the study area seen in Keim (1997). A number of factors make this region suitable for an investigation of urban precipitation processes including the number of large urban centers, such as Atlanta, Dallas-Fort Worth, Houston, New Orleans, and Miami and the rapid growth in population (Karl 2009). Climatologically, many of these cities have already been shown to exhibit evidence of precipitation enhancement (Shepherd et al. 2002, Dixon & Mote 2003, Burian & Shepherd 2005, Diem & Mote 2005, Diem 2006a). However, the distribution of synoptic precipitation delivery mechanisms (e.g., frontal, tropical, convective) differs from city to city, thereby likely contributing to spatial variations in urban-precipitation interactions,

including storm bifurcation. In addition, given the frequency with which extreme weather and climate impacts affect this region, such as tropical storms (Keim & Muller 2009) and severe drought (Seager et al. 2009), an improved understanding of precipitation variability in urban regions and its application to emergency management and hazards analysis is vital.

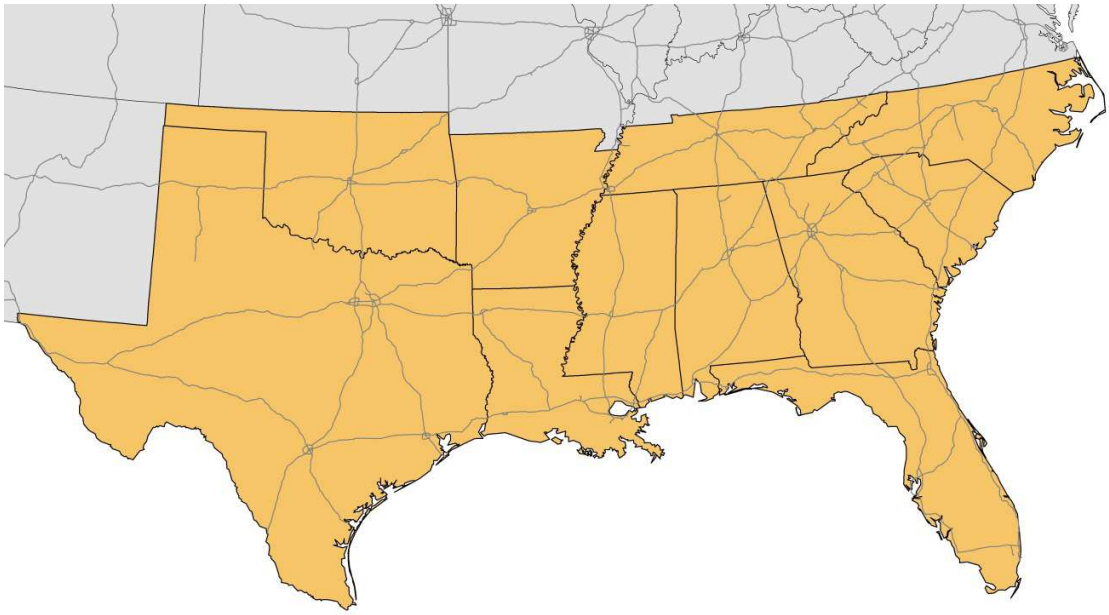

Figure 1.1. The 11 states comprising the southeastern United States and study area.

1.3 Research Questions

This study determines whether the presence of urban areas across the southeastern United States influences precipitation. The proposed research is framed by three research questions:

1) How does evidence of precipitation enhancement vary among urban regions within the southeastern United States?
2) What are the climatological characteristics of storm bifurcation within the southeastern United States?

3) How is synoptic-scale circulation variability linked to the occurrence of storm bifurcation in the southeastern United States?

In Study 1, tests for enhancement of precipitation associated with urban areas will be applied to multiple urban areas across the southeastern U.S. Results of this analysis will characterize the spatial variability of urban-precipitation relationships across the region, as well as guide the identification of potential locations of storm bifurcation. The presence of increased roughness necessary for bifurcation is frequently associated with other urban-precipitation signals such as precipitation enhancement (Dixon & Mote 2003). It is expected that larger urban areas, such as Atlanta, Houston, and Dallas/Fort Worth will exhibit some evidence of precipitation enhancement in their downwind regions. Thus, the comparative analysis framework utilized in Study 1 will constitute an improved understanding of precipitation variability in this region.

In Study 2, storm motion around the urban centers most likely to induce bifurcation is analyzed. This involves tracking the storm motion approaching urban areas using radar imagery and testing the precipitation using a bifurcation detection test. This test is spatially applied to a series of events, designed to characterize specific occurrences of bifurcation at local and regional levels. It is expected that bifurcation, though rare, occurs more frequently around the largest cities.

In Study 3, a circulation-to-environment (Yarnal 1993) classification of synoptic-scale geopotential height flow patterns will be used to determine whether specific circulation patterns promote storm bifurcation at locations within the southeastern United States. It is expected that bifurcation occurs on days with weak synoptic flow, so that mechanical turbulence caused by

surface roughness can play a relatively larger role than thermal turbulence associated with atmospheric instability.

1.4 Implications

By employing multiple detection methods and examining multiple locations within the southeastern U.S., the research proposed in Study 1 will provide a new, robust, and comprehensive assessment of urban-precipitation relationships for this part of the United States. Additionally, this study will provide an updated assessment of some previously studied urban areas within the Southeast, allowing for either support for or disagreement with prior analyses.

Results from Study 2 will be important on numerous levels. First, storm bifurcation has been only minimally catalogued and characterized in a climatological context. The anticipated results from this analysis will expand upon this knowledge base and provide a baseline for future investigations of bifurcation. An improved understanding of bifurcation occurrence can also aid forecasters in urban regions, both on the meteorological level as well as for local and regional climate modeling. Finally, these results could potentially be used to inform urban planners in considerations such as assigning appropriate zoning types for precipitation enhanced regions.

Results from Study 3 will provide insight into the relationship between storm bifurcation processes at the surface and large-scale synoptic circulation conditions aloft. An improved understanding of this relationship could inform forecasting applications and provide a framework for subsequent analyses linking bifurcation to large-scale drivers of climate variability (e.g., North Atlantic Oscillation and El Niño/Southern Oscillation (Yarnal et al. 2001)). It may also be possible to apply this methodology to other urban areas where storm bifurcation occurs.

Together, results of this proposed research will contribute meaningfully toward an increased understanding of storm bifurcation prevalence, enhance the broader understanding of urban-precipitation mechanisms and characteristics, and inform a range of stakeholder communities in the southeastern United States with interest in urban precipitation variability and impacts.

CHAPTER 2. LITERATURE REVIEW

2.1. Introduction

Urban areas have been shown to influence climate on a variety of spatial scales (Carlson & Arthur 2000, Arnfield 2003, Shepherd 2005, Diffenbaugh 2009, Lamptey 2010, McCarthy et al. 2010). It is important to improve our understanding of their impacts on climate because of the rapid growth rate of cities worldwide. Changes in land use/land cover (LULC) and increases in surface roughness and aerosol concentrations continuously alter energy, moisture, and momentum fields as well as circulation patterns above urban environments. Expansion of urban heat islands (UHIs) that result from these changes in turn increase convection and convergence that occur over and downwind of the city center. Pollution has been shown to increase the number of cloud condensation nuclei over urban regions, with a complex series of feedbacks to cloud formation and precipitation. Surface roughness has been shown to affect locations of enhanced convergence.

A robust understanding of precipitation processes over urban regions, driven primarily in the warm season by convergence and convection (Diem & Mote 2005), is essential for understanding a range of environmental and socioeconomic implications. It is particularly important to understand the coupling between the urban area and the local synoptic regime to improve forecasts (Dabberdt et al. 2000) and enhance the efficiency of urban planning for a variety of human benefits (Matzarakis & Endler 2010, Vanos et al. 2010). This is especially true in regions such as the U.S. Southeast, with rapid urbanization, abundant and variable precipitation totals, and numerous precipitation-generating mechanisms, each of which may have a different degree of coupling to the ever-changing urban surface.

Many studies have identified mechanisms responsible for the urban influence on precipitation (Changnon 1976, Diem & Mote 2005, Ntelekos et al. 2007, Lacke et al. 2009, Shem & Shepherd 2009). Collectively, studies such as these suggest that the three primary mechanisms are (1) UHI-induced convection zones which decrease static stability (Lacke et al. 2009), (2) enhanced aerosol concentrations (e.g., Shem and Shepherd 2009), which can either suppress precipitation by producing many small droplets which are too small to fall, or enhance precipitation by increasing the efficiency of the collision-coalescence process, and (3) increased surface roughness which creates areas of convergence at the surface (Dixon & Mote 2003, Diem & Mote 2005).

A final mechanism, confluence/diffluence, remains particularly poorly understood. Bornstein and Lin (2000) showed that when regional winds are strong, surface diffluence occurs, causing the storm to bifurcate, as the storm encounters the increasing surface roughness of the city center. Bornstein and LeRoy (1990) termed this diffluence the "building-barrier effect," a phenomenon also known as storm bifurcation. The process of storm bifurcation tends to produce precipitation maxima on the downwind periphery of the urban region (where confluence occurs) and precipitation minima in the city center (Dixon & Mote 2003). Even though storm bifurcation has been shown to influence the location of maximum rainfall in New York City (NYC) (Loose & Bornstein 1977, Bornstein & Lin 2000), no studies have examined storm bifurcation in detail in urban areas in the southeastern United States. Furthermore, while urban effects on precipitation have been reviewed (Shepherd 2005), an update on the most recent literature and an understanding of general urban-precipitation relationships across the Southeast remains incomplete. This paper reviews the limited findings related to urban influences on precipitation

in the southeastern U.S. and the relatively scarce literature on storm bifurcation, and it calls for increased research on these topics.

2.2. Mechanisms Contributing to Urban Influence on Precipitation

2.2.1 Urban Heat Island

The most widely studied element of urban climate is the UHI (Souch & Grimmond 2006). It is important to understand the UHI effect when examining urban precipitation because it has been shown that the temperature gradient between an urban area and its rural surroundings is partly responsible for precipitation initiation (Bornstein & Lin 2000, Dixon & Mote 2003). An UHI is defined as an urban area where temperatures exceed those of the surrounding (non-urbanized) areas, with the gradient between these regions generally strongest on calm, clear nights. A UHI alters air temperature in the lower layers of the atmosphere, but certainly deeper UHI layers can exist (Voogt & Oke 2003). The general characteristics of an UHI may vary by city due to differences in albedo, anthropogenic heat, emissivity, sky view factor, and thermal inertia (Arnfield 2003). While all of these factors were considered important, a modeled UHI with geographic and climatological characteristics similar to London showed that lack of surface evaporation was the dominant factor producing the UHI (Atkinson 2003).

Regardless of the primary reason for the increased temperatures in the city, differential surface heating between urban and rural areas leads to horizontal temperature gradients and the creation of an urban-breeze circulation (Hidalgo et al. 2008). Hidalgo et al. (2008) simulated the urban-breeze circulation for Toulouse in southwestern France. In part due to the high static stability during the experiment, a daytime July UHI of 1 C° easily formed over the center of the city (detected up to a vertical height of 1100 m), and was advected leeward of the city. These

results were expected to be typical for that time of the year. The urban-breeze was observed soon after the temperature gradients formed. An area of convergence near the city is compensated by divergent winds in the upper levels of the planetary boundary layer, with increased intensity of this circulation in early evening, when it dominated the local wind flow (Hidalgo et al. 2008). Basara et al. (2008) used points along transects through Oklahoma City to show that temperatures vary within the horizontal gradients due to proximity to the central business district, sky view factor, and nearby buildings. A dominant southerly flow advected the center of the UHI north of the central business district (Basara et al. 2008). Cheng and Byun (2008) modeled the effects of land cover on the local circulation for the Houston-Galveston metropolitan area and found that large continuous impervious surface areas produced an unrealistically modeled UHI and caused stronger bay breeze flows than using an area broken down into grass, trees, residential, and impervious surfaces. As a result, by better representing the local wind and heat patterns within the area using detailed land cover representation, the modeled bay breeze more realistically penetrated farther into the city (Cheng & Byun 2008). Such circulations caused by the UHI are responsible for the genesis and/or enhancement of convective storms downwind of the urban area (Bornstein & Lin 2000, Dixon & Mote 2003).

Several studies show that vegetation reduces the magnitude of the UHI by increasing the contribution of latent heating at the expense of sensible heating in the local energy balance (Grimmond et al. 1996, Jauregui & Romales 1996, Hamada & Ohta 2010). Vegetation also shades and changes the albedo of the surface, absorbs solar radiation before it can reach the ground, and increases surface humidity through transpiration. “Green zones” (Grimmond et al. 1996, Shashua-Bar & Hoffman 2000, Gomez et al. 2004, Hirano et al. 2004) are regions within a city consisting of high tree or green vegetative density that lower the air and surface temperature.

Green zones have been shown to modify microclimatic conditions through the regulation of temperature changes, with the influence of green zones dependent on site characteristics (Gomez et al. 2004). Cheng and Byun (2008) showed different land use simulations for the Houston-Galveston metropolitan area where the UHI was responsible for changing the location and strength of the dominant local circulation (sea-breeze) and stated that land cover changes allowed for the influence of local circulation during weak synoptic conditions (Cheng & Byun 2008). With the long growing season and abundant sunshine and moisture, the Southeastern U.S. appears to have good opportunity to mitigate UHI effects via reforestation and strategic landscaping.

Surface albedo of the built environment is another component of urban areas having a direct impact on the UHI effect, which in turn affects urban precipitation. Alterations in small-scale, local heat fluxes of an urban region caused by differing surface albedoes can influence the local surface energy budget. The albedo of a surface is greatly dependent on the color and type of surface; therefore heat storage directly depends on the albedo of the land cover (Asaeda et al. 1996). Because the southeastern U.S. is growing very quickly, changing surface characteristics may play an important role in the urban climate of many cities. Imhoff et al. (2010) studied surface temperatures across the 38 most populated urban areas in the U.S. to determine how the UHI varies according to the biome surrounding the urban area (defined based on a combination of biophysical, climate, botanical, and animal habitats). Results suggest that the percentage of impervious surface area predicts the surface temperature well except in the biomes categorized as deserts and xeric shrublands (Imhoff et al. 2010).

Numerous studies have been conducted to determine the specific UHI effect for various cities across the United States, especially in the Sunbelt. Comrie (2000) studied the UHI of

Tucson, Arizona, one of the rapidly-growing metropolises in the United States. Analysis of minimum temperature in the past 30 years shows UHI growth of ~3 C° over the past 100 years, with more than 2 C° contributed in the past 30 years (Comrie 2000). Hawkins et al. (2004) compared hourly temperature data from two sites in Phoenix: a rural farm southeast of the city and Sky Harbor Airport, near the center of the city. Average UHI effects ranged from 9.4 Cº to 12.9 Cº, confirming that Phoenix may have one of the largest UHIs in the world (Hawkins et al. 2004). UHI values based on minimum temperatures for Phoenix were found to be 4.4 C° in June and 2.4 C° in January (Svoma & Brazel 2010). Basara et al. (2008) found a mean nocturnal UHI greater than 1.5 C° for Oklahoma City (Basara et al. 2008). Using land surface temperatures derived from the Moderate Resolution Imaging Spectroradiometer (MODIS) in 2005 for several counties in Indiana, Rajasekar and Weng (2009) found a UHI effect of 1.5 C° diurnally and 1.3 C° nocturnally (Rajasekar & Weng 2009). A nocturnal rate of increase toward the city core of 0.02 C°/km was observed for Washington and 0.04 C°/km was reported for NYC (Hicks et al. 2010). Zhang et al. (2009) showed that the upwind urban area of Washington, D.C. was responsible for contributing to the heat wave event in Baltimore of 9 July 2007. They found that Baltimore's UHI would be reduced by 1.25 C° if warmer air upwind (Washington D.C.) had not been advected. Other contributing factors such as upward surface heat fluxes and entrainment of warm air aloft were considered (Zhang et al. 2009).

Only a handful of studies have examined the UHI of cities in the southeastern United States. Using MODIS technology, Xie et al. (2006) found a nocturnal UHI of 4 - 5 C° compared to the average temperature of San Antonio. Zhou and Shepherd (2009) found the mean UHI of Atlanta-Athens to be 1.31 C° and Atlanta-Monticello to be 1.71 C° (Zhou & Shepherd 2009). These studies suggest that cities of the Southeast display UHI characteristics despite the

prevalence of many types of broader-scale circulation features, including frontal passages, tropical storm systems, and land-sea breeze circulations.

2.2.2 Increases in Aerosols

The local climatic effects of urban-enhanced air pollution are believed to depend on the concentration and size of solid aerosols serving as cloud condensation nuclei (CCN). Aerosols larger than 1 μm in diameter tend to cause a net increase in precipitation by increasing the efficiency of the collision-coalescence process of converting cloud droplets to raindrops (Rosenfeld et al. 2008a). This conversion efficiency increases because larger cloud droplets are more likely to collide with other cloud droplets (Rosenfeld et al. 2008a). Aerosols smaller than 0.1 μm tend to suppress precipitation because smaller CCNs increase the time required for cloud droplets to coalesce with other droplets (Givati & Rosenfeld 2004, Rosenfeld et al. 2008a). Aerosols also suppress precipitation by attenuating solar radiation, thereby stabilizing the near-surface atmosphere and destabilizing the layer between the height of significant absorption and several meters above it, with the net effect often suppressing convective activity (Ramanathan et al. 2001, Rosenfeld et al. 2008b). The effects of aerosols between 0.1 μm and 1 μm have not been described in the climatological literature.

Anthropogenically-produced CCN have been found to increase precipitation in western Washington, with the magnitude of the effect depending on aerosol size (Hobbs et al. 1970). van den Heever and Cotton (2007) concluded that the influence of aerosols on storms in St. Louis was exceeded by the influence of convergence caused by urban heating. The “Eight Cities Study” (Huff & Changnon 1973) (further discussed in Section 3.1) consisted of an analysis of precipitation for St. Louis, Chicago, Cleveland, Washington, Indianapolis, Tulsa, Houston, and New Orleans. It was concluded that larger concentrations of industrial aerosols, along with

increased condensation, were the causes of the increase in precipitation (Huff & Changnon 1973). Even though aerosols affected the microphysical processes involving precipitation produced by these storms, their influence did not play a large role in the precipitation characteristics of the storm until after development. Simulations of increased urban aerosol concentrations resulted in more intensity increases than with rural aerosols alone (van den Heever & Cotton 2007).

Other studies have found that the net effect of urban-produced aerosols is to decrease precipitation totals. Givati and Rosenfeld (2005) stated that regions with clouds that have warm tops and short lifetimes experience the greatest precipitation suppression, due to pollution contribution by small aerosols. Jirak and Cotton (2006) demonstrated that the decrease in orographic precipitation since 1950 west of urban areas along the Front Range of the Rocky Mountains may be attributable to anthropogenically-produced pollution (Jirak & Cotton 2006). In studying the effects of pollution on orographic winter precipitation across the western U.S., Rosenfeld and Givati (2006) found a decrease in their precipitation factor (R_o) of 24 percent over the last century, which was attributed to the increase in smaller aerosols (Rosenfeld & Givati 2006). In a simulation of various aerosol concentrations associated with a squall line over the south plains of the U.S., Li et al. (2009) concluded that increasing the number of aerosols increases the concentration of CCNs, reducing cloud droplet size. Although a variety of aerosol sizes was simulated, the size responsible for the reduction in cloud droplets was not specified. In the various simulations of the squall line, aerosol concentration was found to influence precipitation intensity but not the spatial pattern. Deep convective clouds were found to be intensified with increases in aerosols, while small cumulus clouds distant to the squall line decreased in intensity (Li et al. 2009). Regardless of whether the net effect of solid aerosol

contribution is toward increasing or decreasing precipitation, indications are that as urban areas continue to grow, so will the transportation, industrial, and/or domestic needs of the city, causing the UHI effect to intensify and increase the number of aerosols emitted (Rosenfeld et al. 1995).

The net effect of aerosols on precipitation variation in time and space has been examined more thoroughly in the Southeast than in most other regions. Using Tropical Rainfall Measuring Mission (TRMM) estimated precipitation, Bell et al. (2008) found a statistically significant weekly signal in precipitation during the summer over the southeastern U.S. where the intensity of precipitation and area covered by rain increased during the middle of the week (and with a minimum on Sunday), very similar to the flux in anthropogenic aerosols, possibly indicating an anthropogenic influence. Over the Atlantic, the signal was very strong but reversed in sign. It was concluded that sea salt -- larger aerosols possibly serving as CCNs -- weakened the effects of anthropogenic pollution by enhancing rainfall (Bell et al. 2008). Lacke et al. (2009) examined radar-derived precipitation for Atlanta to determine the role of aerosols in enhancing or initiating precipitation under maritime tropical air mass conditions (Kalkstein et al. 1996). They found a statistically significant increase in precipitation on Thursdays compared with other days of the week and precipitation maxima in northwestern and eastern metropolitan Atlanta on days with greater aerosol concentrations, while maxima occurred in southeastern Atlanta on low aerosol days (Lacke et al. 2009).

The relationship between aerosols and convective thunderstorms in the U.S. Southeast has been analyzed recently. In a follow-up study focused partially in the U.S. Southeast (Bell et al. 2009), lightning data from the National Lightning Detection Network (NLDN) was used to confirm the results of Bell et al. (2008). The authors claimed that the presence of lightning is an indicator of the effects of aerosols on storm development due to its dependence on ice aloft.

Lightning activity peaked over the southeastern U.S. during the middle of the week and over the Atlantic Ocean and Gulf of Mexico on the weekends. Compared to the strength of the signal found in Bell et al. (2008), the signal was weaker, especially over the urban areas, and more widespread. The authors posit that this result may suggest that the aerosol-influenced growth of the storms has already reached a maximum. When compared to the weekly cycle of lightning, the cycle in pollution was less visible. The UHI may have invigorated the storms so much that any influence caused by aerosols was difficult to distinguish (Bell et al. 2009). Carrio et al. (2010) modeled the effect of aerosols on two convective events in Houston using the Town Energy Budget urban model within the Regional Atmospheric Modeling System (RAMS) from Colorado State University. The first group of storms, not influenced by urban-simulated CCNs due to the "cleaner" air from the incoming sea-breeze, occurred southwest of the city, while the second group was influenced by the CCNs and occurred downwind of the city. High aerosol concentrations prevented growth of ice particles, reducing precipitation efficiency (Carrio et al. 2010).

2.2.3 Surface Roughness

The topography of the urban environment can greatly impact the microclimate, possibly resulting in local changes in precipitation. These changes occur because surface roughness alters energy, mass, and momentum fluxes between the surface and the atmosphere and in the urban mixed layer (Dabberdt et al. 2000). While the direct influence of surface roughness on precipitation has not been widely explored in the literature, its influence has been shown to impact storm movement and dynamics (Dixon & Mote 2003).

Many aspects of urban design regarding roughness elements, such as density of urbanization, street orientation, building height and location, and size of green areas, impact the

local circulation regimes. Givoni (1994) discussed ways that an urban area can be developed to influence local winds which can lead to convergence. For instance, enhancement of ventilation of the city core can occur by designing streets parallel to the direction of prevailing winds; once these winds are set up, they can affect local storm motion by creating areas of convergence (Kishtawal et al. 2010). Also, constructing buildings of different heights perpendicular to the prevailing wind and orienting buildings of similar height parallel to the prevailing wind will increase ventilation and perhaps alter precipitation patterns (Givoni 1994). Grimmond et al. (1998) concluded that the heights of the upwind roughness elements influence winds at a greater distance compared to shorter roughness elements. They also found that roughness length in the winter was 82-87% of the length for the summer and that land cover of an urban area becomes more uniform with increasing height (Grimmond et al. 1998). The importance of adding green zones, including on rooftops (Dvorak & Volder 2010), with varying heights to provide shade, encourage ventilation, and save irrigation costs by increasing humidity is also stressed (Givoni 1994).

Thielen et al. (2000) developed a surface model by testing the sensitivity of parameters within an urban area to find the influence of the surface roughness on developing convective precipitation. It was found that roughness length (Oke 1987) significantly influences downwind precipitation. If the roughness elements are small, simulated UHIs were the dominant surface forcing (Thielen et al. 2000). Childs and Raman (2005) found when studying the interaction between the UHI of NYC with the sea-breeze that events occurring at night under a strong regional flow were subjected to a roughness-induced cyclonic turning over the core of the city, enhancing the chance of precipitation (Childs & Raman 2005). Carraca and Collier (2007) noted that that either the upwind rural–urban discontinuity or the presence of buildings (affecting

upward vertical velocities) may be responsible for initiating convective cloud cover and precipitation in Manchester, UK, with closely-built tall buildings impacting the initiation of convection and sensible heat fluxes similar to that of widely-spaced medium-sized buildings. If the atmospheric boundary layer is unstable, then convection may be initiated by the increase in sensible heat flux (Carraca & Collier 2007).

2.3. Urban Precipitation

2.3.1 Urban Influences on Precipitation Enhancement

When changes in LULC occur in a growing urban area, changes in the frequency, intensity, and amount of precipitation can occur (Shepherd 2005), but this anthropogenic alteration is generally strongest in the warm season although effects have been seen year-round (Changnon et al. 1991, Changnon 2003, Gero et al. 2006, Svoma & Balling 2009). Among the earliest comprehensive investigations of urban-precipitation relationships was Project METROMEX (Illinois State Water Survey 1974), a field study of St. Louis intended to analyse the effects of weather modification by urbanized areas. It was determined that not only did afternoon precipitation increase after urbanization, but clouds over urban areas were more likely to merge with developing storm systems, resulting in stronger storm units (Changnon et al. 1971). The "Eight Cities Study" (Huff & Changnon 1973) expanded upon the findings of METROMEX by analyzing the precipitation climatology of St. Louis, Chicago, Cleveland, Washington, Indianapolis, Tulsa, Houston, and New Orleans. Urban-enhanced increases in average daily and seasonal precipitation, particularly in June through August, were found in St. Louis, Chicago, and Cleveland, while Washington showed most enhancement in September through November, and Houston and New Orleans only experienced enhancement in May

through September and May through October, respectively. No significant evidence of increased precipitation in Indianapolis and Tulsa was found. While the scope of the conclusions was limited by the data and technology available at the time, it was asserted that destabilization of the atmosphere caused by the UHI, along with additional condensation linked to increases in industrial aerosols, were responsible for the observed precipitation enhancement (Huff & Changnon 1973). Subsequent studies in this early period of urban climatology research generally supported the hypothesis that urban areas were prone to enhance precipitation (Dettwiller & Changnon 1976, Huff & Vogel 1978, 1979).

Souch and Grimmond (2006) noted the increase in research on urban precipitation that emerged in the 1990s as longer and more accurate weather station records, along with the advent of new technologies such as satellite-derived precipitation estimates from the TRMM and Doppler radar, became available. Some examples of urban-precipitation studies throughout the United States and other countries from this era include those of Jauregui and Romales (1996), Shepherd et al. (2002), Diem and Brown (2003), Dixon and Mote (2003), Burian and Shepherd (2005), Diem and Mote (2005), Diem (2006), Shepherd (2006), Baumer and Vogel (2007), Mote et al. (2007), and Bell et al. (2008). The increased sophistication of these investigations led to improved hypotheses about the mechanisms responsible for precipitation enhancement in urban regions. These include: the addition of available water vapor into the local atmosphere through changes in moisture-energy fluxes; an increase in low-level convergence driven by surface roughness of the urban landscape; and the complex role of aerosols and CCN (Diem & Brown 2003).

2.3.2 Precipitation Enhancement in the Southeastern United States

The southeastern U.S. has been the focus of a number of urban precipitation studies (Huff & Changnon 1973, Bornstein & Lin 2000, Shepherd et al. 2002, Burian & Shepherd 2005, Diem & Mote 2005, Diem 2006b, Mote et al. 2007, Hand & Shepherd 2009). Also three of the eight metropolitan areas in the "Eight Cities Study" (Huff & Changnon 1973) were located in the southeastern United States (Houston, New Orleans, Tulsa). Huff and Changnon (1973) detected an increase in daily and seasonal precipitation amounts for days synoptically classified as "air-mass" along the coastal cities. Specifically, a 17 percent increase in warm-season precipitation of air-mass origin to the north and northeast of Houston and a 10 percent increase in warm-season precipitation of air-mass origin in the northern part of New Orleans were reported (Huff & Changnon 1973). The strongest evidence for urban influences occurred on days with heavy rainfall during the warm season, although increases in thunder-day frequencies were also observed in other seasons (Huff & Changnon 1973). A convective sequence (increase in convective activity over the city resulting in thunderstorm formation, and further evolution into hailstorms downwind of the urban center) initiated by urban areas is stated to be the cause for these downwind patterns (Huff & Changnon 1973).

All seven cities, chosen because of their limited topographic relief, tested in Shepherd et al. (2002) are located in the southeastern United States: Atlanta, Montgomery, Nashville, San Antonio, Waco, Austin, and Dallas. For the period 1998-2000, TRMM-based precipitation estimates were used to detect and characterize warm-season (May – September) urban rainfall signals around these seven cities (Shepherd et al. 2002). Downwind sections, which were defined based on warm-season 700 hPa average flow for each city, averaged 28.4 percent more rainfall than the areas immediately upwind of the urban center, leading Shepherd et al. (2002) to

conclude that the spatial scale of the urban precipitation modifications was consistent with that of METROMEX and other previous studies. Hand and Shepherd (2009) observed warm-season (June-September) positive precipitation anomalies of mean daily rainfall amounts in the climatologically downwind region of Oklahoma City, leading to their conclusion that urban influences may be the largest contributing factor to local precipitation variability.

Atlanta has been the focus of a large amount of attention in the scholarly research in recent years. Diem and Mote (2005) noted that only one station in the Atlanta metropolitan region experienced a strong temporal trend in the number of heavy precipitation days between 1953 and 2002 and therefore deemed the degree of urban enhancement of precipitation in that city as inconclusive. Using radar data, Mote et al. (2007) found areas of enhanced rainfall up to 80 kilometers east of Atlanta on warm-season, moist tropical (MT and MT+) days in the Spatial Synoptic Classification (Kalkstein et al. 1996, Sheridan 2002), with the greatest positive anomaly centered at a downwind distance of approximately 40 kilometers. Most recently, Bentley et al. (2010) used radar to study convective events in and around Atlanta to define regions of enhanced reflectivity around the central business district (CBD). Enhancement was found over the CBD, and to the northeast and south of the CBD; leading the authors to conclude that aerosols, the UHI, and convergence zones may be responsible for the "augmentation" of lightning downwind (Bentley et al. 2010). They also thought that enhanced reflectivity over the CBD may be a result of bifurcation, while lightning activity around the periphery was highly coupled with the outline of Atlanta (Bentley et al. 2010).

2.4. Urban Influences on Storm Bifurcation

2.4.1 Definition of Bifurcation

Evidence suggests that the interaction between the urban land surface and storm movement is complex. For example, Rose et al. (2008) found both lightning flash and precipitation enhancement in all directions surrounding Atlanta, rather than solely in the upwind region (Rose et al. 2008). Beyond the mechanisms of precipitation enhancement described above, urban areas have a further, and still poorly understood, effect on precipitation by altering the movement, growth, and demise of individual storm cells. Bornstein and Lin (2000) defined *storm bifurcation* as "a group of storms [that] moves in two directions from a specific location (such as upwind of city)". This phenomenon differs from *storm splitting* in that splitting is "a single initial storm [that] splits into two separated supercells, given appropriate vertical wind shear conditions" (Bornstein and Lin 2000, p. 515). While it is possible for storm splitting and bifurcation to occur in multiple types of rainfall events (frontal, convective, tropical), very few studies on the specific phenomenon of storm bifurcation have been undertaken, including for the U.S. Southeast.

2.4.2 Initial Bifurcation Studies and Evidence

Despite the lack of Southeast-specific studies on storm bifurcation, many of the same mechanisms that may initiate bifurcation in the Southeast are present in other regions that have been the focus of bifurcation analysis. Urban areas throughout the U.S. have variable UHIs, pollution emission levels, and surface roughness, contributing to the type of atmosphere that is most susceptible to bifurcation. In studying four different frontal systems that passed NYC, Loose and Bornstein (1977) found that the speed of the front decreased by 50 percent over the central urban area when no UHI was present due to the proportionally greater effects of frictional

drag and surface roughness. In contrast, periods where strong UHIs were established still resulted in the front slowing by 50 percent but only in the upwind half of the city (Loose & Bornstein 1977). The speed of the front increased by 25 percent downwind of the urban core due to horizontal pressure gradients caused by the UHI (Loose & Bornstein 1977). However, research on sea-breeze fronts (Freitas et al. 2007, Cheng & Byun 2008) and convective storm cells (Kishtawal et al. 2010) suggests this may not be the case, and there are complicated underlying factors that still need to be studied. Such modulation of storm movement due to climatic influences of the urban region could result in storm bifurcation, as suggested by Gaffen and Bornstein (1988) who analyzed a slow-moving front passing through NYC on 10-11 March 1966. Due to the initial slow speed of the front, the surface roughness of NYC was able to retard its movement, resulting in a horizontal split in the vertical structure between the surface front and upper segments.

Though the focus was on the initiation of six summer convective storms, the analysis of Bornstein and Lin (2000) sheds light on the relationship between UHI and storm bifurcation in Atlanta. They found that a UHI-initiated convergence zone affected storm movement on days with weak steering wind flows. Days with stronger flows led to a bifurcation of storms, causing storms to move around the city (Bornstein & Lin 2000). Even though individual synoptic situations in an urban area are complex, it can be concluded that when regional winds are strong, surface roughness of an urban area dominates the local synoptic regime, as opposed to a UHI-dominated regime in weaker synoptic settings (Bornstein & Lin 2000). This relationship is analogous to the "mechanical turbulence" versus "thermal turbulence" dichotomy that characterizes atmospheric buoyancy in general.

More recently, WSR-88D radar estimates of precipitation and lightning data revealed a mid-latitude cyclone that allowed for orographic initiation, caused by the Blue Ridge Mountains, of storms on 7 July 2004 which slowed during passage over Baltimore and the Chesapeake Bay (Ntelekos et al. 2007). The Chesapeake Bay, acting as a thermal boundary, not only prevented the storms from propagating eastward, but also provided southerly winds that would normally enhance convergence over Baltimore (Ntelekos et al. 2007). Precipitation totals and lightning flashes were greater along the western edge of Baltimore and Washington D.C. as the storm was shown on radar to split around Baltimore (Ntelekos et al. 2007). Thus, it seems that the urban area influences the evolution and propagation of storm cells as a result of frictional effects caused by the urban canopy (Ntelekos et al. 2007).

2.5. Conclusion

Urban areas have been shown to influence the frequency, intensity, and amount of precipitation through changes in LULC (Shepherd 2005). Project METROMEX (Illinois State Water Survey 1974) established that afternoon precipitation is enhanced in urban areas (Changnon et al. 1971). Huff and Changnon (1973) conducted the first multiple-city analysis of urban influence on precipitation and found possible evidence of urban-enhanced increases in average daily and seasonal precipitation at many of their study sites (Huff & Changnon 1973). Subsequent studies have revealed that while influences occur year-round, the signal is usually strongest in the warm season (Changnon et al. 1991, Changnon 2003, Gero et al. 2006, Svoma & Balling 2009). Recent studies (e.g., Jauregui and Romales 1996, Shepherd et al. 2002, Diem and Brown 2003, Dixon and Mote 2003, Burian and Shepherd 2005, Diem and Mote 2005, Diem 2006, Shepherd 2006, Baumer and Vogel 2007, Mote et al. 2007, Bell et al. 2008) have advanced

knowledge of the urban climate using the increased data availability and technology, allowing for improved hypothesis testing regarding mechanisms responsible for precipitation enhancement.

Many urban precipitation studies have been conducted for locations within the southeastern U.S. (Huff & Changnon 1973, Bornstein & Lin 2000, Sheridan 2002, Burian & Shepherd 2005, Diem & Mote 2005, Diem 2006b, Mote et al. 2007, Hand & Shepherd 2009). Collectively, these studies showed urban influences on “heavy"-precipitation days during the warm season (Huff & Changnon 1973) and enhanced precipitation downwind of the urban area (Shepherd et al. 2002, Mote et al. 2007, Hand & Shepherd 2009).

Further understanding of storm dynamics over urban areas is needed, as storm movement is linked directly to hazards such as lightning strikes and flash flooding. Only a few studies have investigated the occurrence of storm bifurcation and the effects of urban areas on storm movement (Loose & Bornstein 1977, Bornstein & Lin 2000, Dixon & Mote 2003, Ntelekos et al. 2007). Studying bifurcation is important for several reasons. First, applying the proposed methods of bifurcation analysis will provide a baseline for future investigations of bifurcation, a topic which has been only minimally examined and characterized in a climatological context. Second, an improved understanding of bifurcation occurrence can also aid forecasters in urban regions, both on the meteorological level as well as for local and regional climate modeling. Finally, results from such analyses could potentially be used to inform urban planners in considerations such as assigning appropriate zoning types for precipitation enhanced regions. Urban areas have many effects on their local environment. While numerous studies show that downwind enhancement of total precipitation, propagation of individual storm cells, or the slowing of storm systems in and around an urban area can occur, it has been very difficult to

conclude that urban features are the sole cause for such influences. Therefore, it is important to continue to study urban effects on precipitation to obtain a better understanding of this complex and dynamic relationship. If urban influence on rainfall can be predicted successfully, then urban infrastructure can be zoned for green space or reservoirs to maximize rainfall capture. Finally, a broader understanding of precipitation variability across major urban centers in the southeastern U.S. will provide potential benefit to a range of stakeholders, such as city planners and emergency managers, whose work is informed by climatological information.

CHAPTER 3. PRECIPITATION ENHANCEMENT

3.1 Introduction

The previous chapter reviewed the literature of urban influences on precipitation. While studies on urban precipitation have occurred for regions throughout the U.S., this study focuses on major urban areas within the southeastern United States. This chapter discusses methods used to test for urban influence on precipitation for six cities in the region: Atlanta, Birmingham, Dallas/Fort Worth, Houston, Memphis, and Tulsa.

3.2 Background

3.2.1 Urban Influences on Precipitation Enhancement

When changes in land use/land cover (LULC) occur in a growing urban area, changes in the frequency, intensity, and amount of precipitation can occur (Shepherd 2005) on both meteorological and climatological time scales. This anthropogenic alteration is generally strongest in the warm season, when precipitation events are more likely to be convective, but effects have been observed year-round (Changnon et al. 1991, Changnon 2003, Gero et al. 2006, Svoma & Balling 2009). Among the earliest comprehensive investigations of urban-precipitation relationships was Project METROMEX (Illinois State Water Survey 1974), a field study of St. Louis intended to analyze the effects of weather modification by urbanized areas. It was determined that not only did afternoon precipitation increase after urbanization, but clouds over urban areas were more likely to merge with developing storm systems, resulting in stronger storm units (Changnon et al. 1971). A subsequent “Eight Cities Study” (Huff & Changnon 1973) expanded upon the findings of METROMEX by analyzing the precipitation climatology of St.

Louis, Chicago, Cleveland, Washington, Indianapolis, Tulsa, Houston, and New Orleans. Locations were chosen to represent various climate zones, degrees of industrialization, topographic features, and rates of population growth. Possible evidence of urban-enhanced increases in average daily and seasonal precipitation, particularly in June through August, were found in St. Louis, Chicago, and Cleveland, while Washington showed most enhancement in September through November, and Houston and New Orleans only experienced enhancement in May through September and May through October, respectively. No significant evidence of increased precipitation in Indianapolis and Tulsa was found. While the scope of the conclusions was limited by the data (1955-1970) and technology available at the time, it was asserted that destabilization of the atmosphere caused by the urban heat island (UHI), along with additional condensation linked to increases in industrial aerosols, were responsible for the observed precipitation enhancement (Huff & Changnon 1973). Subsequent studies in this early period of urban climatology research generally supported the hypothesis that urban areas were prone to enhance precipitation (Dettwiller & Changnon 1976, Huff & Vogel 1978, 1979).

Souch and Grimmond (2006) noted the increase in research on urban precipitation that emerged in the 1990s as longer and more accurate weather station records, along with the advent of new technologies such as satellite-derived precipitation estimates from the Tropical Rainfall Measuring Mission (NASA and the Japan Aerospace Exploration Agency (JAXA)) and Doppler radar, became available. Some examples of urban-precipitation studies throughout the United States and other countries from this era include those of Jauregui and Romales (1996), Shepherd et al. (2002), Diem and Brown (2003), Dixon and Mote (2003), Burian and Shepherd (2005), Diem and Mote (2005), Diem (2006), Shepherd (2006), Baumer and Vogel (2007), Mote et al. (2007), and Bell et al. (2008). The increased sophistication of these investigations led to

improved hypotheses about the mechanisms responsible for precipitation enhancement in urban regions. These include: the addition of available water vapor into the local atmosphere through changes in moisture-energy fluxes; an increase in low-level convergence driven by surface roughness of the urban landscape; and the complex role of aerosols and cloud condensation nuclei (CCN, Diem & Brown 2003).

3.2.2 Precipitation Enhancement in the Southeastern United States

The southeastern U.S. has been the focus of a number of urban precipitation studies (Huff & Changnon 1973, Bornstein & Lin 2000, Shepherd et al. 2002, Burian & Shepherd 2005, Diem & Mote 2005, Diem 2006b, Mote et al. 2007, Hand & Shepherd 2009). In addition, three of the eight metropolitan areas in the "Eight Cities Study" (Huff & Changnon 1973) are located in the southeastern United States (Houston, New Orleans, Tulsa). Huff and Changnon (1973) detected a long-term increase in daily and seasonal precipitation amounts for days synoptically classified as "air-mass" along the coastal cities. Specifically, a 17 percent increase in warm-season precipitation of air-mass origin to the north and northeast of Houston and a 10 percent increase in warm-season precipitation of air-mass origin in the northern part of New Orleans were reported for the period between 1964 and 1968 (Huff & Changnon 1973). The strongest evidence for urban influences occurred on days with heavy rainfall during the warm season, although increases in thunder-day frequencies were also observed in other seasons (Huff & Changnon 1973). A convective sequence (increase in convective activity over the city resulting in thunderstorm formation, and further evolution into hailstorms downwind of the urban center) initiated by urban areas is stated to be the cause for these downwind patterns (Huff & Changnon 1973).

All seven cities, chosen because of their limited topographic relief, tested in Shepherd et al. (2002) are located in the southeastern United States: Atlanta, Montgomery, Nashville, San Antonio, Waco, Austin, and Dallas. For the period 1998-2000, TRMM-based precipitation estimates were used to detect and characterize warm-season (May – September) urban rainfall signals around these seven cities (Shepherd et al. 2002). Downwind sections, which were defined based on warm-season 700 hPa average flow for each city, averaged 28.4 percent more rainfall than the areas immediately upwind of the urban center, leading Shepherd et al. (2002) to conclude that the spatial scale of the urban precipitation modifications was consistent with that of METROMEX and other previous studies. It is possible that the increase in rainfall might be at least partially explained by the fact that their definition of "downwind" was based only on climatology and therefore covered the same areas regardless of the variation from climatological wind direction in individual storms, thereby including areas that naturally experience more rainfall as "downwind". Hand and Shepherd (2009) observed warm-season (June-September) positive precipitation anomalies of mean daily rainfall amounts in the climatologically downwind region of Oklahoma City, leading to their conclusion that urban influences may be the largest contributing factor to local precipitation variability.

Atlanta has been the focus of a many urban precipitation studies in recent years. Only one station in the Atlanta metropolitan region experienced a statistically significant long-term temporal trend in the number of heavy precipitation days between 1953 and 2002 (Diem & Mote 2005). Mote et al. (2007) used radar data and found areas of enhanced rainfall up to 80 kilometers east of Atlanta, with the greatest positive anomaly centered at a downwind distance of approximately 40 kilometers. Most recently, Bentley et al. (2010) studied convective events in and around Atlanta to define regions of enhanced reflectivity around the central business district

(CBD). Enhancement was found over the CBD, and to the northeast and south of the CBD, leading the authors to conclude that aerosols, the UHI, and convergence zones may be responsible for the "augmentation" of lightning downwind (Bentley et al. 2010). They also hypothesized that enhanced reflectivity over the CBD may be a result of the UHI, while lightning activity around the periphery was highly coupled with the outline of Atlanta and may be due to storm bifurcation (Bentley et al. 2010).

3.2. Data and Methods

3.2.1. Site Selection

U.S. Census Bureau's (2008) population estimates for metropolitan statistical areas (MSA) across the southeastern U.S. are used to identify the 25 largest metropolitan areas (defined as a core urban area having a population greater than 50,000 combined with surrounding counties having a "high degree of economic and social integration with that core") in the 11-state study region (Table 3.1). A list of factors is derived to guide the selection of locations to test for evidence of urban enhancement of precipitation, including: the topographic relief (variability in topography, or change in slope of elevation), proximity to large water bodies, and availability of historical record of precipitation observations (combination of large number of stations and fine spatial resolution). Cities having a greater distance to large water bodies and less relief are prioritized. Precipitation data are compiled into a series of "data availability" matrices for each city to include details about the station record (start date, end date, percent of missing data, length of record) and spatial coverage around the urban area ("Good" if stations are evenly distributed throughout the study area, "Poor" if there are regions within the study area not represented by a station), with MSAs having higher-quality precipitation records

prioritized for analysis. An abundance of precipitation data, both temporally and spatially, is critical to the detection of precipitation enhancement, as well as storm bifurcation occurrence. Other factors that may be considered are whether the city has been previously studied (allowing for direct comparison to previous results) and whether the inclusion of the city improves the spatial representation of study locations across the Southeast.

Topographic data are available from the National Elevation Dataset from USGS (United States Geological Survey (USGS)). The range in elevation is calculated across the 100 km buffer surrounding each urban area. Proximity to water body is calculated by measuring the distance from the edge of the 100 km buffer to the nearer coast (Gulf of Mexico or Atlantic). The purpose of determining these distances is to choose study sites that have minimal significant local influences on precipitation other than urbanization. The sharp precipitation gradients unrelated to the urban effects in coastal MSAs invite caution in the selection of such MSAs for analysis. In cases where a site chosen has a great topographic range or is near water, a study was conducted previously at that site, allowing for direct comparison of results from this analysis. While this methodology has some subjectivity, it provides insight to the characteristics of the study sites.

3.2.2. Climatic Data

Period-of-record daily precipitation data for each of the cities included in the initial pool of urban regions are retrieved from National Oceanic and Atmospheric Administration's (NOAA's) National Climatic Data Center (NCDC), specifically the cooperative observing network of stations (COOP). Longer and more spatially complete precipitation data will best

Table 3.1. Metropolitan areas ranked by population, distance to nearest large water body, range in elevation, number of precipitation stations, and spatial resolution of stations.

Rank	Metropolitan area	Estimated population 2008	Census 2000 population	Distance to H_20 (km)	Range in elevation (m)	Number of stations	Spatial resolution
1	Houston, TX	5,728,143	4,715,407	79.38	201	94	Good
2	Atlanta, GA	5,376,285	4,247,981	412.49	1051	105	Good
3	Dallas, TX	4,226,003	3,451,226	427.6	314.49	143	Good
4	Tampa, FL	2,733,761	2,395,997	35.5	113.14	51	Poor
5	Miami, FL	2,398,245	2,253,362	6.7	26	55	Poor
6	Fort Worth, TX	2,074,003	1,710,318	452.77	365	148	Good
7	Orlando, FL	2,054,574	1,644,561	73.51	113.14	89	Good
8	San Antonio, TX	2,031,445	1,711,703	233.66	673	103	Good
9	Fort Lauderdale, FL	1,751,234	1,623,018	4.86	26	62	Poor
10	Charlotte, NC	1,701,799	1,330,448	249.06	911.23	82	Good
11	Austin, TX	1,652,602	1,249,763	254.34	564	129	Good
12	Nashville, TN	1,550,733	1,311,789	644.27	534.43	145	Good
13	Memphis, TN	1,285,732	1,205,204	536.19	192	74	Good
14	West Palm Beach, FL	1,265,293	1,131,184	10.9	25.95	53	Poor
15	Oklahoma City, OK	1,206,142	1,095,421	722.62	346.98	103	Good
16	New Orleans, LA	1,134,029	1,316,510	63.7	115.13	141	Good
17	Birmingham, AL	1,117,608	1,052,238	350.18	705	99	Good
18	Raleigh, NC	1,088,765	797,071	189.16	296.95	87	Poor
19	Tulsa, OK	916,079	859,532	742	264.48	95	Poor
20	Baton Rouge, LA	774,327	705,973	106.42	143.59	120	Good
21	El Paso, TX	742,062	679,622	1012.94	2639.22	33	Poor
22	Columbia, SC	728,063	647,158	175.54	247.695	89	Good
23	McAllen, TX	726,604	569,463	104.42	310	44	Poor
24	Greensboro, NC	705,684	643,430	277.17	1183.26	96	Good
25	Sarasota, FL	687,823	589,959	4.7	113.14	34	Poor

facilitate comparisons between early and more recent rainfall regimes (Diem & Mote 2005, Shepherd 2006, Diem 2008). Within a MSA, precipitation stations should be selected both within and beyond what is believed to represent the zone of urban influence. As seen in Table 3.2, the distance from a city where urban enhancement precipitation has been identified varies by location and study. In this research, all precipitation stations within 100 kilometers of the city center with less than 10 percent missing daily precipitation data (Burian & Shepherd 2005), and a record length of 20 years or greater are included. For these stations, only the days receiving "heavy amounts" of precipitation (≥ 25 mm/day) are considered for analysis as they have been shown to have the greatest response to urban influence (Huff & Changnon 1973, Huff & Vogel 1978, Burian & Shepherd 2005, Diem & Mote 2005) (Figure 3.1).

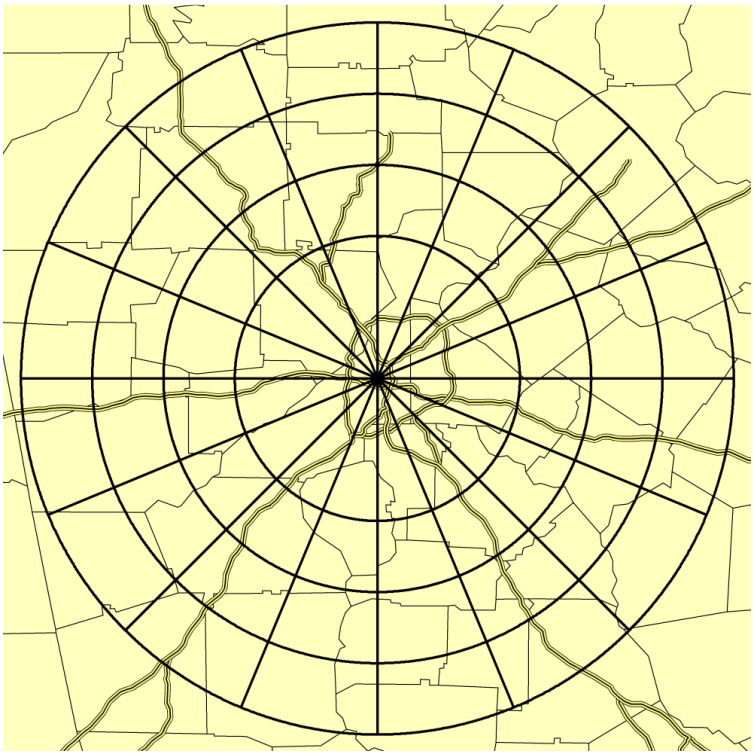

Figure 3.1. Buffers used to test extent of precipitation enhancement for Atlanta. Buffers are as follows starting with the largest buffer: 100 km, 80 km, 60 km, 40 km.

Table 3.2. Distance from city where urban influence on precipitation was detected.

Study	**City**	**Urban influence**
Huff & Changnon 1973	St. Louis	16-20 km
	Chicago	50-55 km
	Cleveland	40-80 km
	Washington D.C.	Urban area
	Baltimore	Urban and northeastward
	Houston	Near urban center
	New Orleans	Northeast side of city
Semonin & Changnon 1974	St. Louis	8-10 mi (12.87-16.09 km)
Changnon 1979	St. Louis	Downwind quadrant
Changnon et al. 1991	St. Louis	Downwind quadrant
Bornstein & Lin 2000	Atlanta	Initiated 25-40 km downwind
Shepherd et al. 2002	Atlanta	~60 km
	Montgomery	~25 km
	Dallas	~20 km
	Waco	~50 km
	San Antonio	~40 km
Diem & Mote 2005	Atlanta	Norcross station (~30 km)
Burian & Shepherd 2005	Houston	Urban area & urban impact regions
Diem 2006	Phoenix	40-100 km
Dixon & Mote 2007	Atlanta	Urban center-15 km
Mote et al. 2007	Atlanta	40-80 km
Diem 2008	Atlanta	50 km, Norcross station (~30 km)
Hand & Shepherd 2009	Oklahoma City	NNE of city

In preparation for the three tests to identify the degree and spatial extent of urban influence on precipitation, a series of concentric buffers at 20–km-radii intervals is drawn around the urban center. The 20 km-minimum buffer was chosen because buffers smaller than 20 km may not include enough stations to depict the precipitation pattern accurately. The 100 km-maximum buffer was selected because larger buffers are increasingly likely to allow non-urban precipitation-generating mechanisms to obscure the measurement of the impact of the urban area. Furthermore, because no previous study has identified an urban influence that extends beyond 100 km (Table 3.2), a maximum distance of 100 km seems reasonable. Each study site is then divided into a downwind region -- a zone situated beyond the city center, and an upwind region -- a zone situated opposite of the downwind region. The placement of these regions is

based upon the traditional location of urban-influenced precipitation anomalies seen in Huff & Changnon (1973), Changnon (1979), Shepherd et al. (2002), Diem and Mote (2005), Mote et al. (2007), Diem (2008), and Hand and Shepherd (2009). But unlike the aforementioned studies, the upwind and downwind regions are unique for each heavy precipitation event, determined by the mean daily wind direction at 700 hPa, the same level used in Burian & Shepherd (2005), Diem (2006; 2008), and Hand & Shepherd (2009). These data are available from the National Centers for Environmental Prediction/National Center for Atmospheric Research (NCEP/NCAR) North American Regional Reanalysis (NARR) dataset provided by the Physical Sciences Division of the Earth System Research Laboratory (Mesinger et al. 2006). Other studies that used only the 700 hPa level are Burian & Shepherd (2005) and Hand & Shepherd (2009).

3.2.3. Enhancement Detection Tests

Once the final selection of cities is made, three tests are employed at each site to detect the existence of urban-enhanced precipitation: (1) "downwind *vs*. upwind" test, (2) temporal analysis, and (3) the "contour" test.

3.2.3.1 Downwind vs. Upwind

The "downwind *vs*. upwind" tests requires that mean 700 hPa wind direction (acquired from NCEP/NCAR regional reanalysis data (Mesinger et al. 2006)) be calculated uniquely for every heavy precipitation day at each city. This level is used because it best represents mean moisture advection in the southeastern U.S. and is preferred over 500 hPa (which is usually considered to represent mean steering flow) as the 700 hPa level generally provides a balance between complete geostrophic flow and friction-influenced surface-level flow. Even though both 700 and 850 hPa levels have been used in previous studies, 700 hPa is preferred in studies that involve higher-elevation sites (e.g. Atlanta).

For each heavy precipitation day measured at any station in the study area, the mean wind direction is derived by determining the angle formed by using the mean u- and v-wind vectors at the 700 hPa level. Once the calculations are performed, these values are verified using the reanalysis data viewer online. The daily mean wind direction is assigned one of the sixteen 22.5°-wide azimuths. For example, a daily mean wind direction from an azimuth of 179° is assigned to the section between 157.5° and 180°. Precipitation stations are then grouped according to whether they fall into a "downwind" or "upwind" wedge of the city. For a given event, all stations situated within the eight wedges adjacent to the actual wind direction are considered "upwind," and all stations situated within the eight wedges on the opposite side of the circle are considered "downwind". If the angle of wind direction is equal to a boundary angle, it is classified into the wedge with the smaller azimuth values (e.g., a wind direction with an angle of 180° is placed in the section between 157.5° and 180°).

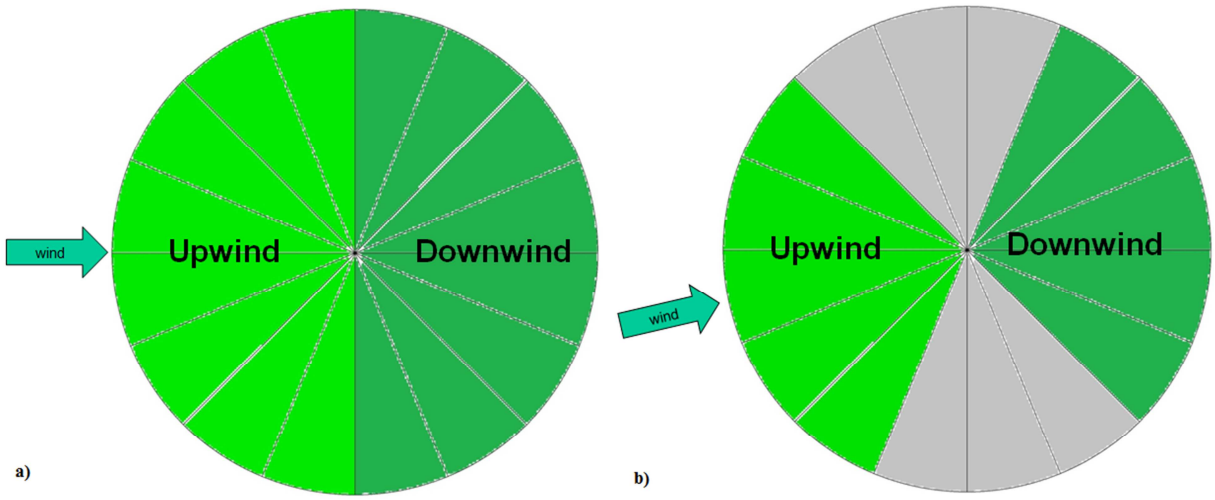

Figure 3.2. Upwind and downwind sections according to the two tests used: a) traditional test; b) 90° test.

Two upwind/downwind comparisons are made (Figure 3.2). The first one-- the "traditional test"-- involves dividing the azimuths centered on the city center in half, with the mean wind direction for that day in a wedge near the center of the "upwind" half. The study area includes all stations within a 100 km buffer around the city center. The second comparison, the "90° test", is conducted by comparing precipitation totals only in those stations that are within the four wedges nearest to the mean wind ("upwind") vs. the totals in stations within the four wedges opposite to the mean wind ("downwind"). In the 90° test, stations that are located in the eight wedges nearest to a 90° angle to the mean wind are removed from the test. The rationale behind this experimental design is that the stations in the eight wedges most perpendicular to the mean wind are so far removed from being truly "upwind" or "downwind" from the main urban LULC that they could contaminate comparisons between the other stations. The 90° test contains a smaller number of days because stations not located in the upwind/downwind sections were removed from the analysis. If no other stations within the upwind or downwind regions measured heavy precipitation (i.e., $\geq$ 25 mm) from an event analyzed in the traditional test, the event is removed from the list altogether.

For each heavy precipitation event, mean precipitation at upwind and downwind stations is calculated. Differences in mean precipitation between the upwind and downwind regions are then tested for statistical significance using a two-tailed Student's t-test and the Wilcoxon rank-sum test in Matlab® (a test equivalent to the Mann-Whitney u-test). The two-tailed t-test is selected because no assumptions are made regarding whether it is the upwind or downwind region that receive rainfall enhancement; there are theoretical reasons for precipitation enhancement at upwind sites (i.e., increasing surface convergence initiated by increasing surface roughness caused by the urban elements) and for downwind sites (i.e., increasing presence of

CCN as air flows over the city and/or increased surface convergence after storm cells merge downwind of the city following bifurcation upwind of the CBD). The two statistical tests are used for comparison and verification of results as they have been used in previous studies (Diem & Brown 2003, Diem & Mote 2005, Shepherd 2006, Diem 2008). At each site, these difference of mean tests are performed on the overall mean precipitation values for heavy precipitation days in the upwind and downwind sections, and also by season (spring = March, April, May; summer = June, July, August; fall = September, October, November; winter = December, January, February). If one region receives significantly more rainfall than the other, it is possible that the precipitation has been enhanced by one or more of the previously discussed mechanisms.

3.2.3.2 Temporal Analysis

The "temporal analysis" tests for trends in the precipitation record of each MSA using the Poisson Process (Keim & Cruise 1998) and a linear regression of the inter-arrival times between days above a specified threshold value (annual frequency series (Keim & Cruise 1998)). To determine the series at a given MSA, regional average heavy-event precipitation is calculated, and then the heavy precipitation days are ranked from largest to smallest. In most extreme event research, an annual frequency series consists of approximately 1-2 events per year in the record. According to this idea, with a record in this study of up to 31 years (actual length of record varies by MSA), there should be no more than 62 events. The equality of mean and variance is one of the characteristics of a Poisson distribution. To determine whether the null hypothesis (that the mean and variance are equal) should be rejected, the R-value (variance/mean ratio) is computed for each site. The rejection region is determined using the chi-square table for a given n (number of years) and α, (0.10). If the rejection value exceeds the R-value, then the null hypothesis cannot be rejected (meaning that the mean and variance are not found to differ at a statistically

significant level). If the rejection value is less than the R-value, then the null hypothesis is rejected (meaning the mean and variance largely differ). Whenever the null hypothesis is rejected, the precipitation threshold (the precipitation value of the event with rank 62) is increased by 12.7 mm (0.5 in) to produce a dataset representing a Poisson distribution (Keim & Cruise 1998). The threshold increase of 0.5 inches is chosen to remove multiple events from the series until it becomes Poisson distributed as is done in Keim & Cruise (1998). The R-value is then recalculated and null hypothesis re-tested.

The second portion of the temporal analysis determines inter-arrival times between heavy precipitation days. The inter-arrival times between events are then clustered in groups of two to reduce the variance and allow for a more normal distribution so that a linear regression can be performed. The natural logarithm of the clustered inter-arrival times is used in the computation to normalize the data distribution (Chow 1954). If the inter-arrival times for a given MSA are decreasing over the period of record, heavy precipitation days are occurring more frequently, and the urban influence may be a cause.

3.2.3.3 Contour Test

The final test, the "contour" test, is a comparison between urban and non-urban precipitation stations similar to the comparison between urban stations and reference network (non-urban) stations done in Diem (2008). At each site, all precipitation stations between 80 and 100 km of the city center are considered "non-urban," while those within 80 km are considered "urban." While it is possible to consider stations in this region as "urban", precipitation at these stations are being used to predict rainfall closer to the central business district.

Period-of-record-mean precipitation on heavy-precipitation days is then calculated by station (both overall and by season), for each of the non-urban stations. These values are then

interpolated spatially using the inverse distance weighting (IDW) scheme as used in Diem (2008) and Bornstein & Lin (2000) to estimate "urban" precipitation (i.e., within a 40 km radius of the city center). For each urban precipitation station, actual period-of-record-mean precipitation is compared to its corresponding interpolated value through the calculation of anomalies. "Urban" locations at which observed precipitation exceeds the spatially interpolated value are likely candidates for urban enhancement. If such enhanced stations are concentrated toward the upwind or downwind side of the city center, circumstantial evidence for urban enhancement from one of the mechanisms described previously may exist. The analysis is then repeated at each site using an urban/non-urban threshold of 60 km, and 40 km, again both for all heavy-precipitation days and for heavy-precipitation days by season.

3.3 Results

3.3.1 Enhancement Detection

Based on the factors guiding the site selection (Section 3.2.1), six MSAs, out of 25, were found to be appropriate for further analysis and were selected for Study 1: Atlanta, Houston, Dallas/Fort Worth, Tulsa, Memphis, and Birmingham. These cities represent both large and smaller populations as well as the various precipitation regimes in the southeastern U.S. and include previously studied locations to provide some precedent for the results. Results of these tests are reported in Tables 3.3 to 3.14, where h=1 indicates that the null hypothesis (precipitation is equal between upwind and downwind regions) is rejected.

It is noteworthy that the significance values for the t-test are in some cases very different from those of the Mann Whitney u-test. Such results are indeed valid when it is considered that the two tests are examining different features of the data set. The t-test requires that the

investigator test the data for normality and ensure equality of variances in the upwind and downwind region. While precipitation data are not usually normal, the t-test is used in this research because it has been used in previous urban precipitation studies. By contrast, the u-test is very flexible and the data do not have to meet the same rigid standards as the t-test. However, the u-test examines a very different feature of the data set because it evaluates the rank of the data, not the data itself. Therefore, even though both tests are appropriate to apply, they would not necessarily be expected to give the same results because one is based on actual value (mean precipitation in upwind and downwind regions) and the other is based on rank of the data distribution.

- **Atlanta**

The t-test using the traditional upwind and downwind sections did not reveal any significant differences in precipitation on heavy precipitation days ($\geq$ 25 mm) between the upwind and downwind regions, either annually or in any of the four seasons (Table 3.3). The u-test revealed that the only significant difference in precipitation between the downwind and upwind sections was for more precipitation in the downwind region and for overall precipitation at the 60 km buffer.

The 90° test revealed similar results to the traditional one, except, not surprisingly, that larger means are measured (Table 3.4). Only the 40 km winter heavy-precipitation days differ significantly between downwind and upwind sites using the t-test, and only the 60 km winter and 40 km overall, fall, and winter events showed statistically significant differences using the u-test. Again, in all cases, the downwind direction experienced more precipitation. Interestingly, though not statistically significant, more precipitation was measured during the spring in the upwind regions.

As almost no seasonal differences in the upwind and downwind heavy-event precipitation were detected, precipitation-generating mechanisms due to the urbanized land cover are unlikely to cause differential effects upwind and downwind of Atlanta. More seasonally-independent factors may be the cause for the differences between upwind and downwind precipitation, such as local topography. Aerosol production may also be a factor, as it has been shown to influence precipitation in this region (Bell et al. 2008, Bell et al. 2009, Lacke et al. 2009).

- **Birmingham**

Results for this study site show that none of the traditional mean downwind *vs*. upwind differences for all comparisons (overall and seasonal) were found to be statistically significant using the t-test, while only the 60 km summer and 40 km overall, summer, fall, and winter comparisons using the u-test were significant (Table 3.5), again with more precipitation on heavy precipitation days occurring downwind than upwind. Results of the 90°comparison showed no significant differences using the t-test except for more precipitation downwind than upwind at the 60 km summer and 40 km overall and summer with the u-test. For this site, the least amount of heavy precipitation was measured during summer while spring, fall, and winter all had comparable rainfall totals.

- **Dallas/Fort Worth**

The "traditional" test shows statistically significant differences in heavy precipitation totals between the upwind and downwind regions (with more precipitation downwind than upwind) for many of the comparisons (Table 3.7). While a strong natural gradient in precipitation exists at this study site, this was accounted for through the use of varying the wind direction for each precipitation event studied. Significant comparisons include 100 km

Table 3.3. Results of the t-test and u-test for comparison of upwind and downwind mean precipitation for "traditional" upwind and downwind sections in Atlanta.

	Traditional t-test				Traditional u-test	
100 km	**Reject H_0?**	**p**	**up mean (mm)**	**down mean (mm)**	**Reject H_0?**	**p**
Overall	n	0.93	48.29	48.42	n	0.21
Spring	n	0.74	54.62	53.56	n	0.35
Summer	n	0.66	35.13	34.34	n	0.37
Fall	n	0.99	54.76	54.73	n	0.51
Winter	n	0.33	57.56	60.71	n	0.69
80 km	**Reject H_0?**	**p**	**up mean (mm)**	**down mean (mm)**	**Reject H_0?**	**p**
Overall	n	0.68	48.29	48.89	n	0.10
Spring	n	0.94	54.36	54.59	n	0.37
Summer	n	0.96	35.32	35.21	n	0.27
Fall	n	0.89	55.00	54.52	n	0.37
Winter	n	0.33	57.29	60.53	n	0.98
60 km	**Reject H_0?**	**p**	**up mean (mm)**	**down mean (mm)**	**Reject H_0?**	**p**
Overall	n	0.62	48.18	48.96	y	0.02
Spring	n	0.79	53.45	54.31	n	0.30
Summer	n	0.87	35.63	35.28	n	0.15
Fall	n	0.96	55.29	55.09	n	0.23
Winter	n	0.31	57.00	60.52	n	0.64
40 km	**Reject H_0?**	**p**	**up mean (mm)**	**down mean (mm)**	**Reject H_0?**	**p**
Overall	n	0.24	47.43	49.28	n	0.12
Spring	n	0.99	53.82	53.86	n	0.14
Summer	n	0.57	34.81	36.15	n	0.49
Fall	n	0.64	54.69	56.57	n	0.73
Winter	n	0.16	54.96	59.72	n	0.97

Table 3.4. Results of the t-test and u-test for comparison of upwind and downwind mean precipitation excluding quadrants 90° to the mean wind in Atlanta.

	90° t-test				90° u-test	
100 km	**Reject H_0?**	**P**	**up mean (mm)**	**down mean (mm)**	**Reject H_0?**	**p**
Overall	n	0.67	55.14	55.85	n	0.69
Spring	n	0.62	61.08	59.28	n	0.51
Summer	n	0.81	40.40	39.85	n	0.49
Fall	n	0.58	63.88	66.27	n	0.59
Winter	n	0.26	65.32	69.54	n	0.56
80 km	**Reject H_0?**	**p**	**up mean (mm)**	**down mean (mm)**	**Reject H_0?**	**p**
Overall	n	0.25	65.70	68.23	n	0.66
Spring	n	0.88	72.56	71.83	n	0.89
Summer	n	0.50	48.57	50.77	n	0.85
Fall	n	0.40	75.33	79.75	n	0.36
Winter	n	0.29	77.73	82.83	n	0.55
60 km	**Reject H_0?**	**p**	**up mean (mm)**	**down mean (mm)**	**Reject H_0?**	**p**
Overall	n	0.07	82.80	88.35	n	0.06
Spring	n	0.46	89.05	93.40	n	0.40
Summer	n	0.87	69.29	70.23	n	0.99
Fall	n	0.23	91.25	99.03	n	0.20
Winter	n	0.05	87.25	98.65	y	0.02
40 km	**Reject H_0?**	**p**	**up mean (mm)**	**down mean (mm)**	**Reject H_0?**	**p**
Overall	n	0.11	94.16	100.32	y	0.00
Spring	n	0.77	102.92	105.07	n	0.49
Summer	n	0.95	86.91	87.41	n	0.33
Fall	n	0.22	99.55	109.37	y	0.04
Winter	y	0.05	88.86	102.68	y	0.01

Table 3.5. Results of the t-test and u-test for comparison of upwind and downwind mean precipitation for "traditional" upwind and downwind sections in Birmingham.

	Traditional t-test				Traditional u-test	
100 km	**Reject H_0?**	**P**	**up mean (mm)**	**down mean (mm)**	**Reject H_0?**	**p**
Overall	n	0.76	48.35	48.75	n	0.67
Spring	n	0.89	56.21	56.64	n	0.71
Summer	n	0.88	32.61	32.41	n	0.54
Fall	n	0.85	53.21	53.79	n	0.52
Winter	n	0.69	61.67	62.92	n	0.38
80 km	**Reject H_0?**	**P**	**up mean (mm)**	**down mean (mm)**	**Reject H_0?**	**p**
Overall	n	0.78	48.48	48.86	n	0.23
Spring	n	0.82	56.49	57.26	n	0.66
Summer	n	0.87	32.42	32.66	n	0.44
Fall	n	0.89	53.81	53.35	n	0.85
Winter	n	0.76	61.75	62.78	n	0.19
60 km	**Reject H_0?**	**P**	**up mean (mm)**	**down mean (mm)**	**Reject H_0?**	**p**
Overall	n	0.93	48.62	48.48	n	0.07
Spring	n	0.78	57.78	56.82	n	0.83
Summer	n	0.45	31.65	32.91	y	0.00
Fall	n	0.89	54.13	53.64	n	0.82
Winter	n	0.72	61.96	60.70	n	0.62
40 km	**Reject H_0?**	**P**	**up mean (mm)**	**down mean (mm)**	**Reject H_0?**	**p**
Overall	n	0.36	47.75	49.20	y	0.00
Spring	n	0.91	57.88	57.47	n	0.11
Summer	n	0.39	31.81	33.58	y	0.00
Fall	n	0.45	52.87	55.78	y	0.01
Winter	n	0.68	58.59	60.16	y	0.00

Table 3.6. Results of the t-test and u-test for comparison of upwind and downwind mean precipitation excluding quadrants 90° to the mean wind in Birmingham.

	90° t-test				90° u-test	
100 km	**Reject H_0?**	**P**	**up mean (mm)**	**down mean (mm)**	**Reject H_0?**	**p**
Overall	n	0.44	54.95	56.17	n	0.47
Spring	n	0.47	63.38	66.07	n	0.86
Summer	n	0.69	37.13	37.83	n	0.50
Fall	n	0.79	60.57	61.54	n	0.20
Winter	n	0.86	69.50	70.16	n	0.70
80 km	**Reject H_0?**	**P**	**up mean (mm)**	**down mean (mm)**	**Reject H_0?**	**p**
Overall	n	0.46	61.63	62.97	n	0.29
Spring	n	0.56	70.85	73.33	n	0.47
Summer	n	0.33	41.43	43.52	n	0.25
Fall	n	0.94	68.48	68.82	n	0.61
Winter	n	0.99	75.96	75.89	n	0.51
60 km	**Reject H_0?**	**p**	**up mean (mm)**	**down mean (mm)**	**Reject H_0?**	**p**
Overall	n	0.53	75.27	76.81	n	0.24
Spring	n	0.53	81.48	84.69	n	0.98
Summer	n	0.24	52.88	57.42	y	0.00
Fall	n	0.98	81.89	81.74	n	0.69
Winter	n	0.67	87.34	85.26	n	0.91
40 km	**Reject H_0?**	**p**	**up mean (mm)**	**down mean (mm)**	**Reject H_0?**	**p**
Overall	n	0.66	86.69	88.11	y	0.02
Spring	n	0.93	94.88	94.36	n	0.99
Summer	n	0.43	68.58	73.64	y	0.00
Fall	n	0.76	88.84	90.79	n	0.68
Winter	y	0.97	91.88	91.67	n	0.12

overall and winter, 80 km winter, and 60 km winter. The u-test revealed significantly different magnitudes of downwind *vs*. upwind heavy-precipitation totals for all comparisons except 100 km spring and summer, 80 km spring and summer, 60 km summer, and 40 km spring and summer. It should be noted that the large difference in means for small buffers does not always appear as statistically significant likely due to the small number of stations included in such buffers.

The 90° section t-test showed statistically-significant differences between upwind and downwind heavy precipitation for 40 km summer in addition to the same comparisons as seen in the traditional sections (Table 3.8). All u-test comparisons were found to be significant except 100 km, 80 km and 60 km summer and 40 km overall, spring, summer and fall. Mean downwind precipitation is greater for all seasons except the summer in the traditional and 90° upwind and downwind comparisons.

The fact that the downwind precipitation is statistically greater than the upwind rainfall only for the larger buffers may imply that inner city precipitation is very similar between upwind and downwind regions and that urbanization may be causing an increasingly prominent footprint at successively larger scales, at least up to 100 km, in this very large metroplex. To determine how far this urban influence can extend, it would be beneficial for future studies to compare precipitation for stations outside the 100 km buffer for this MSA. Also, there is little evidence from the tests in this study showing that summer precipitation is influenced by urbanization, contrary to some previous studies (Shepherd et al. 2002), unless an influence on the type of precipitation occurring during these months could not be detected with methods used in this research.

Table 3.7. Results of the t-test and u-test for comparison of upwind and downwind mean precipitation for "traditional" upwind and downwind sections in Dallas/Fort Worth.

	Traditional t-test				Traditional u-test	
100 km	**Reject H_0?**	**p**	**up mean (mm)**	**down mean (mm)**	**Reject H_0?**	**p**
Overall	y	0.02	40.54	43.98	y	0.00
Spring	n	0.20	43.61	47.15	n	0.05
Summer	n	0.49	34.13	32.56	n	0.89
Fall	n	0.16	42.40	46.54	y	0.01
Winter	y	0.00	43.35	53.92	y	0.00
80 km	**Reject H_0?**	**p**	**up mean (mm)**	**down mean (mm)**	**Reject H_0?**	**p**
Overall	n	0.10	41.43	43.85	y	0.00
Spring	n	0.41	44.73	47.06	n	0.06
Summer	n	0.37	34.95	32.74	n	0.65
Fall	n	0.34	43.15	46.06	y	0.03
Winter	y	0.01	44.19	53.75	y	0.00
60 km	**Reject H_0?**	**p**	**up mean (mm)**	**down mean (mm)**	**Reject H_0?**	**p**
Overall	n	0.08	40.84	43.48	y	0.00
Spring	n	0.36	44.01	46.72	y	0.00
Summer	n	0.41	35.07	32.90	n	0.93
Fall	n	0.21	41.70	45.60	y	0.00
Winter	y	0.02	43.92	52.58	y	0.00
40 km	**Reject H_0?**	**P**	**up mean (mm)**	**down mean (mm)**	**Reject H_0?**	**p**
Overall	n	0.57	43.98	43.00	y	0.02
Spring	n	0.37	48.40	45.41	n	0.26
Summer	n	0.17	37.06	32.80	n	0.34
Fall	n	0.75	44.32	45.39	y	0.03
Winter	n	0.25	47.70	52.40	y	0.02

Table 3.8. Results of the t-test and u-test for comparison of upwind and downwind mean precipitation excluding quadrants 90° to the mean wind in Dallas/Fort Worth.

	90° t-test				90° u-test	
100 km	**Reject H_0?**	**p**	**up mean (mm)**	**down mean (mm)**	**Reject H_0?**	**p**
Overall	y	0.00	45.54	51.14	y	0.00
Spring	n	0.08	49.08	55.06	y	0.01
Summer	n	0.69	39.88	38.73	n	0.75
Fall	n	0.05	46.42	53.07	y	0.00
Winter	y	0.00	47.62	62.25	y	0.00
80 km	**Reject H_0?**	**p**	**up mean (mm)**	**down mean (mm)**	**Reject H_0?**	**p**
Overall	n	0.07	52.03	55.65	y	0.00
Spring	n	0.31	56.67	60.71	y	0.03
Summer	n	0.31	45.29	41.86	n	0.58
Fall	n	0.29	53.39	57.58	y	0.02
Winter	y	0.00	53.39	67.23	y	0.00
60 km	**Reject H_0?**	**p**	**up mean (mm)**	**down mean (mm)**	**Reject H_0?**	**p**
Overall	n	0.14	63.55	67.33	y	0.00
Spring	n	0.45	67.53	71.23	y	0.02
Summer	n	0.26	59.02	53.65	n	0.64
Fall	n	0.44	65.41	69.36	y	0.02
Winter	y	0.00	61.07	79.25	y	0.00
40 km	**Reject H_0?**	**p**	**up mean (mm)**	**down mean (mm)**	**Reject H_0?**	**p**
Overall	n	0.23	88.60	84.01	n	0.29
Spring	n	0.17	93.12	83.52	n	0.94
Summer	y	0.01	88.97	69.85	n	0.05
Fall	n	0.81	87.49	89.23	n	0.16
Winter	n	0.07	82.03	97.39	y	0.00

- **Houston**

Results from Houston were also very interesting, as the t-test for the traditional analysis showed significantly more precipitation on heavy precipitation days received in the downwind than upwind regions for the following comparisons: 100 km, 80 km and 60 km winter (Table 3.9). Results for the u-test showed significant differences between upwind and downwind regions for the 100 km overall and winter, 80 km overall, spring, and winter, 60 km overall and winter, and 40 km overall and winter. Similar to the strong natural gradient in precipitation seen at Dallas/Fort Worth, the gradient in precipitation at Houston was likely a result of a varying wind direction for each precipitation event studied.

The t-tests at 90° showed significance for the same comparisons as the traditional t-test (Table 3.10). The u-test showed only the 100 km fall comparison to be significant.

It is possible that urbanization may be causing an influence in precipitation between the upwind and downwind regions, as was confirmed for Houston by previous studies (Orville et al. 2001, Shepherd et al. 2002, Burian & Shepherd 2005, Shepherd et al. 2010). This may be due to the large number of aerosols (Carrio et al. 2010, Carrio & Cotton 2011) or the presence of an urban heat island (Zhou et al. 2011). Similar to Dallas/Fort Worth, it is possible that an influence can be detected at stations beyond the 100 km buffer. Future research should include a larger zone of analysis in this rapidly-growing city.

- **Memphis**

The t-test for the traditional comparisons showed statistically significant downwind *vs*. upwind differences for 100 km overall and summer, 80 km overall, 60 km overall, spring, and winter, and for overall and all-season precipitation on heavy precipitation days at 40 km (Table 3.11). Results from the u-tests showed all downwind *vs*. upwind comparisons as significant.

Results from the 90° tests show overall precipitation at 100 km, 80 km, 60 km, and 40 km to be significant in addition to 40 km spring and winter (Table 3.12). The u-test results showed significance for all comparisons except the 60 km summer and 40 km summer.

Collectively, these results provide strong evidence that an urban influence on precipitation in Memphis may exist.

- **Tulsa**

On heavy precipitation days, the only "traditional" test comparison found to be statistically significant using the t-test is 100 km overall precipitation (Table 3.13). The u-test found only overall precipitation at 100 km and 80 km to be significant. All of these differences showed more precipitation downwind than upwind.

Results from the 90° t-test showed significant differences between upwind and downwind heavy precipitation days for 100 km overall and 40 km overall and spring, again, with more precipitation downwind than upwind (Table 3.14). The u-test showed significant differences for these same comparisons in addition to 100 km summer.

3.3.2 Temporal Analysis

The temporal analysis is performed on the annual frequency series (the largest 62 heavy precipitation days in the 30-year record) to test for trends in extreme events. Because the annual frequency series is derived by ranking the events from largest to smallest, these days are the largest of all heavy precipitation days and can be considered extreme precipitation days. Table 3.15 shows the results of the Poisson tests.

- **Atlanta**

Plotting the annual frequency series over time shows no apparent trends (Figure 3.3) using a threshold of 293.20 mm/year. Some years have high numbers of extreme precipitation

Table 3.9. Results of the t-test and u-test for comparison of upwind and downwind mean precipitation for "traditional" upwind and downwind sections in Houston.

	Traditional t-test				Traditional u-test	
100 km	**Reject H_0?**	**p**	**up mean (mm)**	**down mean (mm)**	**Reject H_0?**	**p**
Overall	n	0.37	42.30	43.54	y	0.02
Spring	n	0.33	41.61	44.22	n	0.11
Summer	n	0.88	36.10	35.76	n	0.65
Fall	n	0.58	53.32	51.30	n	0.67
Winter	y	0.02	39.37	44.92	y	0.00
80 km	**Reject H_0?**	**p**	**up mean (mm)**	**down mean (mm)**	**Reject H_0?**	**p**
Overall	n	0.18	43.33	45.39	y	0.00
Spring	n	0.29	43.15	46.31	y	0.04
Summer	n	0.92	37.04	37.28	n	0.42
Fall	n	1.00	53.90	53.92	n	0.57
Winter	y	0.04	40.49	46.10	y	0.00
60 km	**Reject H_0?**	**p**	**up mean (mm)**	**down mean (mm)**	**Reject H_0?**	**p**
Overall	n	0.17	43.44	45.62	y	0.00
Spring	n	0.38	43.72	46.51	n	0.06
Summer	n	0.40	37.13	39.34	n	0.13
Fall	n	0.90	53.30	52.80	n	0.46
Winter	n	0.11	40.92	45.37	y	0.00
40 km	**Reject H_0?**	**p**	**up mean (mm)**	**down mean (mm)**	**Reject H_0?**	**p**
Overall	n	0.12	44.33	47.04	y	0.00
Spring	n	0.93	46.08	45.80	n	0.31
Summer	n	0.25	38.65	42.00	n	0.16
Fall	n	0.79	52.30	53.47	n	0.24
Winter	y	0.03	41.44	48.17	y	0.00

Table 3.10. Results of the t-test and u-test for comparison of upwind and downwind mean precipitation excluding quadrants 90° to the mean wind in Houston.

	90° t-test				90° u-test	
100 km	**Reject H_0?**	**p**	**up mean (mm)**	**down mean (mm)**	**Reject H_0?**	**p**
Overall	n	0.34	52.82	54.68	n	1.00
Spring	n	0.54	54.40	56.72	n	0.69
Summer	n	0.92	43.00	43.30	n	0.11
Fall	n	0.71	64.47	62.62	y	0.04
Winter	y	0.02	51.68	60.28	n	0.12
80 km	**Reject H_0?**	**p**	**up mean (mm)**	**down mean (mm)**	**Reject H_0?**	**p**
Overall	n	0.22	60.65	63.54	n	0.45
Spring	n	0.61	62.70	65.06	n	0.97
Summer	n	0.97	51.01	50.87	n	0.34
Fall	n	0.72	72.30	74.46	n	0.56
Winter	y	0.04	58.34	67.33	n	0.10
60 km	**Reject H_0?**	**p**	**up mean (mm)**	**down mean (mm)**	**Reject H_0?**	**p**
Overall	n	0.33	70.06	73.04	n	0.65
Spring	n	0.60	71.73	74.90	n	0.44
Summer	n	0.77	59.74	61.21	n	0.54
Fall	n	0.75	83.16	85.53	n	0.34
Winter	n	0.27	67.14	73.02	n	0.71
40 km	**Reject H_0?**	**p**	**up mean (mm)**	**down mean (mm)**	**Reject H_0?**	**p**
Overall	n	0.15	81.82	87.87	n	0.73
Spring	n	0.62	88.87	84.94	n	0.13
Summer	n	0.34	69.12	76.84	n	0.46
Fall	n	0.63	95.42	100.11	n	0.77
Winter	y	0.03	75.57	90.93	n	0.06

Table 3.11. Results of the t-test and u-test for comparison of upwind and downwind mean precipitation for "traditional" upwind and downwind sections in Memphis.

	Traditional t-test				Traditional u-test	
100 km	**Reject H_0?**	**p**	**up mean (mm)**	**down mean (mm)**	**Reject H_0?**	**p**
Overall	y	0.00	35.36	38.63	y	0.00
Spring	n	0.21	36.03	38.68	y	0.00
Summer	y	0.05	31.56	35.23	y	0.00
Fall	n	0.25	38.94	42.11	y	0.00
Winter	n	0.10	35.05	38.76	y	0.00
80 km	**Reject H_0?**	**p**	**up mean (mm)**	**down mean (mm)**	**Reject H_0?**	**p**
Overall	y	0.00	36.37	40.30	y	0.00
Spring	n	0.06	37.05	41.15	y	0.00
Summer	n	0.05	32.44	36.31	y	0.00
Fall	n	0.26	40.17	43.40	y	0.00
Winter	n	0.06	36.00	40.34	y	0.00
60 km	**Reject H_0?**	**p**	**up mean (mm)**	**down mean (mm)**	**Reject H_0?**	**p**
Overall	y	0.00	37.12	41.60	y	0.00
Spring	y	0.03	37.83	42.80	y	0.00
Summer	n	0.16	33.64	36.62	y	0.00
Fall	n	0.28	40.75	43.89	y	0.00
Winter	y	0.01	36.46	42.76	y	0.00
40 km	**Reject H_0?**	**p**	**up mean (mm)**	**down mean (mm)**	**Reject H_0?**	**p**
Overall	y	0.00	36.06	48.02	y	0.00
Spring	y	0.00	36.31	50.27	y	0.00
Summer	y	0.00	32.90	40.53	y	0.00
Fall	y	0.01	40.66	49.20	y	0.00
Winter	y	0.00	34.99	51.00	y	0.00

Table 3.12. Results of the t-test and u-test for comparison of upwind and downwind mean precipitation excluding quadrants 90° to the mean wind in Memphis.

	90° t-test				90° u-test	
100 km	**Reject H_0?**	**p**	**up mean (mm)**	**down mean (mm)**	**Reject H_0?**	**p**
Overall	y	0.01	45.83	49.68	y	0.00
Spring	n	0.36	49.99	52.83	y	0.00
Summer	n	0.09	37.74	41.86	y	0.00
Fall	n	0.20	49.62	54.45	y	0.00
Winter	n	0.23	46.15	50.02	y	0.00
80 km	**Reject H_0?**	**p**	**up mean (mm)**	**down mean (mm)**	**Reject H_0?**	**p**
Overall	y	0.04	56.15	60.52	y	0.00
Spring	n	0.19	58.37	63.65	y	0.00
Summer	n	0.49	52.18	54.79	y	0.01
Fall	n	0.26	61.29	66.95	y	0.01
Winter	n	0.35	52.91	56.76	y	0.00
60 km	**Reject H_0?**	**p**	**up mean (mm)**	**down mean (mm)**	**Reject H_0?**	**p**
Overall	y	0.03	61.32	66.85	y	0.00
Spring	n	0.23	63.03	68.61	y	0.00
Summer	n	0.74	59.13	60.66	n	0.06
Fall	n	0.36	66.51	71.93	y	0.04
Winter	n	0.07	56.93	65.70	y	0.00
40 km	**Reject H_0?**	**p**	**up mean (mm)**	**down mean (mm)**	**Reject H_0?**	**p**
Overall	y	0.00	56.25	74.04	y	0.00
Spring	y	0.00	51.44	71.59	y	0.00
Summer	n	0.25	68.85	76.56	n	0.07
Fall	n	0.07	68.38	84.85	y	0.00
Winter	y	0.00	44.89	67.75	y	0.00

Table 3.13. Results of the t-test and u-test for comparison of upwind and downwind mean precipitation for "traditional" upwind and downwind sections in Tulsa.

	Traditional t-test				Traditional u-test	
100 km	**Reject H_0?**	**P**	**up mean (mm)**	**down mean (mm)**	**Reject H_0?**	**p**
Overall	y	0.04	53.57	57.35	y	0.01
Spring	n	0.68	57.53	58.83	n	0.32
Summer	n	0.18	43.09	46.58	n	0.08
Fall	n	0.12	61.48	68.42	n	0.06
Winter	n	0.38	56.76	61.00	n	0.25
80 km	**Reject H_0?**	**P**	**up mean (mm)**	**down mean (mm)**	**Reject H_0?**	**p**
Overall	n	0.16	54.66	57.25	y	0.02
Spring	n	0.83	57.94	58.64	n	0.52
Summer	n	0.52	44.55	46.33	n	0.11
Fall	n	0.24	62.93	68.25	n	0.16
Winter	n	0.43	57.84	61.70	n	0.29
60 km	**Reject H_0?**	**p**	**up mean (mm)**	**down mean (mm)**	**Reject H_0?**	**p**
Overall	n	0.38	55.18	57.00	n	0.96
Spring	n	0.91	59.10	58.71	n	0.49
Summer	n	0.48	44.65	46.98	n	0.75
Fall	n	0.42	63.29	67.23	n	0.72
Winter	n	0.77	58.04	59.59	n	0.96
40 km	**Reject H_0?**	**p**	**up mean (mm)**	**down mean (mm)**	**Reject H_0?**	**p**
Overall	n	0.23	51.92	55.15	n	0.12
Spring	n	0.26	55.77	61.33	n	0.59
Summer	n	0.61	41.32	43.49	n	0.06
Fall	n	0.47	60.53	64.74	n	0.77
Winter	n	0.81	54.31	52.50	n	0.30

Table 3.14. Results of the t-test and u-test for comparison of upwind and downwind mean precipitation excluding quadrants 90° to the mean wind in Tulsa.

	90° t-test				90° u-test	
100 km	**Reject H_0?**	**p**	**up mean (mm)**	**down mean (mm)**	**Reject H_0?**	**p**
Overall	y	0.01	61.67	67.33	y	0.00
Spring	n	0.35	64.37	67.93	n	0.14
Summer	n	0.05	50.54	57.12	y	0.03
Fall	n	0.19	70.76	77.83	n	0.21
Winter	n	0.34	66.26	71.75	n	0.41
80 km	**Reject H_0?**	**p**	**up mean (mm)**	**down mean (mm)**	**Reject H_0?**	**p**
Overall	n	0.14	70.45	74.23	n	0.06
Spring	n	0.59	71.51	73.76	n	0.31
Summer	n	0.17	59.38	65.10	n	0.06
Fall	n	0.49	80.64	84.92	n	0.41
Winter	n	0.81	74.89	76.44	n	0.90
60 km	**Reject H_0?**	**p**	**up mean (mm)**	**down mean (mm)**	**Reject H_0?**	**p**
Overall	n	0.49	96.65	99.29	n	0.64
Spring	n	0.94	97.03	96.52	n	0.66
Summer	n	0.21	85.04	93.75	n	0.26
Fall	n	0.63	108.89	113.11	n	0.45
Winter	n	0.40	97.56	90.73	n	0.33
40 km	**Reject H_0?**	**p**	**up mean (mm)**	**down mean (mm)**	**Reject H_0?**	**p**
Overall	y	0.00	97.58	123.51	y	0.00
Spring	y	0.01	98.92	138.05	y	0.02
Summer	n	0.23	85.31	100.65	n	0.22
Fall	n	0.08	100.70	130.70	n	0.08
Winter	n	1.00	117.26	117.29	n	0.96

Table 3.15. Results of Poisson test for each city.

	n	mean	variance	R-value	Reject region	alpha	Reject?
Atlanta	31	2.03	2.83	0.72	0.66	0.1	yes
	31	1.92	1.91	1.00	1.30	0.1	no
Birmingham	31	2.03	2.50	0.81	0.66	0.1	yes
	31	1.96	1.43	1.37	1.30	0.1	yes
	31	1.54	1.56	0.99	0.66	0.1	yes
	31	1.38	1.29	1.07	1.30	0.1	no
Dallas/Fort Worth	31	2.03	6.63	0.31	0.66	0.1	no
Houston	31	2.03	4.17	0.49	0.66	0.1	no
Memphis	31	2.03	2.77	0.73	0.66	0.1	yes
	31	1.96	2.04	0.96	0.66	0.1	yes
	31	1.56	1.76	0.89	0.66	0.1	yes
	31	1.28	1.29	0.99	0.66	0.1	yes
	31	0.96	0.62	1.54	1.30	0.1	yes
	31	0.72	0.63	1.15	1.30	0.1	no
Tulsa	31	2.03	2.77	0.73	0.66	0.1	yes
	31	2.08	0.91	2.29	1.30	0.1	yes
	31	1.68	1.14	1.47	1.30	0.1	yes
	31	1.32	0.89	1.48	1.30	0.1	yes
	31	1.12	1.03	1.09	1.30	0.1	no

events (e.g., 1995), but most years have only 1 or 2 events. Extreme precipitation in this region occurs frequently and is not exhibiting any trends. The natural logarithmic transformation of inter-arrival times of heavy precipitation days does not show significant linear trends (p-value = 0.84).

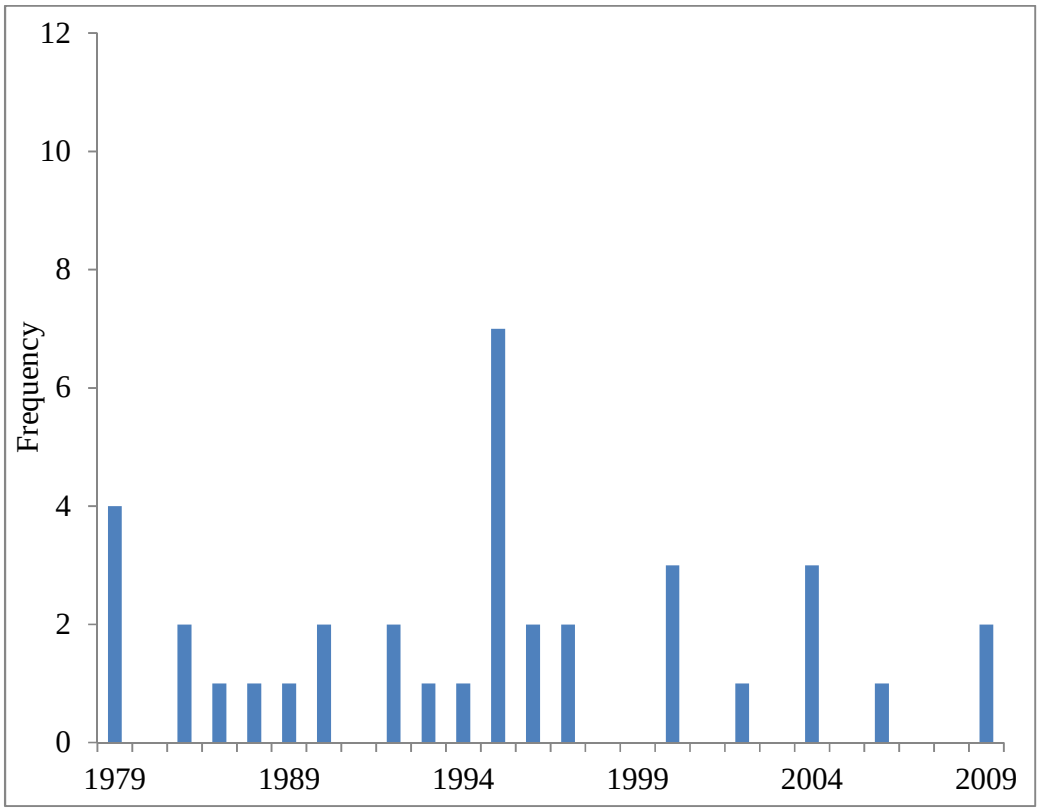

Figure 3.3. Annual frequency series of heavy precipitation days for Atlanta.

- **Birmingham**

The annual frequency series for Birmingham exhibits no trends (Figure 3.4) with a threshold of 328.10 mm/year. Heavy precipitation days occur consistently throughout the record. The inter-arrival time between paired events exhibits a slight, but not significant (p-value = 0.41), upward trend (Figure 3.5).

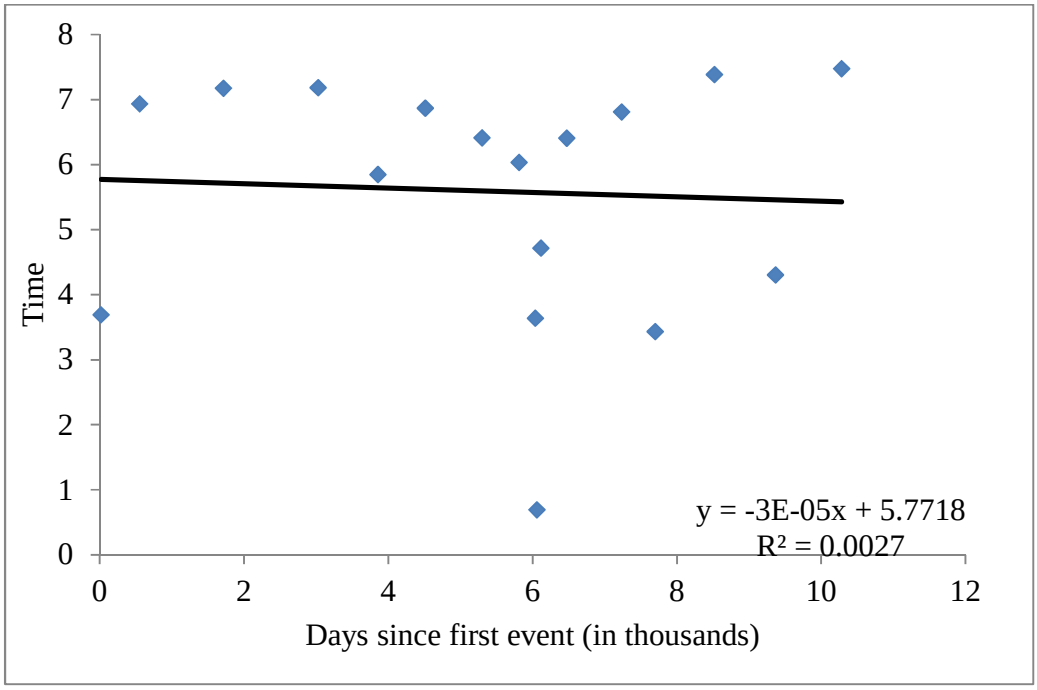

Figure 3.4. Inter-arrival time between paired events from the annual frequency series for Atlanta.

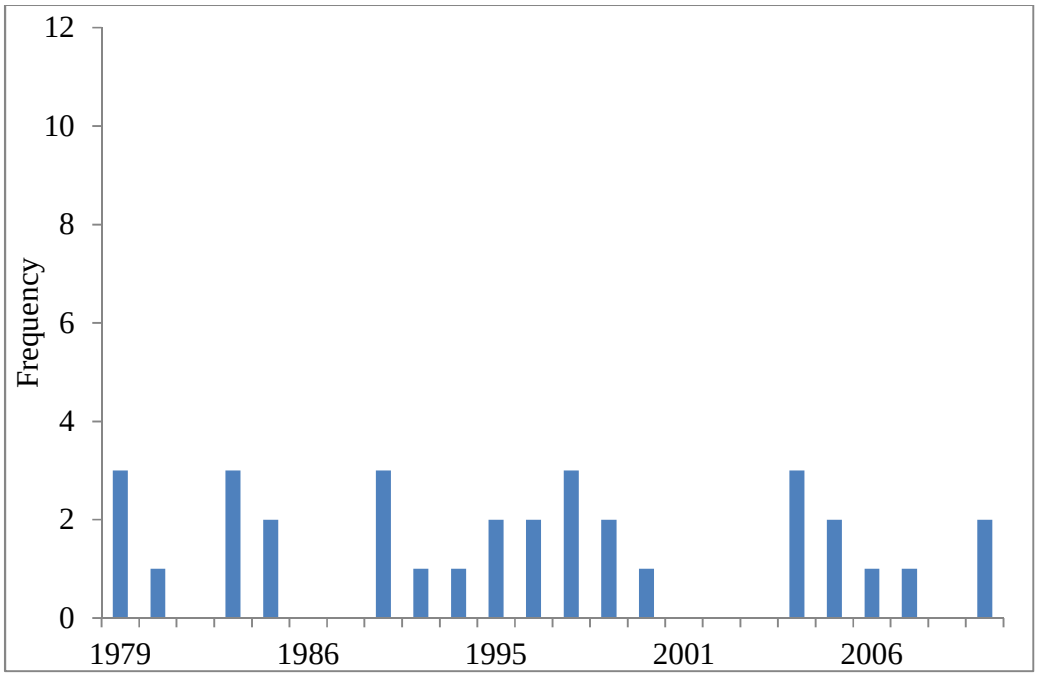

Figure 3.5. Annual frequency series of heavy precipitation days for Birmingham.

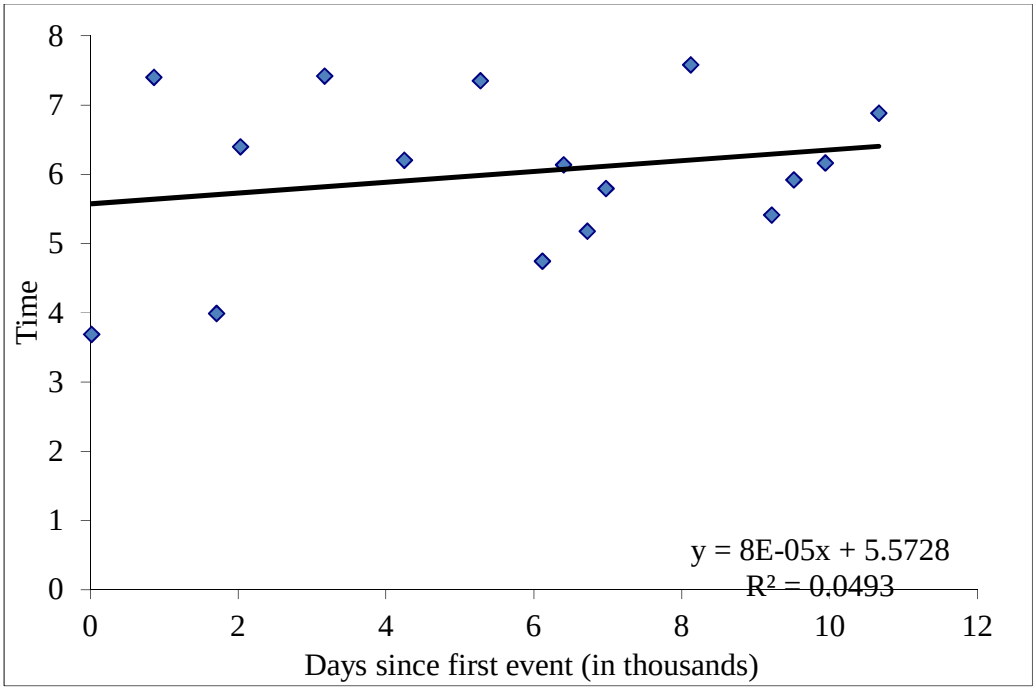

Figure 3.6. Inter-arrival time between paired events from the annual frequency series for Birmingham.

- **Dallas/Fort Worth**

The annual frequency series of the Dallas/Fort Worth MSA shows a strong trend in the most extreme of precipitation days, with the highest number of events occurring in the last five years of the record (Figure 3.6). The threshold used was 320.00 mm/year. A strong downward trend is seen in the inter-arrival time between the most extreme events (p-value = 0.00).

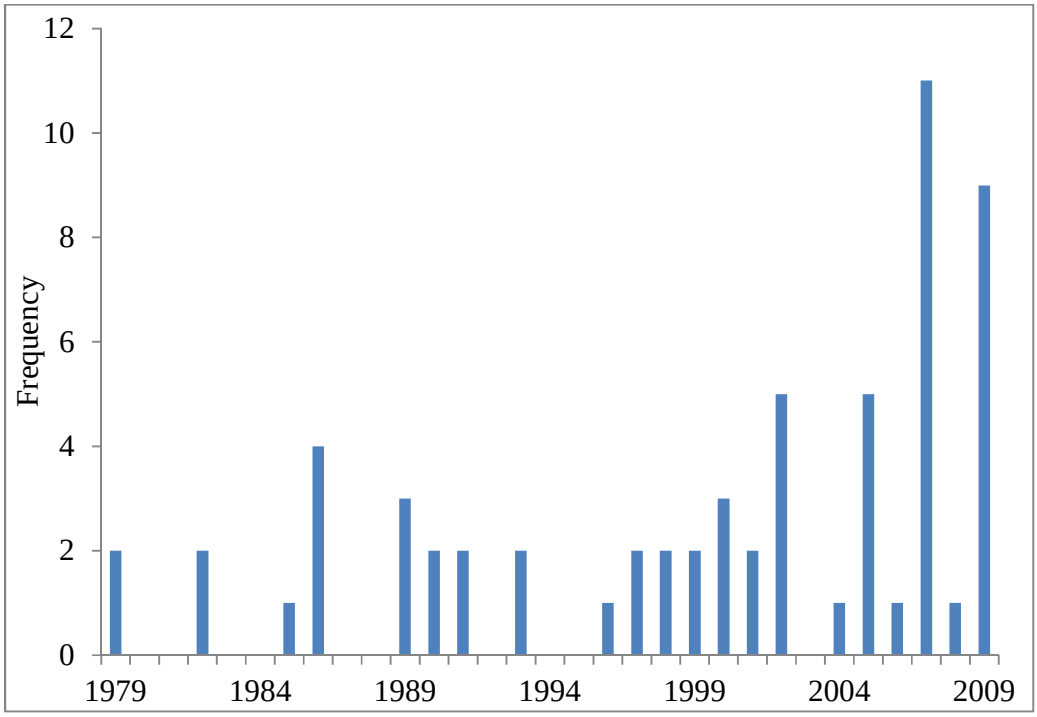

Figure 3.7. Annual frequency series of heavy precipitation days for Dallas/Fort Worth.

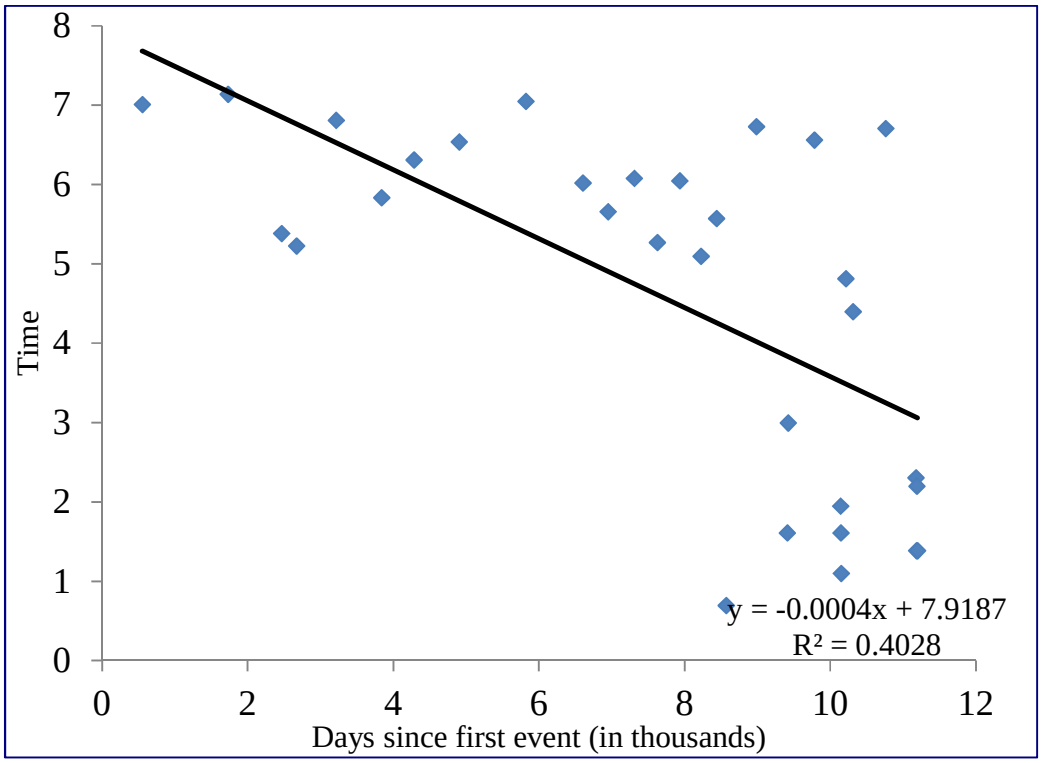

Figure 3.8. Inter-arrival time between paired events from the annual frequency series for Dallas/Fort Worth.

- **Houston**

The annual frequency series shows no trends in extreme events (Figure 3.8) using a threshold of 360.00 mm/year. Similar to Atlanta, extreme precipitation events occur fairly frequently. A non-significant downward slope is seen in inter-arrival times (p-value = 0.59) (Figure 3.9).

- **Memphis**

A plot of the annual frequency series for Memphis shows no trends (Figure 3.10) using a threshold of 351.50 mm/year. There is an even distribution of heavy events with no discernible patterns except the relatively large number of events occurring in 1982 and 2002. There is also no temporal trend in inter-arrival times between paired extreme events (p-value = 0.84) (Figure 3.11).

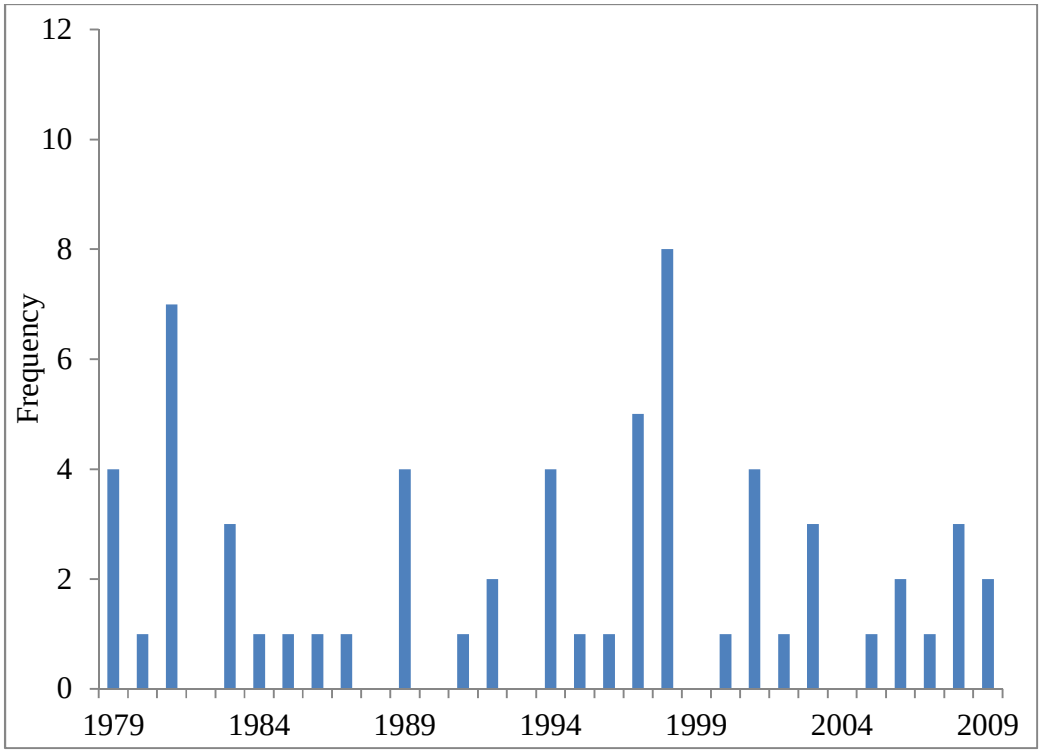

Figure 3.9. Annual frequency series of heavy precipitation days for Houston.

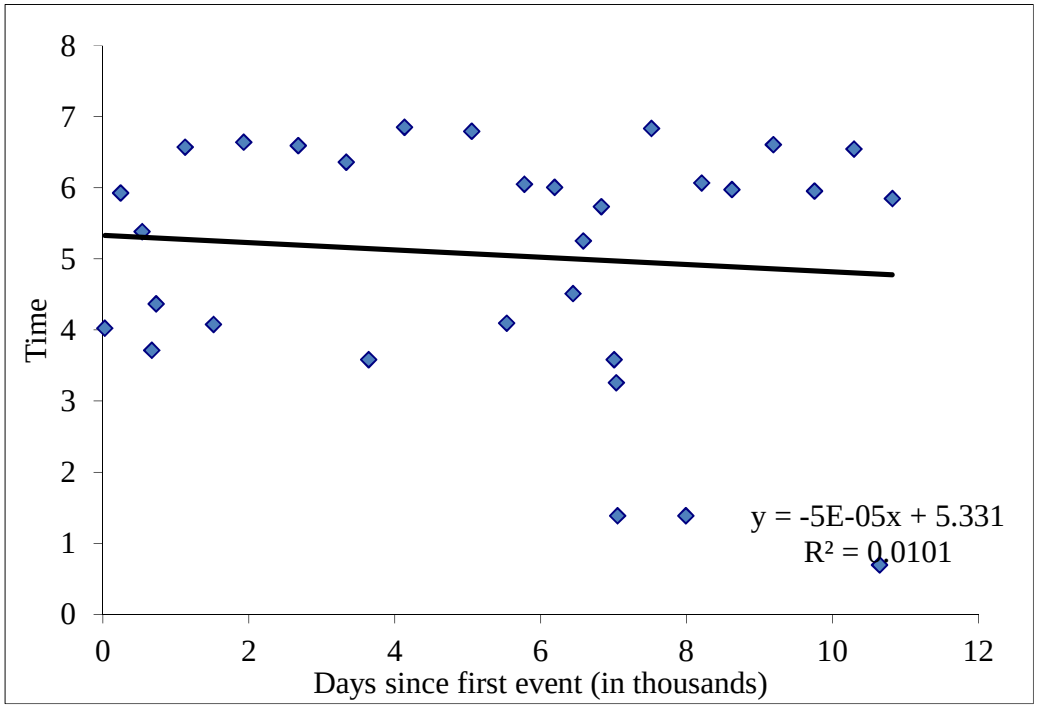

Figure 3.10. Inter-arrival time between paired events from the annual frequency series for Houston.

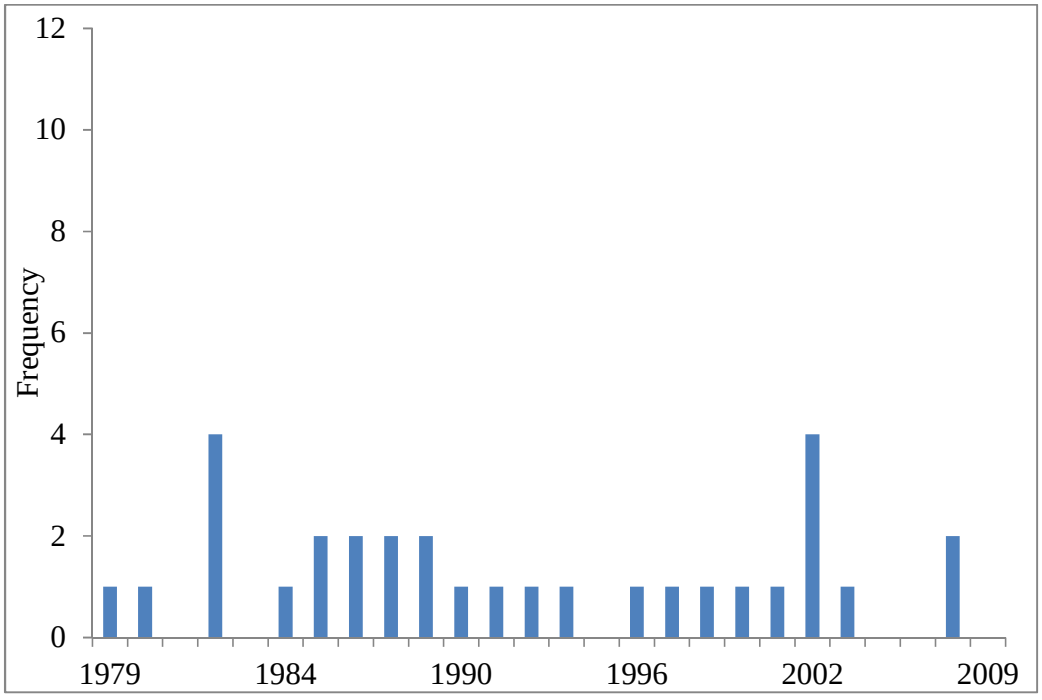

Figure 3.11. Annual frequency series of heavy precipitation days for Memphis.

- **Tulsa**

The annual frequency series shows an evenly-spaced number of extreme events throughout the entire record (Figure 3.12) with occasional, short dry periods (1980 – 1982 and 2000 – 2001) with a threshold of 326.84 mm/year. There is no discernible trend of the inter-arrival times in Tulsa (p-value = 0.70) (Figure 3.13).

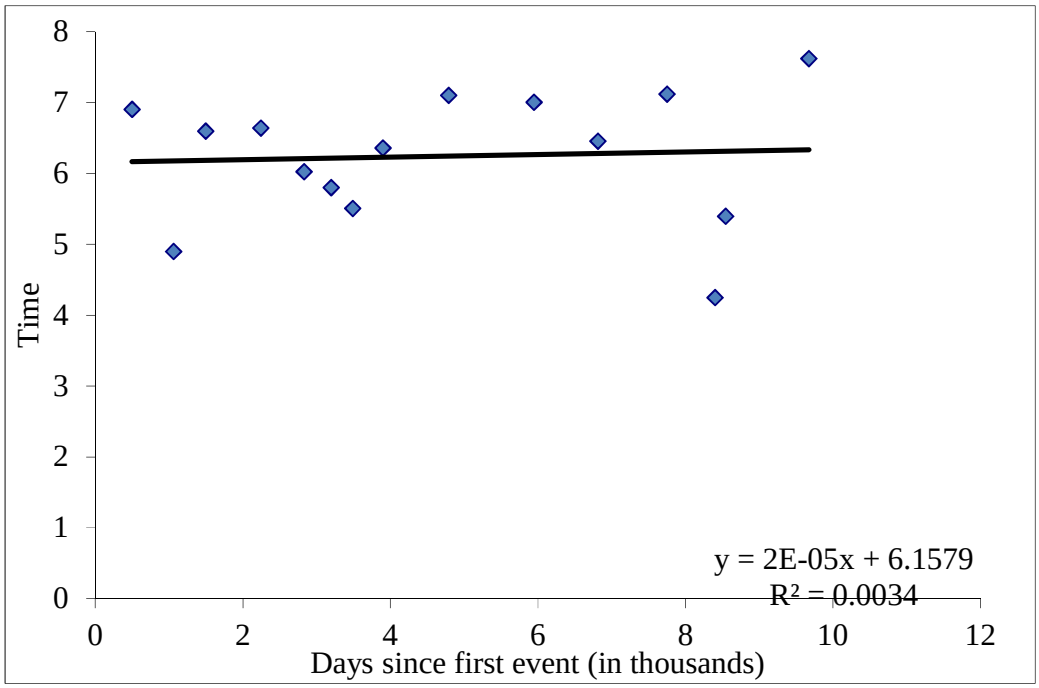

Figure 3.12. Inter-arrival time between paired events from the annual frequency series for Memphis.

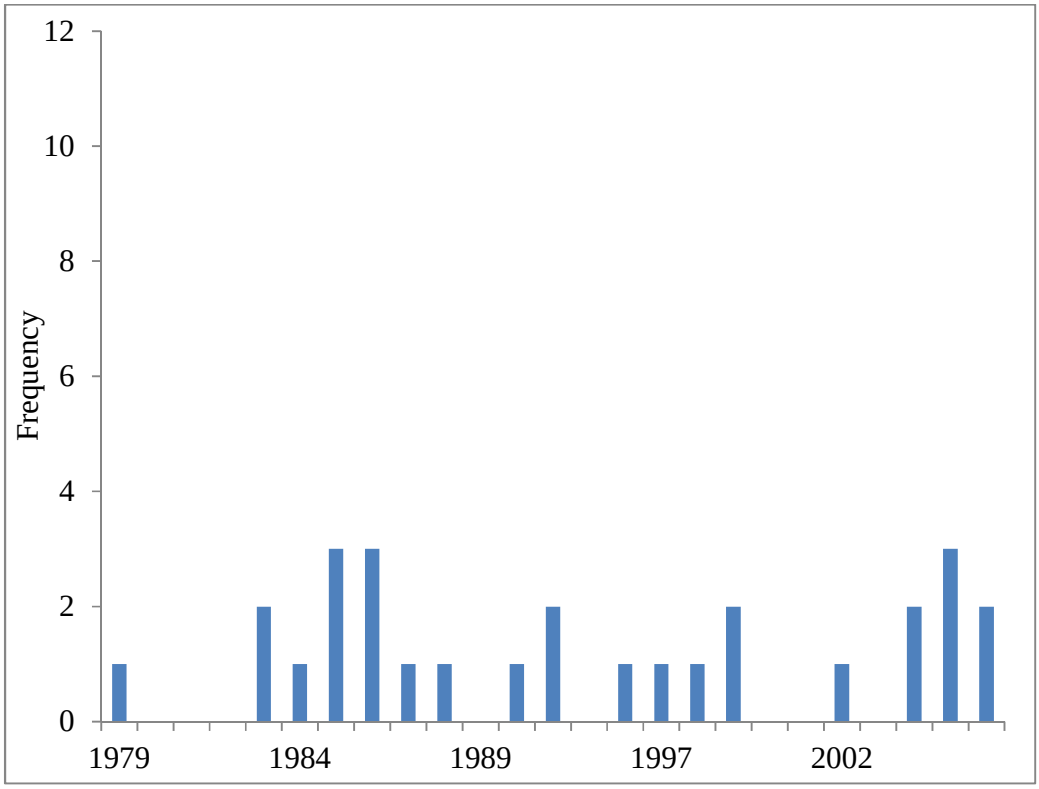

Figure 3.13. Annual frequency series of heavy precipitation days for Tulsa.

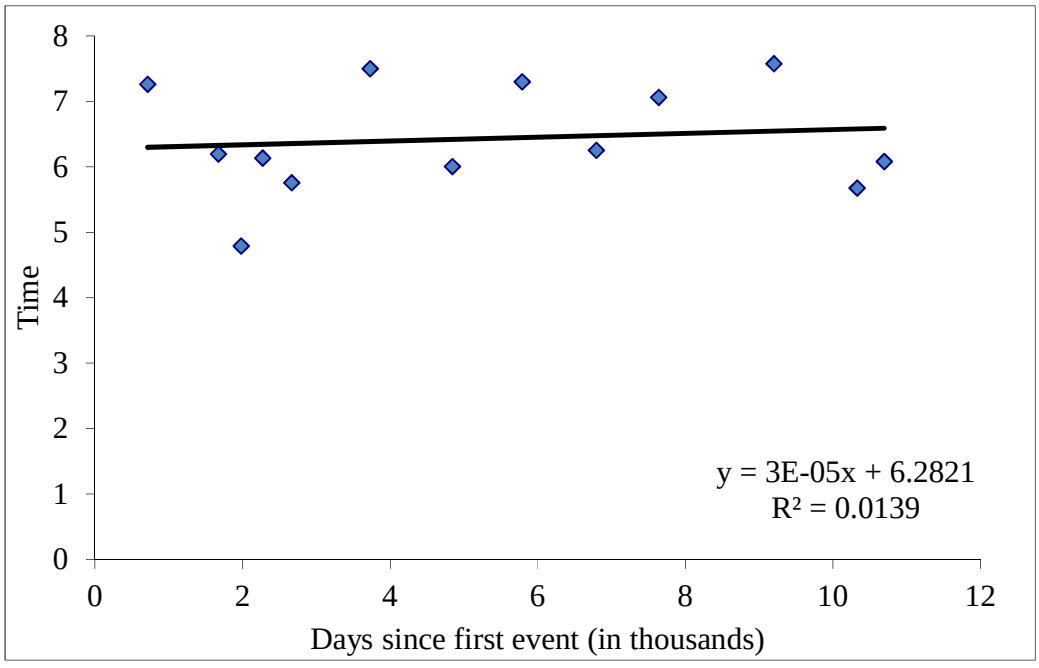

Figure 3.14. Inter-arrival time between paired events from the annual frequency series for Tulsa.

3.3.3 Contour Test

- **Atlanta**

Results of the contour test for Atlanta are shown in Figures 3.14 through 3.16. The interpolation using only the non-urban stations did a relatively accurate job of "predicting" the urban precipitation at all runs (seen inside the inner buffer). The colors and contour lines

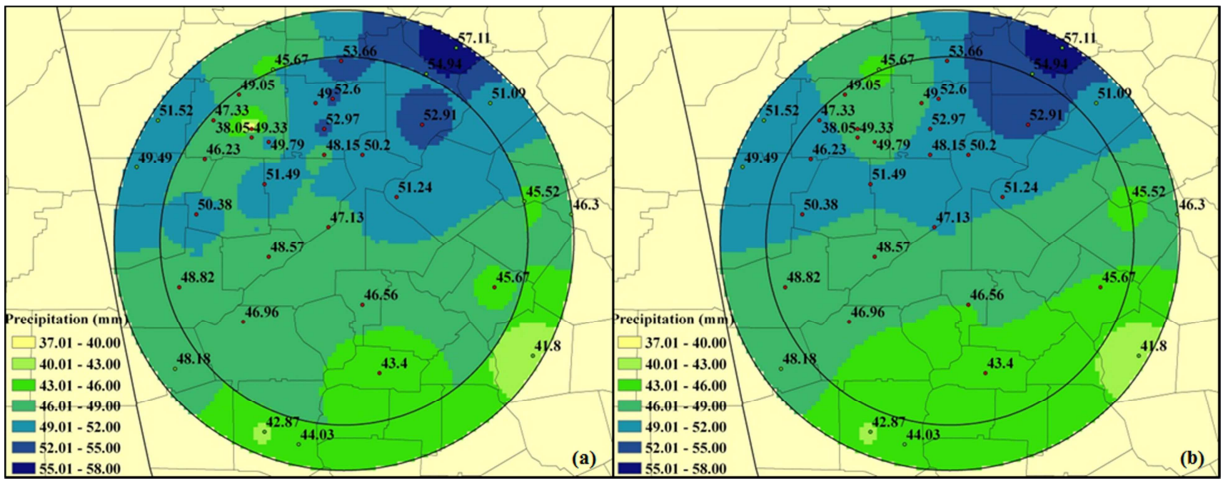

Figure 3.15. Results of the contour test for Atlanta at the 80 km buffer. Stations are represented by the dots with their overall mean precipitation (mm) from heavy precipitation events. The inner circle for Figure A shows precipitation based only on urban station data. Figure B shows urban station precipitation interpolated using non-urban stations.

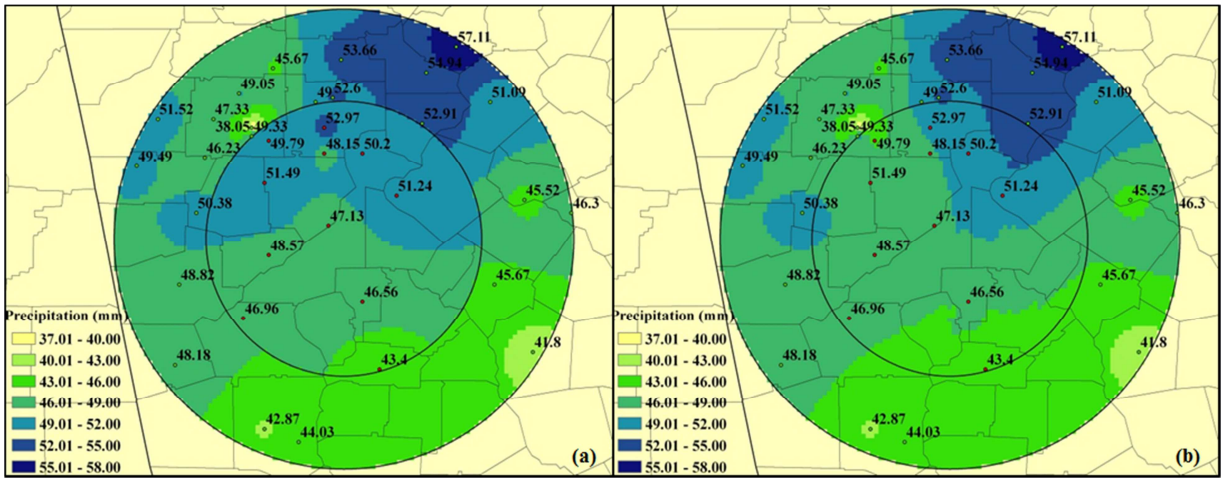

Figure 3.16. Results of the contour test for Atlanta at the 60 km buffer. Stations are represented by the dots with their overall mean precipitation (mm) from heavy precipitation events. The inner circle for Figure A shows precipitation based only on urban station data. Figure B shows urban station precipitation interpolated using non-urban stations.

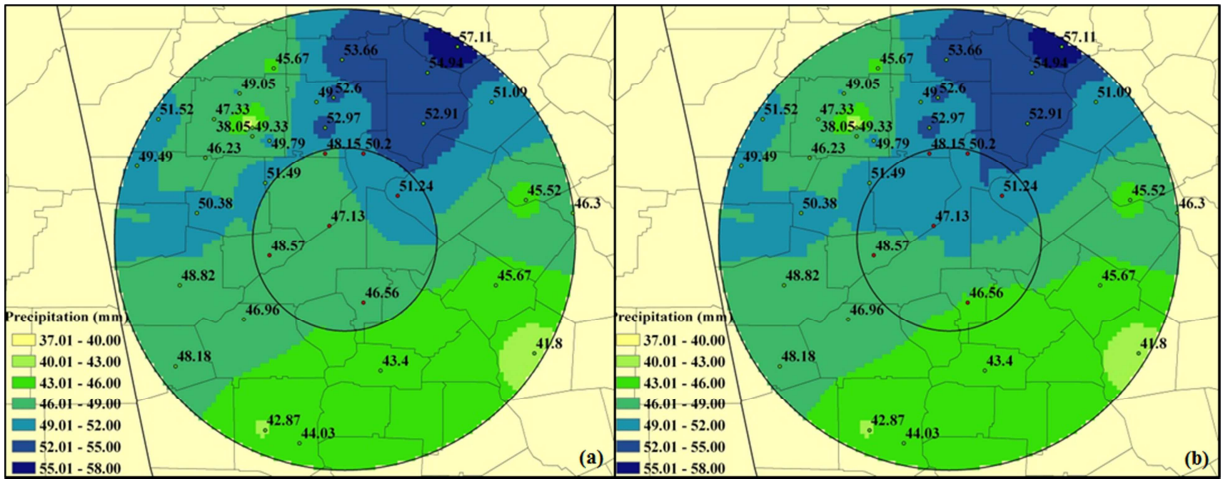

Figure 3.17. Results of the contour test for Atlanta at the 40 km buffer. Stations are represented by the dots with their overall mean precipitation (mm) from heavy precipitation events. The inner circle for Figure A shows precipitation based only on urban station data. Figure B shows urban station precipitation interpolated using non-urban stations.

correspond closely and no significant areas of precipitation are estimated inaccurately.

- **Birmingham**

Similar to Atlanta, the contour test shows that interpolating precipitation from non-urban stations did not exhibit many differences with the interpolated urban precipitation (Figures 3.17 through 3.19).

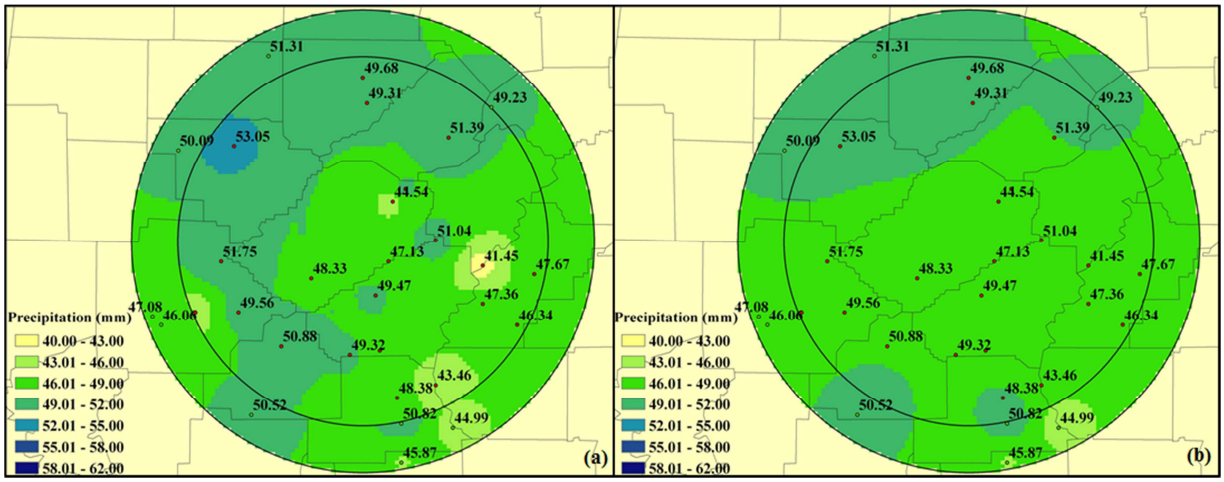

Figure 3.18. Results of the contour test for Birmingham at the 80 km buffer. Stations are represented by the dots with their overall mean precipitation (mm) from heavy precipitation events. The inner circle for Figure A shows precipitation based only on urban station data. Figure B shows urban station precipitation interpolated using non-urban stations.

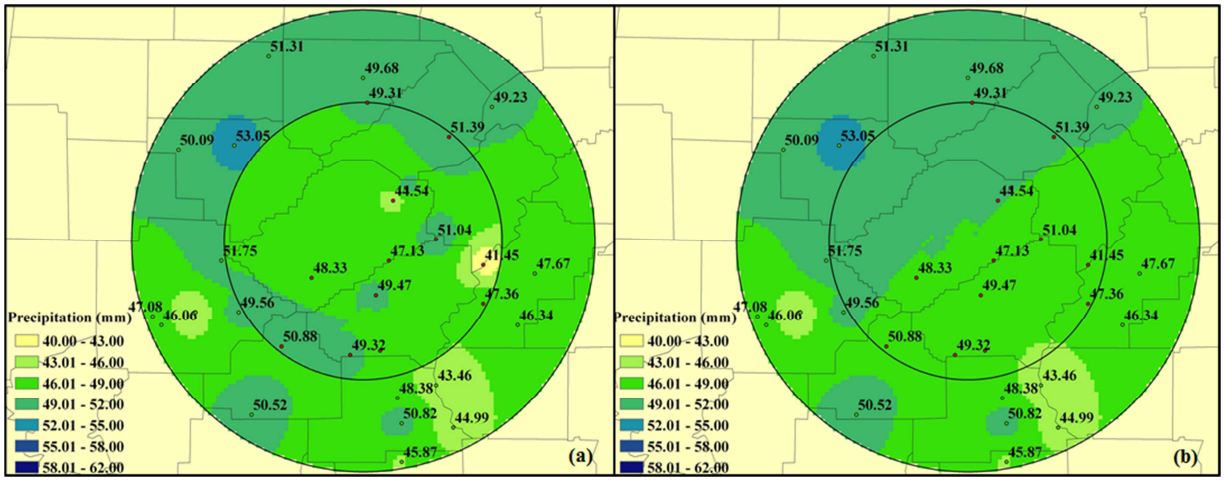

Figure 3.19. Results of the contour test for Birmingham at the 60 km buffer. Stations are represented by the dots with their overall mean precipitation (mm) from heavy precipitation events. The inner circle for Figure A shows precipitation based only on urban station data. Figure B shows urban station precipitation interpolated using non-urban stations.

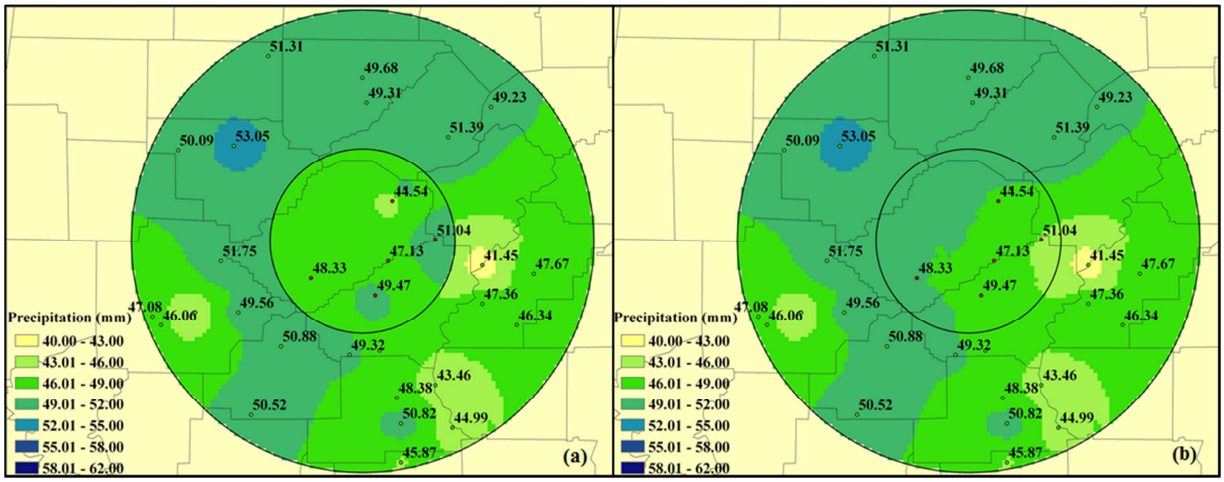

Figure 3.20. Results of the contour test for Birmingham at the 40 km buffer. Stations are represented by the dots with their overall mean precipitation (mm) from heavy precipitation events. The inner circle for Figure A shows precipitation based only on urban station data. Figure B shows urban station precipitation interpolated using non-urban stations.

- **Dallas/Fort Worth**

Results from the contour test show that there may be an urban influence in precipitation (Figures 3.20 through 3.22). There is an area of greater precipitation inside the urban buffers

that is missed when using non-urban only precipitation. This region is most defined within the 60 km buffer.

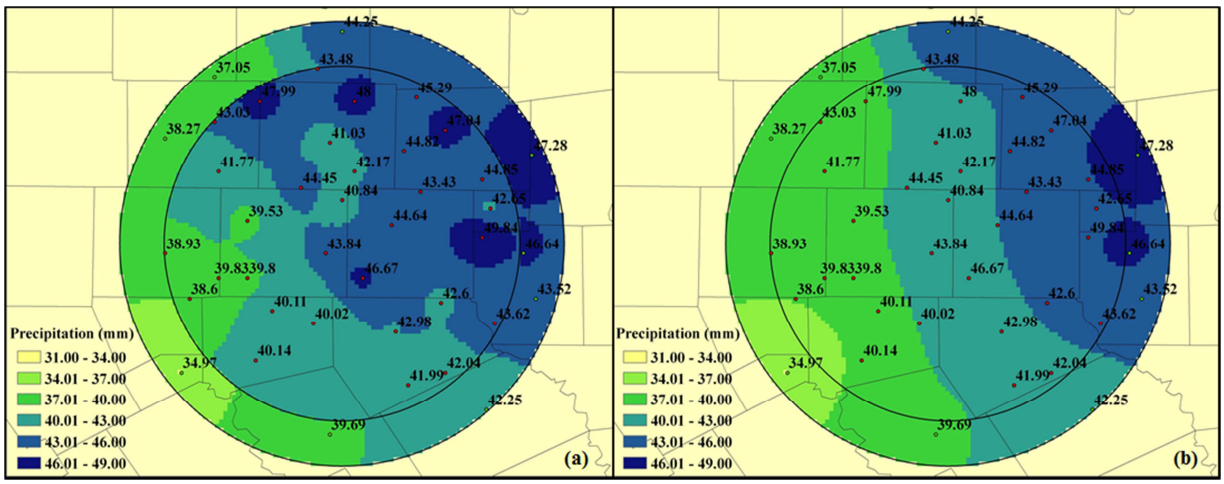

Figure 3.21. Results of the contour test for Dallas/Fort Worth at the 80 km buffer. Stations are represented by the dots with their overall mean precipitation (mm) from heavy precipitation events. The inner circle for Figure A shows precipitation based only on urban station data. Figure B shows urban station precipitation interpolated using non-urban stations.

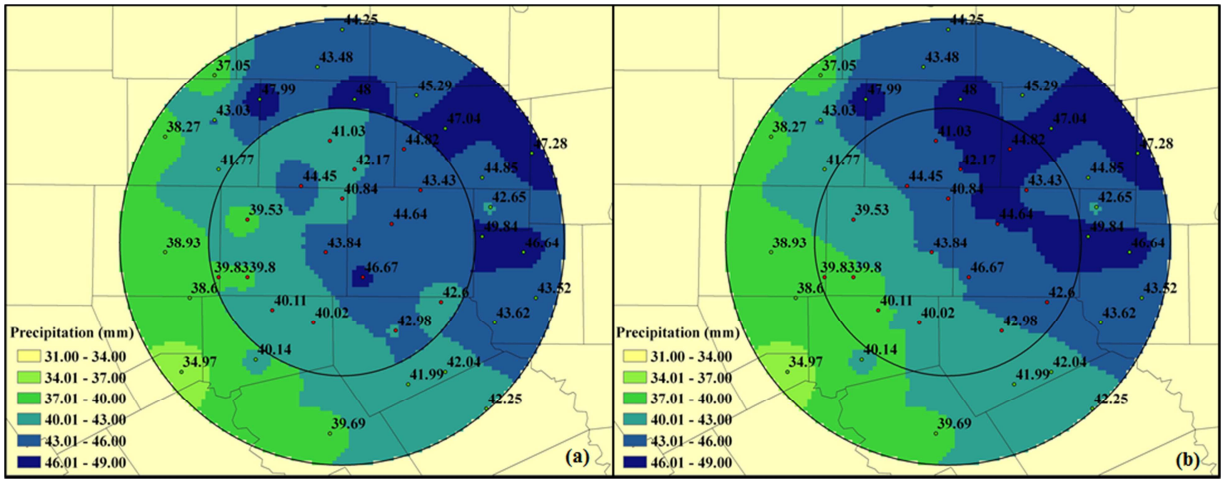

Figure 3.22. Results of the contour test for Dallas/Fort Worth at the 60 km buffer. Stations are represented by the dots with their overall mean precipitation (mm) from heavy precipitation events. The inner circle for Figure A shows precipitation based only on urban station data. Figure B shows urban station precipitation interpolated using non-urban stations.

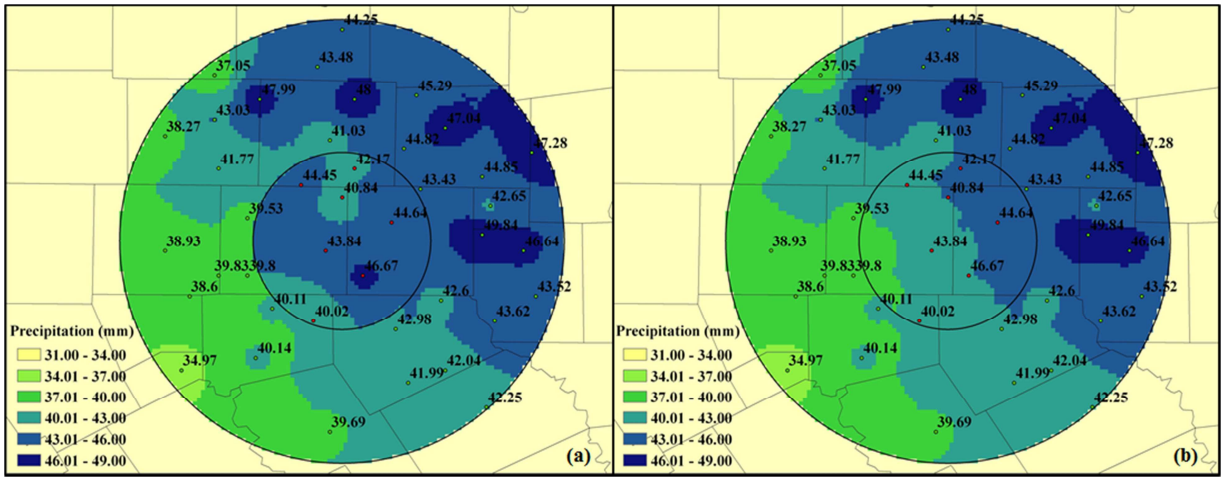

Figure 3.23. Results of the contour test for Dallas/Fort Worth at the 40 km buffer. Stations are represented by the dots with their overall mean precipitation (mm) from heavy precipitation events. The inner circle for Figure A shows precipitation based only on urban station data. Figure B shows urban station precipitation interpolated using non-urban stations.

- **Houston**

The contour test (Figures 3.23 through 3.25) shows that the interpolation of precipitation from the non-urban stations did not produce any unexpected patterns based upon the urban station precipitation (at all runs). One station within the urban area seems to receive greater precipitation in all buffers, possibly influencing the pattern of the contours, but this result may be due to local effects.

- **Memphis**

The non-urban interpolation predicted the urban precipitation fairly well at all buffers as the contours of the interpolations corresponded consistently (Figures 3.26 through 3.28).

- **Tulsa**

The contour test for Tulsa shows precipitation at some urban stations measuring higher precipitation that is not seen when interpolating precipitation at non-urban stations (for the 80 km (Figure 3.29) and 60 km buffer (Figure 3.30)). Run 3 shows the opposite: a region of lesser

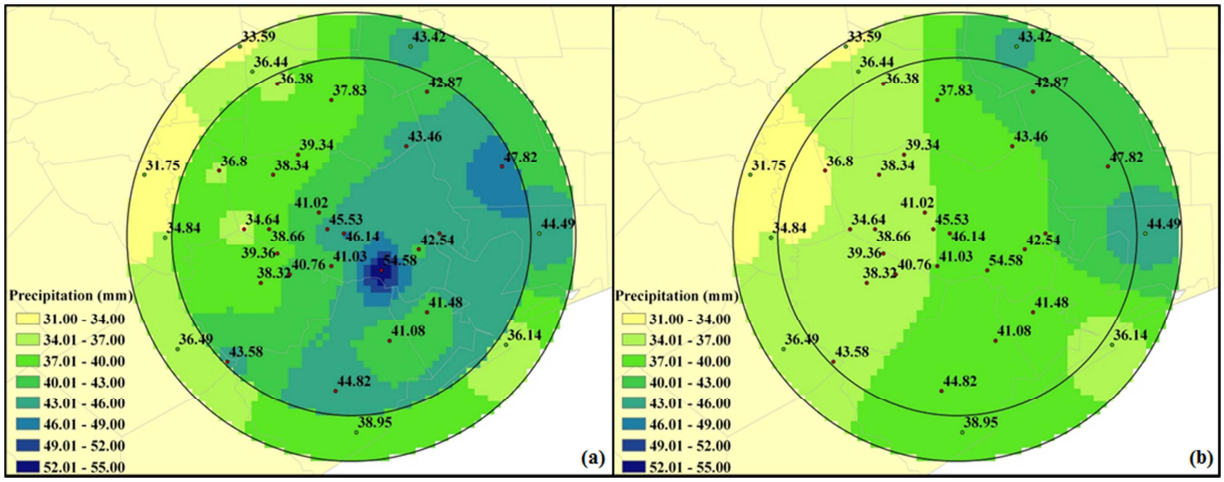

Figure 3.24. Results of the contour test for Houston at the 80 km buffer. Stations are represented by the dots with their overall mean precipitation (mm) from heavy precipitation events. The inner circle for Figure A shows precipitation based only on urban station data. Figure B shows urban station precipitation interpolated using non-urban stations.

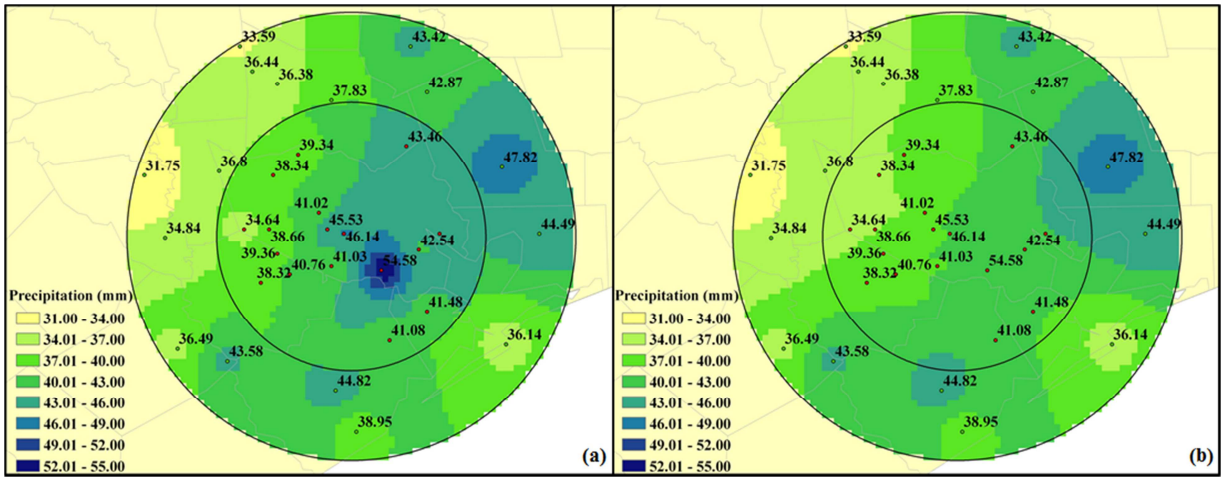

Figure 3.25. Results of the contour test for Houston at the 60 km buffer. Stations are represented by the dots with their overall mean precipitation (mm) from heavy precipitation events. The inner circle for Figure A shows precipitation based only on urban station data. Figure B shows urban station precipitation interpolated using non-urban stations.

precipitation in the urban area rather than outside the urban area (Figure 3.31). It is possible that these anomalous regions are due to local effects on precipitation (nearby vegetation, buildings, etc.) and are not representing a true urban influence on precipitation.

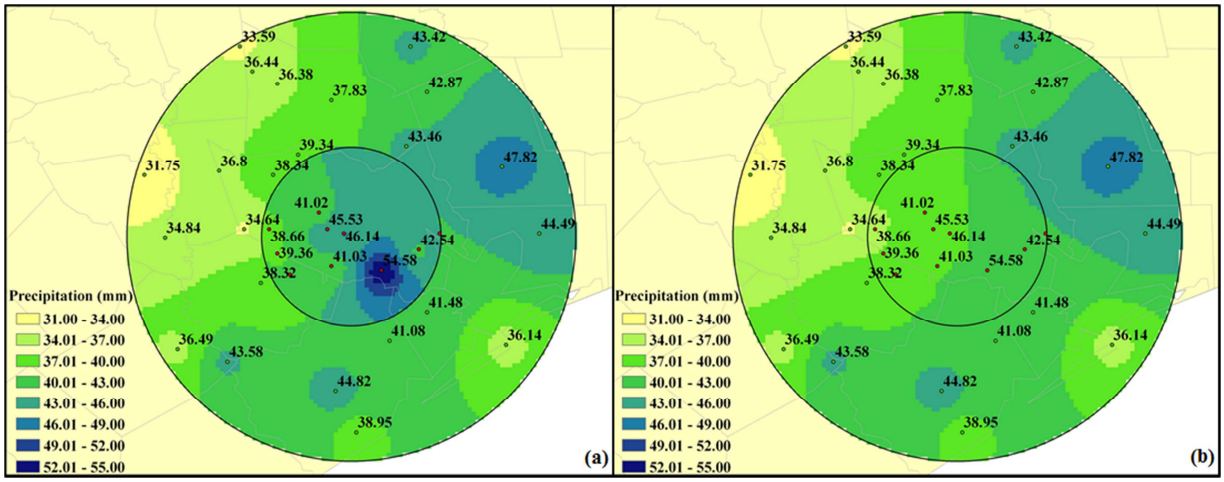

Figure 3.26. Results of the contour test for Houston at the 40 km buffer. Stations are represented by the dots with their overall mean precipitation (mm) from heavy precipitation events. The inner circle for Figure A shows precipitation based only on urban station data. Figure B shows urban station precipitation interpolated using non-urban stations.

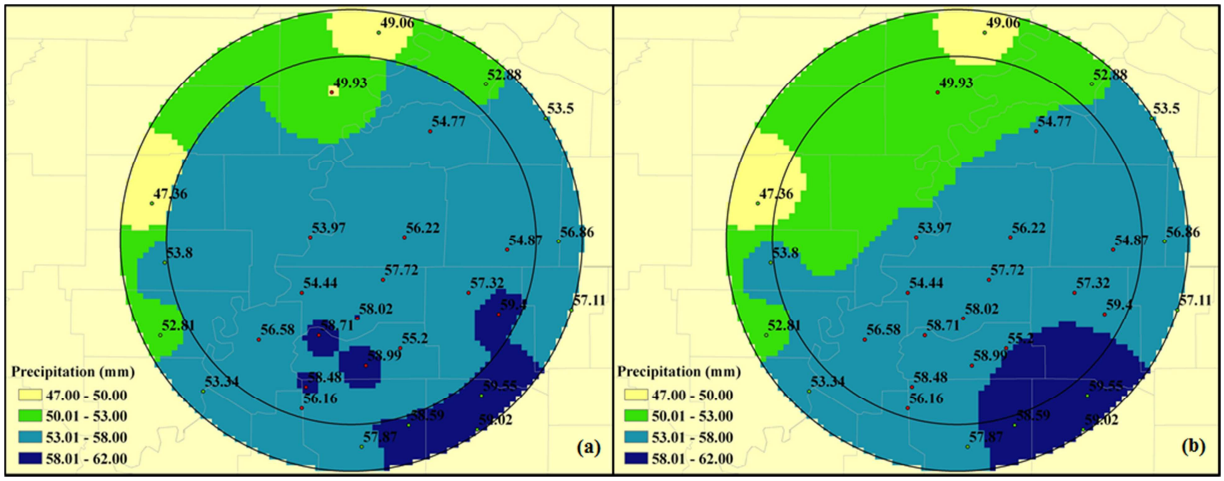

Figure 3.27. Results of the contour test for Memphis at the 80 km buffer. Stations are represented by the dots with their overall mean precipitation (mm) from heavy precipitation events. The inner circle for Figure A shows precipitation based only on urban station data. Figure B shows urban station precipitation interpolated using non-urban stations.

3.4 Summary/Conclusion

3.4.1 Overall Results

By employing multiple detection methods and examining multiple locations within the southeastern U.S., the research proposed in Study 1 provides a new, robust, and comprehensive

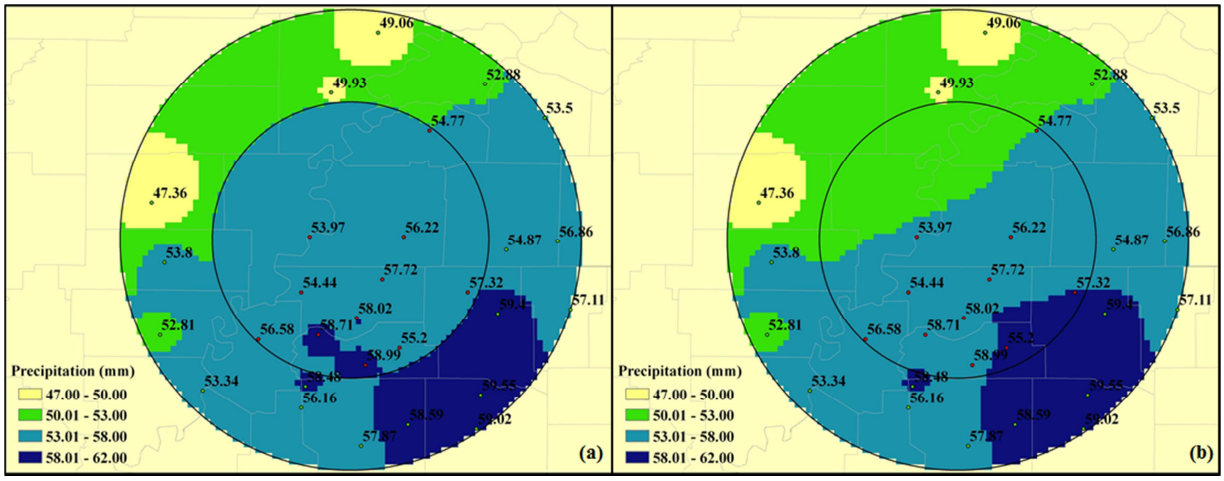

Figure 3.28. Results of the contour test for Memphis at the 60 km buffer. Stations are represented by the dots with their overall mean precipitation (mm) from heavy precipitation events. The inner circle for Figure A shows precipitation based only on urban station data. Figure B shows urban station precipitation interpolated using non-urban stations.

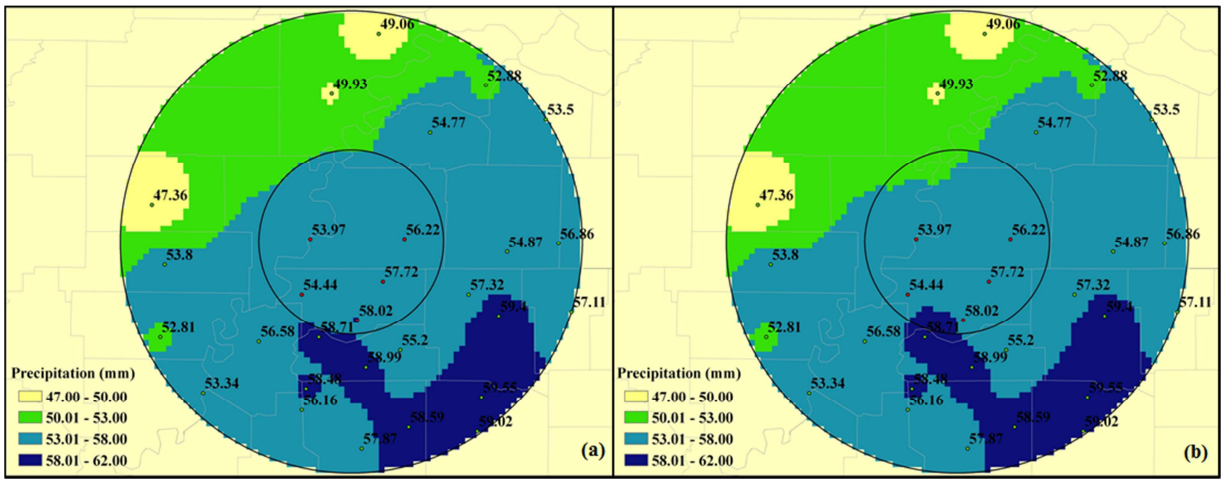

Figure 3.29. Results of the contour test for Memphis at the 40 km buffer. Stations are represented by the dots with their overall mean precipitation (mm) from heavy precipitation events. The inner circle for Figure A shows precipitation based only on urban station data. Figure B shows urban station precipitation interpolated using non-urban stations.

assessment of urban-precipitation relationships for this part of the United States. Additionally, this study provides an updated assessment of Atlanta, allowing for either support of studies showing little to no precipitation enhancement (Diem & Mote 2005, Diem 2006b, 2008)

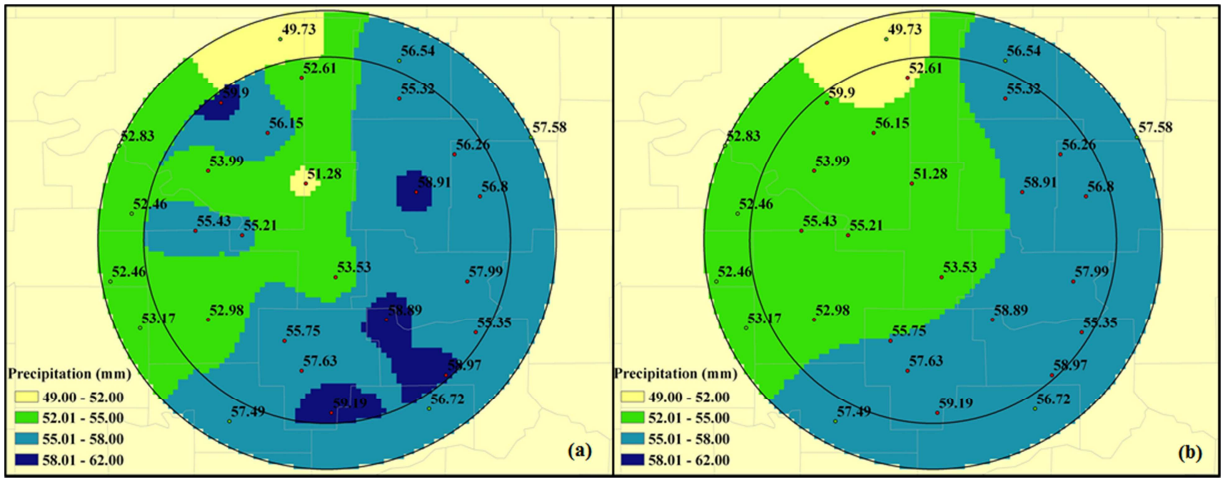

Figure 3.30. Results of the contour test for Tulsa at the 80 km buffer. Stations are represented by the dots with their overall mean precipitation (mm) from heavy precipitation events. The inner circle for Figure A shows precipitation based only on urban station data. Figure B shows urban station precipitation interpolated using non-urban stations.

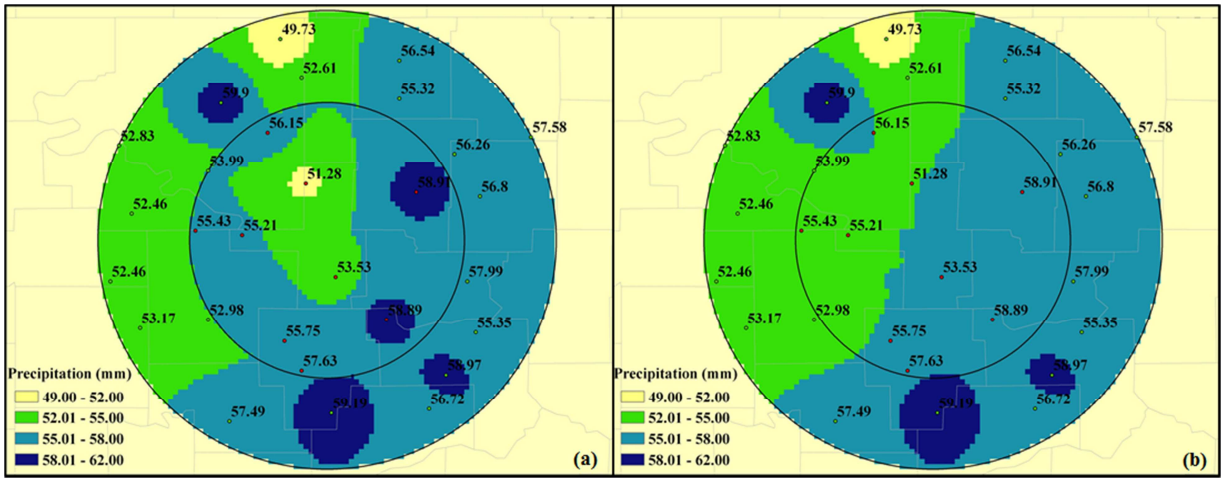

Figure 3.31. Results of the contour test for Tulsa at the 60 km buffer. Stations are represented by the dots with their overall mean precipitation (mm) from heavy precipitation events. The inner circle for Figure A shows precipitation based only on urban station data. Figure B shows urban station precipitation interpolated using non-urban stations.

or disagreement with results showing strong precipitation enhancement (Shepherd et al. 2002, Lacke et al. 2009, Shem & Shepherd 2009). Finally, a broader understanding of precipitation variability across major urban centers in the southeastern U.S. provides potential

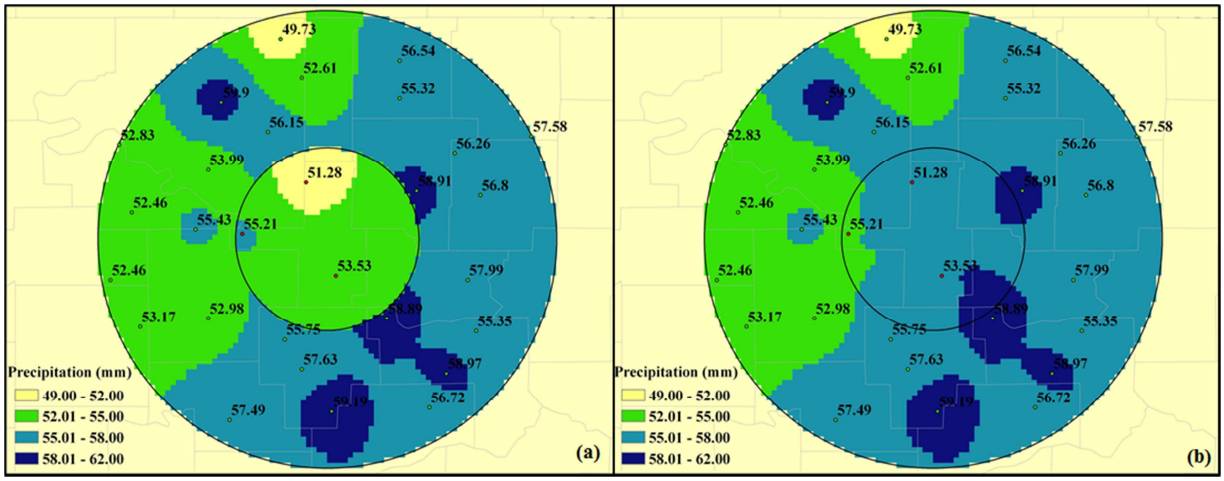

Figure 3.32. Results of the contour test for Tulsa at the 40 km buffer. Stations are represented by the dots with their overall mean precipitation (mm) from heavy precipitation events. The inner circle for Figure A shows precipitation based only on urban station data. Figure B shows urban station precipitation interpolated using non-urban stations.

benefit to a range of stakeholders, such as city planners and emergency managers, whose work is informed by climate information. If urban influence on rainfall can be predicted consistently, then urban infrastructure can be zoned for green space or reservoirs to maximize capture of anticipated increases in heavy precipitation.

A summary of the results of the tests in this study can be found in Table 3.15. Cities that appear to have some urban influence for one out of the three tests are described as having "possible urban influence" (two out of three = "some urban influence"; all three = "likely urban influence"). Houston, Memphis, and Tulsa are the only cities to exhibit possible urban influence, while Birmingham shows some urban influence. Dallas/Fort Worth is the only city to show likely urban influence while Atlanta shows little to no urban influence based upon the tests employed in this study. The recommendation of a study site for the bifurcation analysis (Chapter 4) is based upon two factors: (1) strong evidence of an urban influence on heavy precipitation events ("likely urban influence") and (2) evidence of storm bifurcation seen in the literature.

- **Atlanta**

Few comparisons from the downwind *vs.* upwind tests show significant differences in precipitation on heavy precipitation days (Table 3.6), similar to results seen in (Diem & Mote 2005, Diem 2008) where significantly different precipitation was found at only one station. The temporal analysis does not show any trends in heavy precipitation. The contour test also shows no evidence for urban influence as the interpolation using only non-urban heavy precipitation succeeds in calculating urban precipitation. Therefore, it is concluded that according to the tests in this analysis, an urban influence was not detected for Atlanta, but this city is recommended as a study site for bifurcation analysis due to evidence of possible bifurcation seen in previous studies (Dixon & Mote 2003).

- **Birmingham**

Few comparisons from the downwind *vs.* upwind tests show significant differences in precipitation on heavy precipitation days (Table 3.7). The temporal analysis does not show any trends in heavy precipitation and the contour test shows some evidence of urban influence but only at 80 km. Therefore, it is concluded that Birmingham has some evidence of urban influence on precipitation but is not recommended as a study site for bifurcation analysis. It has been shown that pollution plays a role in the precipitation regime in Birmingham and may be an influencing factor in these results (Trainer et al. 1995, Greene et al. 1999).

- **Dallas/Fort Worth**

The downwind *vs.* upwind tests reveal significant differences in precipitation on heavy precipitation days between the two regions for many of the comparisons (Table 3.8). The temporal analysis shows some evidence of trends, but was not trustworthy due to the lack of normality in the data. The contour test suggests some areas within the urban center that are not

predicted well by the non-urban data, inferring some degree of urban enhancement. Therefore, it is concluded that Dallas/Fort Worth has likely urban influence on heavy precipitation events and is recommended as a study site for bifurcation analysis.

- **Houston**

Many of the comparisons for the downwind *vs.* upwind tests are shown to be significant. There are no trends in the temporal analysis or contour tests that show evidence of urban influence on heavy precipitation events. Therefore, Houston is concluded to have possible urban influence but is not recommended as a bifurcation study site. Factors in the urban environment that may be contributing to these results are the available aerosols and strong urban heat island (Carrio et al. 2010, Carrio & Cotton 2011, Zhou et al. 2011).

- **Memphis**

The downwind *vs.* upwind tests show evidence of urban influence for some comparisons (Table 3.10). The temporal analysis identifies no trends and the contour test shows no difficulty in the non-urban stations predicting urban precipitation. Geographic features within Memphis that may be contributing to these results are the proximity of the Mississippi River, providing an abundant moisture source, and large green spaces throughout the urban landscape. (Wikipedia 2012a). Therefore, Memphis is concluded to have possible urban influence on heavy precipitation events but is not recommended for the bifurcation analysis.

- **Tulsa**

The downwind *vs.* upwind tests reveal some evidence urban influence (Table 3.11). The temporal analysis shows no trends in heavy precipitation events while the contour test provides some evidence of urban influence due to the lack of representation of high precipitation regions

Table 3.16. Study 1 results by city ranked by level of precipitation enhancement.

	Downwind *vs.* Upwind		**Temporal analysis**		**Contour test**			
	Traditional	**90°**	**Annual Frequency**	**Inter-arrival times**	**80 km**	**60 km**	**40 km**	**Conclusion**
Dallas/Fort Worth	some	some	some	some	some	some	none	likely urban influence
Birmingham	some	some	none	none	some	some	none	some urban influence
Houston	some	some	none	none	none	none	none	possible urban influence
Memphis	some	some	none	none	none	none	none	possible urban influence
Tulsa	some	some	none	none	some	some	none	possible urban influence
Atlanta	none	some	none	none	none	none	none	unlikely urban influence

in the urban area. These results are likely influenced by the features of the local topography: rolling hills, prominent vegetation, and presence of the Arkansas River splitting the city in half (The City of Tulsa 2012, Wikipedia 2012). Therefore, Tulsa is concluded as having some urban influence on precipitation but is not recommended for bifurcation analysis.

3.4.2 The Next Steps

The next chapter will examine the frequency of bifurcation of individual storms around Atlanta and Dallas/Fort Worth. To identify whether these frequencies are higher than would be expected without the urban centers present, a control site was chosen where no large city exists. Because no National Weather Service radars in the area are situated in truly rural areas, it was necessary to accept a small town as the control site. The town chosen was Columbus, Mississippi.

CHAPTER 4. STORM BIFURCATION

4.1 Introduction

Results of Study 1 (Chapter 3) identified some likely locations in the southeastern U.S. for precipitation enhancement due to urbanization. However, a further understanding of storm dynamics over urban areas is also needed, as storm movement is linked directly to hazards such as lightning strikes, severe winds, and flash flooding. Ntelekos et al. (2007) is one of the few studies that has investigated the occurrence of storm bifurcation. A few others have examined the effects of urban areas on storm movement (Loose & Bornstein 1977, Bornstein & Lin 2000, Dixon & Mote 2003). Although the present research hypothesizes that storm bifurcation is likely to occur in cities that produce precipitation enhancement, evidence suggests that the interaction between the urban land surface and storm movement is complex. For example, Rose et al. (2008) found both lightning flash and precipitation enhancement in all directions surrounding Atlanta, rather than solely in the upwind region. Because so little is known about how urban areas influence storm movement, and in particular storm bifurcation, the purpose of this chapter (Study 2) provides a thorough, case study-based analysis of bifurcation occurrence in an urban area shown in Chapter 3 to also exhibit likely precipitation enhancement (Dallas/Fort Worth), and in an urban area that has been previously shown by Dixon and Mote (2003) to experience bifurcation (Atlanta).

4.2 Background

Urban areas further affect precipitation by altering the movement, growth, and demise of individual storm cells (Bornstein & Lin 2000). Bornstein and Lin (2000) defined storm

bifurcation as “a group of storms [that] moves in two directions from a specific location (such as upwind of city)” (Bornstein & Lin 2000). While bifurcation is possible in multiple types of rainfall events (frontal, convective, tropical), little is known about the relative importance of each causal mechanism for urban storm bifurcation in the southeastern United States.

Despite the lack of Southeast-specific studies on storm bifurcation, many of the same mechanisms that may initiate bifurcation in other areas (urban heat islands (UHIs), pollution emissions, and surface roughness) occur in the Southeast. Frontal speed and surface roughness affect storm motion over New York City (Loose and Bornstein 1977). However, research on the extent of the effect of cities on speed changes of sea-breeze fronts (Freitas et al. 2007, Cheng and Byun 2008) and convective storm cells (Kishtawal et al. 2010) is inconclusive. Gaffen and Bornstein (1988) suggested that urban modulation of storm movement may result in storm bifurcation. Ntelekos et al. (2007) confirmed this suggestion by observing a multicell storm that split into two elements as it reached Baltimore, and by attributing the bifurcation to frictional effects caused by the urban canopy, resulting in increased precipitation totals and lightning flashes along the western edge of Baltimore and Washington D.C.

Bornstein and Lin (2000) found that on days with weak steering wind flows over Atlanta, the UHI-initiated convergence zone allowed precipitation to propagate upwind of the urban center with no appreciable bifurcation; but on days with stronger flows, bifurcation of storms around the city tended to occur. Even though individual synoptic situations are complex, it can be concluded that when regional winds are strong, surface roughness dominates the local thermally-induced circulation in urban areas, as opposed to a UHI-dominated regime in weaker synoptic settings (Bornstein and Lin 2000). This relationship is analogous to the "mechanical

turbulence" versus "thermal turbulence" dichotomy that characterizes atmospheric buoyancy in general.

4.3 Data and Methods

4.3.1 Site Selection

Because the analysis portion of this objective is thorough and in-depth, the number of cities is restricted to two (Atlanta and Dallas/Fort Worth) plus a non-urban location to serve as a control site (Columbus, Mississippi). The cities are selected on the basis of evidence of urban influence on precipitation (such as precipitation enhancement or storm bifurcation) as determined by previous studies and evidence of urban influence arising from the results of Study 1. Columbus, Mississippi (Figure 4.1) has a population of 23,640 (U.S.A. Census Bureau: Population Division 2010), which is ideal for a control site as it is very unlikely to have a large area of urbanized land cover. Also, it is ideally located between the two urban study sites of Atlanta and Dallas/Fort Worth, likely experiencing similar precipitation events, such as the same mid-latitude cyclone.

4.3.2 Data and Methods

Radar-derived precipitation estimates at six-minute intervals are utilized to identify bifurcation because of their spatial homogeneity (Mote et al. 2007). These data (Level III precipitation, which accounts for both storm total precipitation and base reflectivity) are collected from National Climatic Data Center (NCDC) for each urban area examined each day in the years 2008 – 2009. In addition, daily 900 hPa flow from National Centers for Environmental Prediction/National Center for Atmospheric Research (NCEP/NCAR) reanalysis data (Mesinger et al. 2006) are obtained for the same period, to represent wind speed and direction across the

Figure 4.1. Downtown Columbus, Mississippi (Wikimedia Commons).

urban core. Loose and Bornstein (1977) showed that 4 m s^{-1} is the critical speed that determines whether urban surface roughness (leading to bifurcation) or horizontal pressure gradients (leading to urban-induced convection where storm structure remains intact) will dominate. Oke (1973) showed that UHI conditions are unlikely to form above a regional wind speed of 10 m s^{-1} (Oke 1973).

For each study site, calendar days reporting heavy precipitation ($\geq$ 25 mm day^{-1}) are identified as possible bifurcation case study days (Huff & Changnon 1973, Huff & Vogel 1978, Burian & Shepherd 2005, Diem & Mote 2005). In cases for which the coordinated universal time (UTC) suggests that the precipitation event could have straddled two calendar days (i.e. early morning in Greenwich and the previous evening in the southeastern U.S.), multiple days of radar images are evaluated to ensure the analysis of the entire precipitation event. Consecutive

precipitation days are then combined into a single precipitation "event." If multiple bands pass over the urban area, they are analyzed individually (yet still considered the same event) in case the storm structure or changing surface dynamics play a role in bifurcation. Days with missing radar data within an event were removed from further analysis. For each day, the time and location of storm passage relative to the CBD were noted. For Atlanta, a total of 15 missing days were removed from the analysis (11% total), while 38 days were removed from Columbus (19% total), and 41 days were removed from Dallas/Fort Worth (26% total) (2008 – 2009). It is important to remember that each precipitation event can consist of multiple days; therefore, these days represent a small number of missing data. If the storm did not pass over the CBD then urban surface roughness could not have been a factor in any bifurcation that may have occurred; therefore, such storms were also removed from the analysis.

4.3.3 Bifurcation Detection Test

The spatial characteristics of each event are studied for evidence of an urban signal in the form of bifurcation. It is hypothesized that for bifurcation events, there is a greater amount of rainfall received in the periphery than within the city center. There may also be an area of greater rainfall in the downwind region in the event that the storm cells re-converge after they pass the city center, but this may not be distinguishable from UHI-related precipitation enhancement and is not used as a criterion for determining bifurcation. If a larger amount of precipitation in the periphery is found then it is possible that bifurcation has occurred.

Using the list of potential bifurcation events (i.e., the collection of days with precipitation $\geq$ 25 mm at any single station in the urban area), the distribution of base reflectivity for each event is evaluated to determine visually whether storm bifurcation has occurred. If a storm does not pass over the city (e.g., if a convective event only passes through the outskirts of the study

area and not over the urban core), then it will not be considered for further analysis as there was no opportunity for the urban core to initiate bifurcation. Storm precipitation totals for each of these bifurcation events are imported into a geographic information system (GIS, e.g. ArcMap®). For each event, a bifurcation index consisting of a comparison of precipitation received along the periphery of an urban area to that received within the urban center is calculated. A series of 64 sections is drawn around the urban center (Figure 4.2). Three variations of the index are applied. In Test 1, the urban core includes all sections within 40 km while the periphery includes sections between the 40 km and 100 km buffers. In Test 2, the urban core includes all sections within 60 km while the periphery includes sections between the 60 km and 100 km buffers. In Test 3, the urban core includes all sections within 80 km while the periphery includes the sections between the 80 km and 100 km buffers. The calculation of the bifurcation index is as follows:

$$P_{periphery\ n} - P_{urban\ core}$$

where $P_{periphery\ n}$ is the average precipitation within periphery section *n*, and $P_{urban\ core}$ is the average precipitation within the urban core.

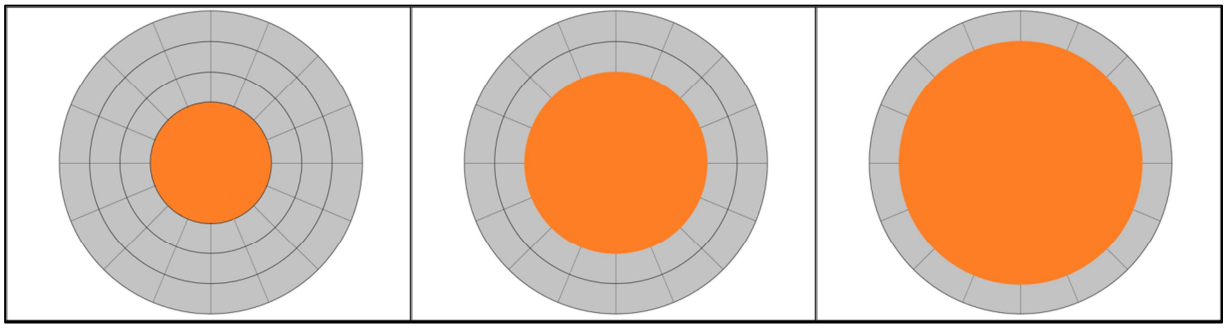

Figure 4.2. Sections drawn to calculate bifurcation index for Test 1 where the urban core includes sections up to 40 km (left), Test 2 where the urban core includes sections up to 60 km (center) and Test 3 where the urban core includes sections up to 80 km (right). The grey sections indicate the urban periphery while the orange section indicates the urban core.

Index values are calculated at all periphery sections and for all heavy precipitation events, with the storm total precipitation data retained in ArcMap. After all events are identified for a particular city, two-tailed paired t-tests are used to determine whether precipitation received in the periphery regions is significantly greater than that within the urban core. The t-test must be two-tailed because it is not known whether periphery precipitation will be larger or smaller than that observed in the core, although it is expected that bifurcating storms exhibit more precipitation in the periphery than in the core. The two-tailed t-test is preferred over the one-tailed t-test due to this uncertainty in the spatial distribution of precipitation. The t-tests must be paired because core precipitation should only be compared to periphery precipitation for the same event (and not comparing core precipitation for a specific event to periphery precipitation at a different event). Based on event-specific radar precipitation totals, storm events exhibiting significant precipitation differences between the core and periphery are classified as storm bifurcation events. To ascertain whether the bifurcation index values are physically meaningful, the difference of means test is also used to compare precipitation of periphery boxes to that of the urban core for all non-bifurcation heavy precipitation events.

4.4 Results

4.4.1 Potential Bifurcation Events

Table 4.1 shows the number of heavy precipitation events analyzed for each city by year. These events have 25 mm or greater of precipitation at any station within 100 km of the city center (Chapter 3).

Table 4.1. Number of heavy precipitation events for each study site by year.

	2008	2009	Total
Atlanta	28	41	69
Dallas/Fort Worth	30	46	76
Columbus	46	67	113

4.4.2 Atlanta

There were 69 events over the two-year study period for Atlanta. Eight of these were thought to experience bifurcation based on visual inspection of the radar imagery. Each radar image was exported from the NOAA data and toolkit as a shapefile. Using Arcmap Model Builder, precipitation values were clipped to each section (Figure 4.3) and an average precipitation value was calculated. A two-tailed paired t-test was implemented using SPSS. Figure 4.4 shows the labeled sections that were compared to core precipitation.

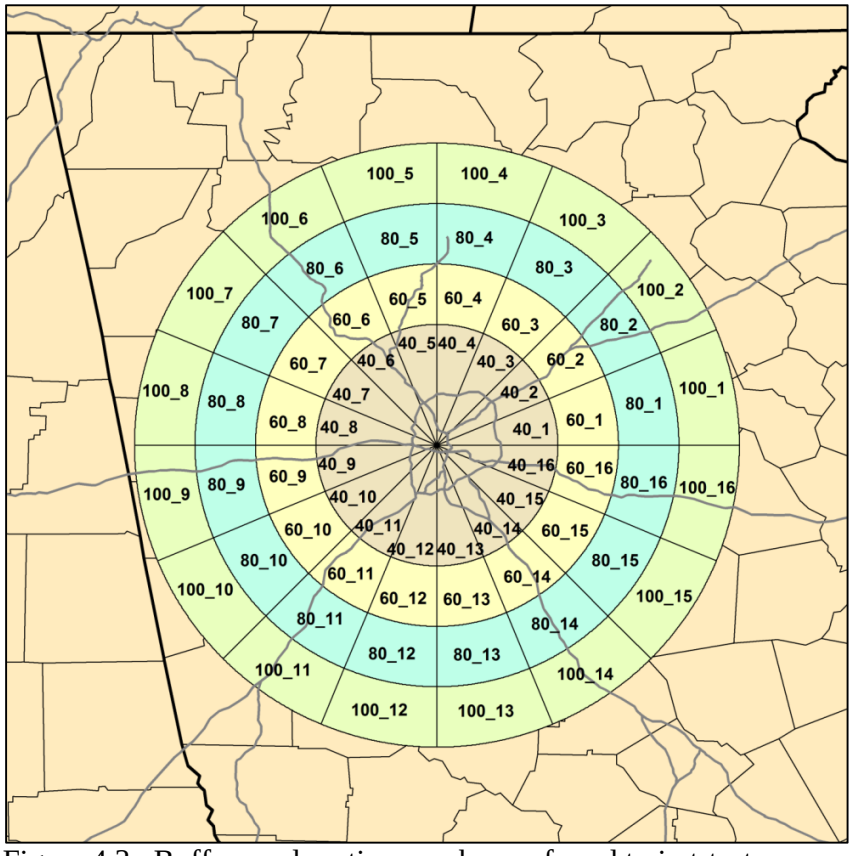

Figure 4.3. Buffers and section numbers referred to in t-tests.

The t-test results of the eight bifurcation events showed that precipitation averages in the southeastern sections of the Atlanta study area differ significantly from those in the core. In Test 1, where the core consisted of sections within 40 km, the periphery sections that were significantly different from core precipitation were Section 15 of Buffer 80 and Sections 11, 12, and 13 within Buffer 60 (Table 4.2). In Test 2, where the core consisted of sections within 60 km, the periphery sections in which precipitation was significantly different from core precipitation were Section 2 of Buffer 100 and Section 15 of Buffer 80 (Table 4.3). In Test 3, where the core consisted of sections within 80 km, the only periphery section with significantly different precipitation from that within the core was Section 2 of Buffer 100 (Table 4.4). It is important to keep in mind that these results are based on only eight events but each section is a mean of precipitation, representing all of the events in a sample of two years: 2008-2009. These relatively recent years were chosen due to the availability of radar data and the likelihood of years in which bifurcation could be present (due to the increased precipitation in the southeastern U.S. caused by a positive ENSO phase (Kurtzman & Scanlon 2007, Mo & Schemm 2008)). The t-test results of the non-bifurcation events showed precipitation at none of the periphery sections to be statistically different from that in the core (Tables 4.5, 4.6, and 4.7).

4.4.3 Dallas/Fort Worth

Of the 76 events over the two-year study period for Dallas/Fort Worth, nine experienced bifurcation. The t-test results of the bifurcation events identified two sections that were significantly different from precipitation in the core. These were located to the west and the east. In Test 1, the periphery sections with precipitation differing significantly from core precipitation were Sections 2 and 10 of Buffers 100 and 80, and Section 2 of Buffer 60 (Table 4.8). In Test 2, the periphery sections with precipitation that differed significantly from core precipitation were

again Sections 2 and 10 of Buffers 100 and 80 (Table 4.9). In Test 3, the only periphery sections with significantly different precipitation from that in the core were Sections 2 and 10 of Buffer 100 (Table 4.10). The t-test results of the non-bifurcation events revealed precipitation at Section 1 of Buffer 60 to be statistically significantly different from that in the core for Test 1 (Table 4.11). Similarly, Section 7 and Section 10 of Buffer 80 had statistically significant differences from the core precipitation for Test 2 (Table 4.12), while in Test 3, Section 10 of Buffer 100 displayed statistically significant differences (Table 4.13). These sections are near those showing significance for the bifurcation events.

4.4.4 Columbus

Of the 113 events for Columbus, only two experienced bifurcation. The t-test results of the bifurcation events identified no sections with precipitation means that differed significantly from precipitation in the core (Tables 4.14, 4.15, and 4.16). The t-test results of the non-bifurcation events revealed precipitation at Sections 1, 3, 4, 5, 14, 15, and 16 of Buffer 100, Sections 1, 2, 4, 5, 9, 14, 15, and 16 of Buffer 80, and Sections 1, 2, 3, 4, 9, 15, and 16 of Buffer 60 to be statistically significantly different from that in the core for Test 1 (Table 4.17).

Similarly, Sections 1, 4, 5, 9, 14, 15, and 16 of Buffer 100 and Sections 1, 2, 4, 8, 9, 14, 15, and 16 of Buffer 80 had statistically significant differences from the core precipitation for Test 2 (Table 4.18). In Test 3, Sections 1, 4, 8, 9, 10, 14, 15, and 16 of Buffer 100 displayed statistically significant differences (Table 4.19).

4.4.5 900 hPa Wind Values

900 hPa flow from National Centers for Environmental Prediction/National Center for Atmospheric Research (NCEP/NCAR) reanalysis data (Mesinger et al. 2006) was analyzed for bifurcation days, to determine whether any potential relationship exists between wind speed and

bifurcation/non-bifurcation of storm systems, but none was found for any of the three study areas. There were some spuriously large wind values in the dataset (some values even greater than 100 ms^{-1}) at every location and especially in 2009, and so the data may not be accurate. It is recommended that another source of wind data be used for future analysis or that near-surface wind speed be calculated.

4.5 Summary/Conclusion

4.5.1 Overall Results

Results from this study are important on numerous levels. First, storm bifurcation has not been thoroughly studied in the literature. This study suggests that bifurcation is likely occurring for Atlanta, but due to the rarity of these events, statistical testing is difficult and unlikely to disprove the existence of bifurcation. Little convincing evidence for bifurcation occurred in 2008-2009 for Dallas/Fort Worth, unless opposing factors masked the effects of bifurcation. The sections that have precipitation that differs significantly from the core are on opposite sides of the study area from each other, even in cases when the wind direction is similar. Some influences that are likely contributing are the multiple CBDs in the Metroplex and the placement of the radar (near Section 10). The position of the radar may be "hiding" precipitation totals in blind spots, to a greater extent in DFW than in other cities examined here.

Finally, bifurcation is unlikely to be an important component of the weather/climate of the Columbus study area, as only two possible events were found. The sections for the Columbus area that were found to display significant differences in precipitation occurred only on non-bifurcation days and are likely reflective of the natural precipitation signal of the study area. This study confirms evidence of bifurcation in Atlanta that was suggested in recent literature (Dixon & Mote 2003).

There are some limitations to this type of analysis. For example, analysis of bifurcation using radar-derived precipitation was done despite potential impacts of the "cone of silence" effect caused by the inability of radar to detect precipitation directly above. Storms that may have bifurcated near the radar may be missed. Another limitation is the small "n" caused by the small number of bifurcation days. Having a longer period of record for analysis may improve this issue, but due to the rarity of bifurcation events and the short records in which radar data has been available, this may not be possible.

4.5.2 The Next Steps

The next chapter (Chapter 5) utilizes 500 hPa geopotential heights to identify possible relationships between bifurcation and atmospheric circulation. This will be done by using an eigenvector-based approach to typing synoptic circulation at the 500 hPa level.

CHAPTER 5. SYNOPTIC ANALYSIS OF STORM BIFURCATION

5.1 Introduction

In addition to a baseline climatological understanding of storm bifurcation characteristics at the surface, it is important to link bifurcation to the larger-scale synoptic processes that may either enhance or inhibit its occurrence. While the greatest enhancement of precipitation has typically been seen in convective, air mass-type storms and during the warm season (Changnon et al. 1991, Changnon 2003, Gero et al. 2006, Svoma & Balling 2009), bifurcation may also occur in cold season, cyclonic situations (Loose & Bornstein 1977). Therefore, it is important to characterize all synoptic settings that may be in place during bifurcation events, both at the surface and aloft.

In Chapter 3, the degree to which selected urban areas in the southeastern U.S. may enhance precipitation in heavy precipitation events ($\geq$ 25 mm) was analyzed. Chapter 4 analyzed the degree to which two of these urban areas, along with a non-urban control site, are linked to bifurcation of individual storm lines. This chapter assesses the degree of synoptic control over the heavy precipitation events and the cases of bifurcation described in Chapter 4. To address this research question, the days of precipitation enhancement and bifurcation days are examined, using a circulation-to-environment approach (Yarnal 1993), to determine the likelihood that they fall into the same category of 500 hPa circulation types.

5.2 Background

Eigenvector-based map-pattern classifications have been utilized very prominently in synoptic climatology since the 1980s (e.g., Diaz 1981, Diaz & Fulbright 1981, Kalkstein et al.

1987, Skinner et al. 2002, Yarnal 1993). Although many variants of eigenvector-based techniques can be used for a wide variety of purposes, in synoptic circulation classification eigenvector analysis is generally employed on standardized geopotential height fields for a collection of observational units (typically the daily or the mean monthly scale). The purpose is to identify the most common modes of variability in the observational unit (i.e., geopotential height at a particular level). Because the eigenvector analysis analyzes relationships between two (space and time) of the three essential variables for understanding climate (space, time, and atmospheric variable) simultaneously, it is a very powerful technique when the geography and temporal variability/change in only one atmospheric variable (i.e., geopotential height at a particular variable) is to be understood. In the atmospheric sciences, principal components analysis (PCA) is the most typical model of the eigenvector-based techniques employed (e.g., Craddock & Flood 1969, Davis & Kalkstein 1990, Davis et al. 1991, Yarnal 1993, Comrie 1996, Yarnal et al. 2001, Cuell & Bonsal 2009), because the PCA model assumes no "uniqueness" among the input variables (i.e., geopotential heights at a particular level in the atmosphere); because atmospheric flow is continuous, no unique conditions at a gridpoint that would not also affect neighboring points should be expected.

The PCA scheme produces the same number of components as original variables (i.e., gridpoints on a daily map), with each successive component explaining a successively smaller percentage of the original dataset variance. For all practical purposes, only the first few components will generally be useful in climatological analysis. Researchers will typically employ a somewhat subjective determination of the number of components to be retained for further analysis based on three criteria summarized by Yarnal (1993): a) the exceedance of a preconceived threshold of total cumulative explained dataset variance; b) "natural breaks" in the

scree slope of eigenvalues by component; and c) retaining components whose eigenvalue exceeds 1.0 (thereby ensuring that the new component explains more variance than the original variable).

Rotation of principal components is necessary in eigenvector-based map-pattern classification studies to minimize the effect of the position of the data point in the spatial domain. Specifically, without rotating, it is likely that the greatest proportion of explained variance (i.e., the first component) will be represented strongly at data points near the middle of the study area, with the second through fifth components identifying strongly with explained variance in each of the four quadrants of the study region (Buell 1975, 1979). An orthogonal rotation scheme mitigates the effects of such "Buell sequences" while still maintaining the constraint that each new component explains a previously-unexplained component of variability in the model (i.e., the orthogonality constraint).

5.3 Data and Methods

Daily 500 hPa geopotential height fields are standardized statistically by gridpoint against the same Julian day in the year, to produce a field of 500 hPa geopotential height anomalies (mean = 0.0, standard deviation = 1.0 for each point) on each heavy precipitation day for the geographic domain from 1 January 1971 to 31 December 2010. The domain consists of all gridded data points in the National Center for Atmospheric Research/National Centers for Environmental Prediction Reanalysis Dataset for 500 hPa geopotential heights bounded by 20°N, 40°N, 110°W, and 75°W. A computer program (referred to as "Synoptic Typer") was used to conduct the PCA and determine the optimal number of components to retain for orthogonal rotation, using the criteria described above. The varimax criterion was chosen as the rotation

scheme because of its popularity in the literature among orthogonal rotation algorithms (e.g., Bloomfield & Davis 1994, Yarnal et al. 2001, Hannachi et al. 2007).

In eigenvector-based map-pattern classification, once the PCA is run (and rotation is done if appropriate), the output of PCA-derived scores for a given observational unit (i.e., in this case, days) is collected. Each observational unit will have *n* scores, one for each retained component, thereby allowing the scores to be plotted in *n*-dimensional space. A clustering algorithm is then selected to classify these points so that those nearest to each other are put into the same group. Each observational unit (one corresponding to each point in *n*-dimensional space) is clustered in this manner, without the need for identifying keydays *a priori*. A pre-existing air mass classification scheme is also linked to the frequencies of heavy precipitation days in 2008 – 2009, to confirm results of the eigenvalue-based map-pattern classification. Finally, composite 500 hPa and 700 hPa geopotential height maps are generated for days of heavy precipitation ($\geq$ 25 mm) when bifurcation was observed at each of the three sites individually. The composite analysis provides a third indication of the synoptic controls during bifurcation events. While the 500 hPa level is generally considered to represent the steering circulation, the 700 hPa level is also included in this analysis because of its importance in advecting low-level moisture.

5.4 Results

5.4.1 Map-pattern Classifications

K-means clustering was run but because it produced a "flat" distribution of types (Cannon et al. 2002, Cuell & Bonsal 2009, Kassomenos et al. 2010), Ward's analysis was used to produce the 17 different synoptic types for this study (Appendix A). Table 5.1 shows the

frequency of each of the 17 types over the initial synoptic window study period (1971 – 2010) and then broken down by city for heavy precipitation days for the bifurcation study period (2008 – 2009) (Chapter 4). This number of types was chosen based upon the scree plots shown in Figure 5.1. The number of types was appropriate due to the large longitudinal range of this study area, which was likely to support ridge/trough axes in multiple positions across the region, and with ridge/trough amplitudes that stretch meridionally through the entire range of latitudes in some cases but are positioned only in the northernmost part of the study area in others. For Atlanta, the synoptic types found to be directly linked to heavy precipitation days were Types 4 (Figure 5.2), 8 (Figure 5.3), 12 (Figure 5.4), 13 (Figure 5.5), and 16 (Figure 5.6). The two dominating synoptic types that are associated with heavy precipitation days show Atlanta beneath the trough-to-ridge side of a Rossby wave and having a pattern of steep geopotential height gradients suggestive of strong baroclinicity. The trough-to-ridge type is likely to cause heavy precipitation events due to upper-level divergence which draws surface air upward, thereby enhancing vertical cloud development, condensation, and precipitation. A strong baroclinic zone would result in heavy precipitation events caused by the stark difference in temperature of nearby cold and warm air masses.

For Dallas/Fort Worth, the synoptic types found to be most directly linked to heavy precipitation days were Types 13 (Figure 5.5), 14 (Figure 5.7), 15 (Figure 5.8), and 16 (Figure 5.6). Two of these four types were the "trough-to-ridge" type, one was suggestive ofa steep isohypse gradient with zonal flow, and one positioned Dallas/Fort Worth under a very deep trough. This deep trough could have likely produced heavy precipitation events similar to the trough-to-ridge types. It is important to remember that the types consist of averages of the

atmospheric circulation for heavy precipitation days, but the within-type variability could be great between each event.

For Columbus, the synoptic types found to be directly linked to heavy precipitation days were Types 5 (Figure 5.9), 13 (Figure 5.5), 14 (Figure 5.7), and 16 (Figure 5.6). Similar to Atlanta, 2 types were trough-to-ridge and 2 types were nearby baroclinic zones.

Table 5.1. Frequency of each synoptic type for the entire synoptic window (1971 – 2010) and for the bifurcation study period (2008 – 2009) (Chapter 4).

Type	**Frequency of all days (1971 – 2010)**	**Frequency of heavy precipitation days (2008 – 2009)**		
		Atlanta	**Columbus**	**Dallas/Fort Worth**
1	42	7	3	1
2	27	4	5	1
3	34	3	8	5
4	51	15	13	6
5	35	4	11	5
6	41	5	8	3
7	71	4	4	2
8	53	11	12	9
9	19	0	2	2
10	15	0	2	0
11	58	9	9	8
12	59	14	9	2
13	67	17	25	18
14	46	8	17	16
15	30	4	8	14
16	49	9	17	17
17	34	3	2	5

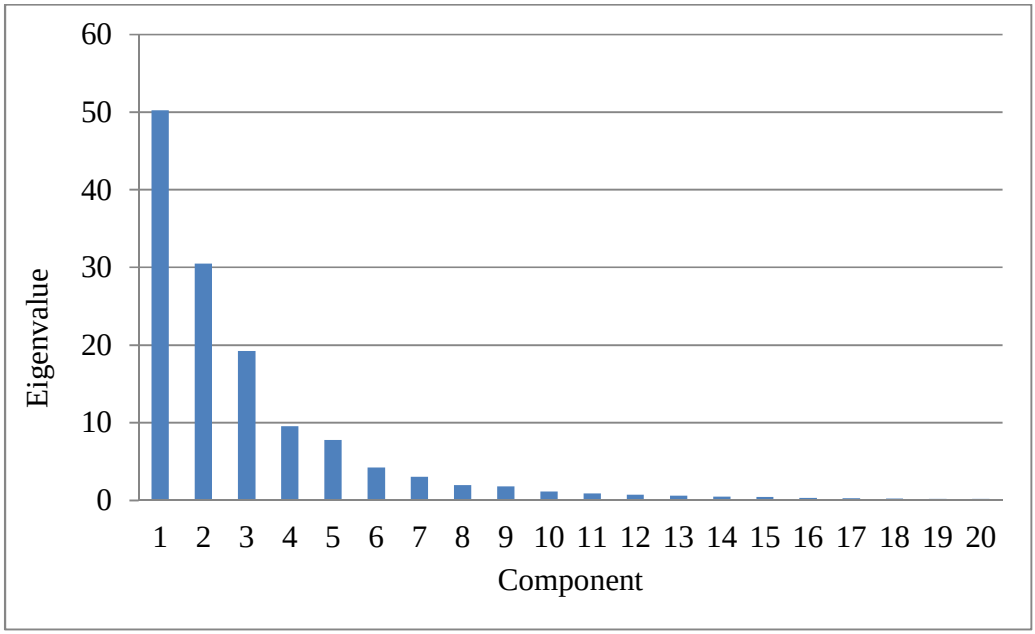

Figure 5.1 Scree plot showing eigenvalues for each of the types.

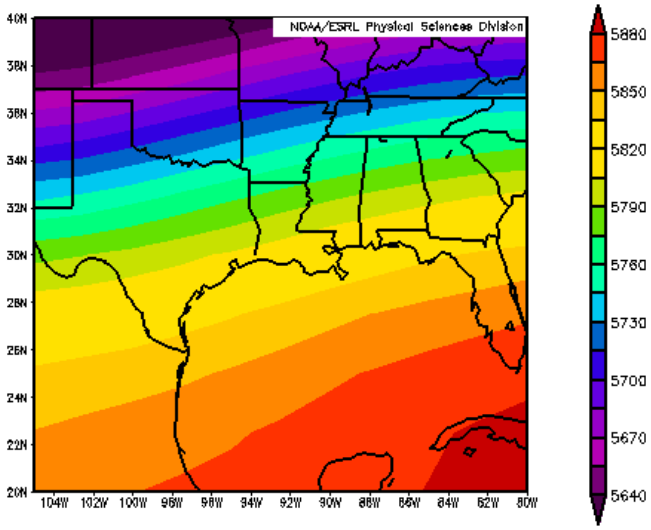

Figure 5.2. Synoptic Type 4 for all days (1971-2010).

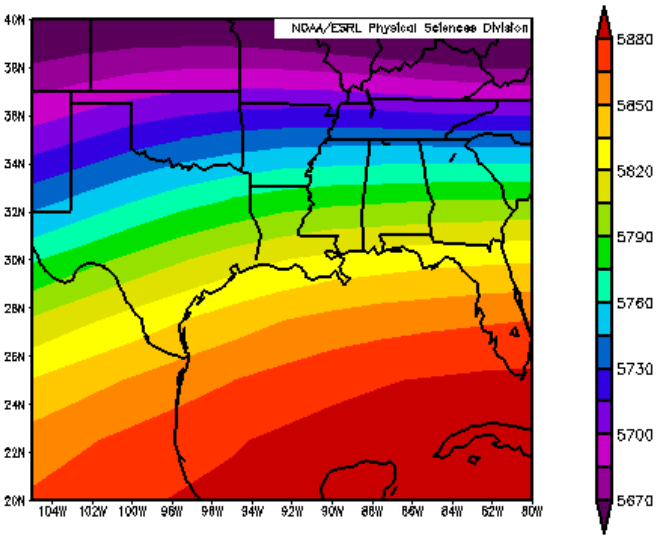

Figure 5.3. Synoptic Type 8 for all days (1971 – 2010).

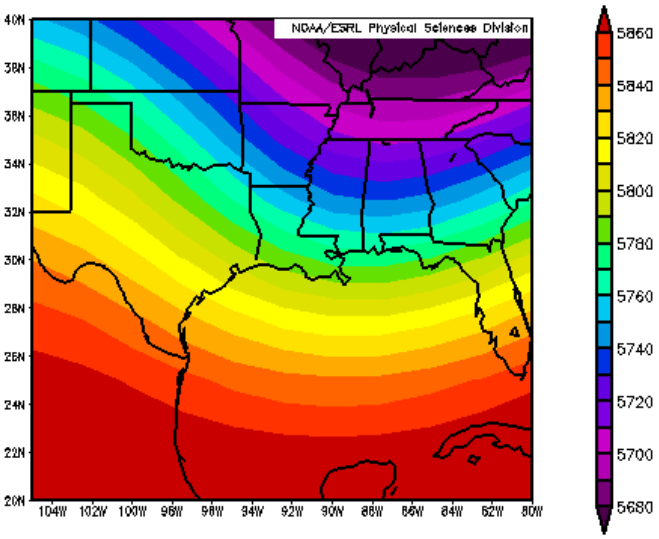

Figure 5.4. Synoptic Type 12 for all days (1971 – 2010).

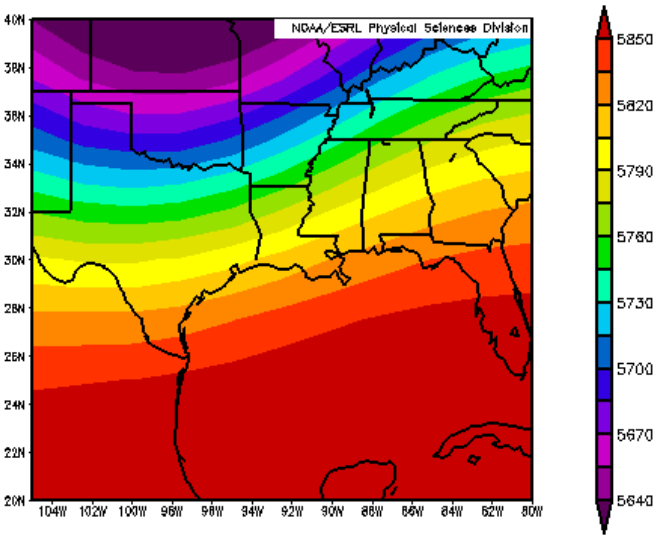

Figure 5.5. Synoptic Type 13 for all days (1971 – 2010).

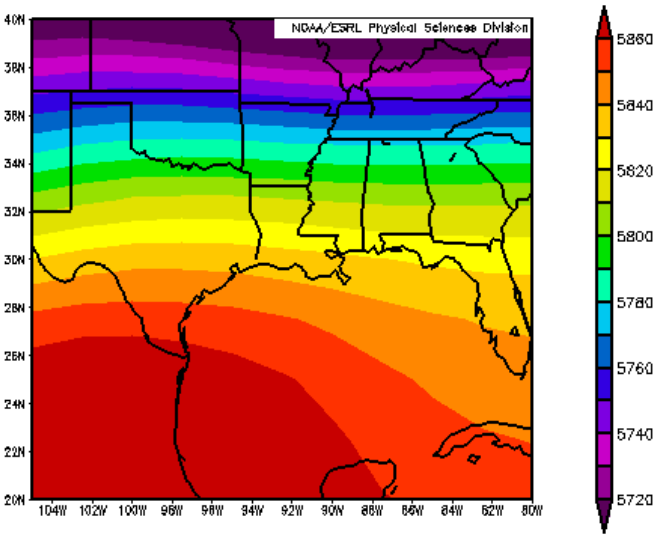

Figure 5.6. Synoptic Type 16 for all days (1971 – 2010).

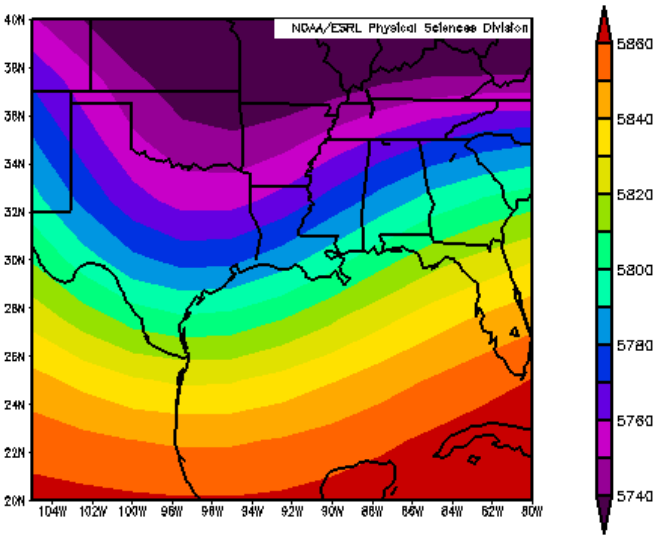

Figure 5.7. Synoptic Type 14 for all days (1971 – 2010).

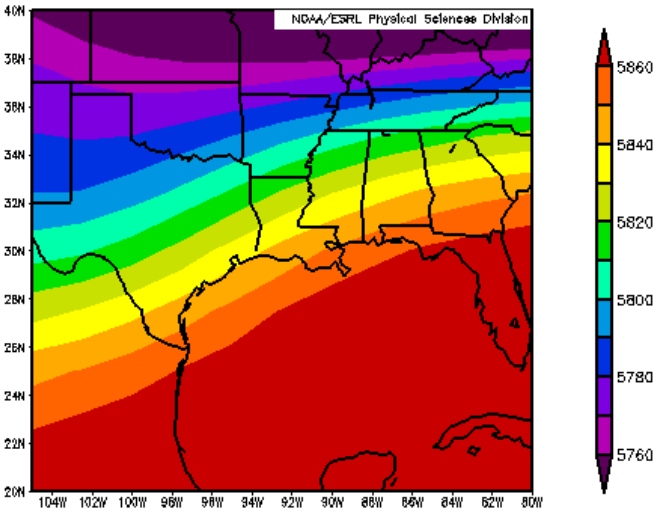

Figure 5.8. Synoptic Type 15 for all days (1971 – 2010).

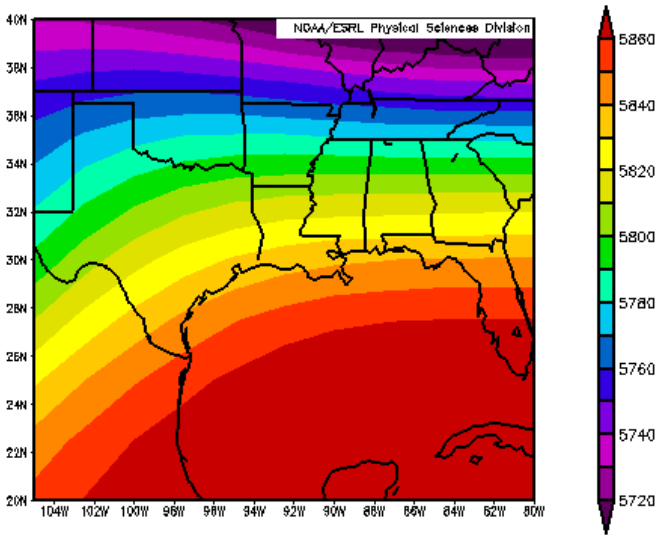

Figure 5.9. Synoptic Type 5 for all days (1971 – 2010).

5.4.2 Spatial Synoptic Classification

To supplement the results suggested by the eigenvector-based map pattern classification (PCA scheme), the Spatial Synoptic Classification (SSC) air mass classification scheme (Kalkstein et al. 1996, Sheridan 2002) was also employed. The SSC is based on a combination of manual and automated processes (Sheridan 2002). There are ten synoptic types within the SSC scheme (Table 5.2). The frequency of each of these types was determined for both bifurcation (Figure 5.10) and non-bifurcation days (Figure 5.11) for Atlanta, Columbus, and Dallas/Fort Worth.

On bifurcation days, Atlanta types are distributed between moist moderate (3 days), moist tropical (1 day) and transition days (1 day) (days on which two weather types were found to occur based on large shifts in pressure, dew point, and wind). Columbus only had two moist tropical days among its bifurcating heavy precipitation events (SSC data were missing for the one other event), while heavy precipitation bifurcating events in Dallas/Fort Worth had a wider

assortment of air masses represented: three dry moderate days, one moist moderate day, one moist polar day, three moist tropical days, and one transition day (i.e., between two air masses, but not necessarily because of a surface frontal passage). Heavy precipitation (≥ 25 mm) days between 2008 and 2009 on which no bifurcation occurred for any of the three sites were more widely-distributed among nine of the ten types (no dry polar types were found). The most frequently occurring type was moist moderate, although moist polar, moist tropical, and transition occurred frequently.

Table 5.2. The ten air mass classification types from the Synoptic Scale Classification (SSC) scheme (Kalkstein et al. 1996, Sheridan 2002).

Classification
Dry Moderate
Dry Polar
Dry Tropical
Moist Moderate
Moist Polar
Moist Tropical
Transition
Day is missing
Moist Tropical Plus
Moist Tropical Double Plus

The SSC scheme did not reveal discrimination among synoptic types for bifurcation vs. non-bifurcation days, likely due to the small number of bifurcation events. Based on these results, it is suspected that such a circulation-to-environment approach may not be optimal for such extreme events, but an environment-to-circulation methodology may allow for more effective discrimination between extreme events. In a final attempt to understand the synoptic controls of bifurcation days, composite maps of 500 hPa and 700 hPa geopotential heights were produced (Kalnay et al. 1996).

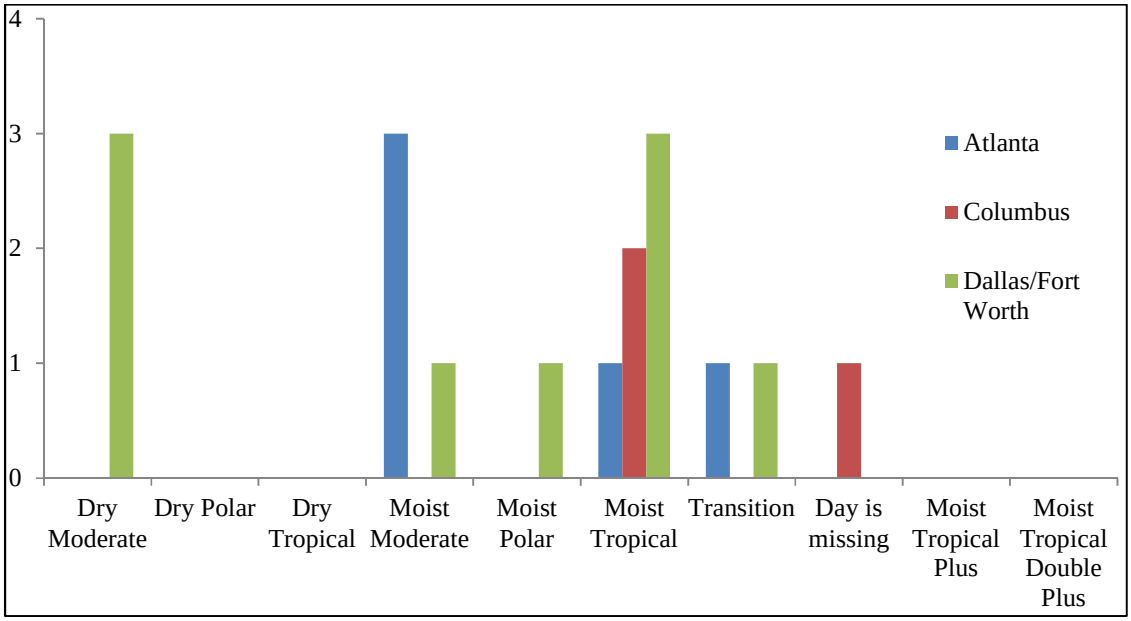

Figure 5.10. SSC classification types for bifurcation days (2008-2009).

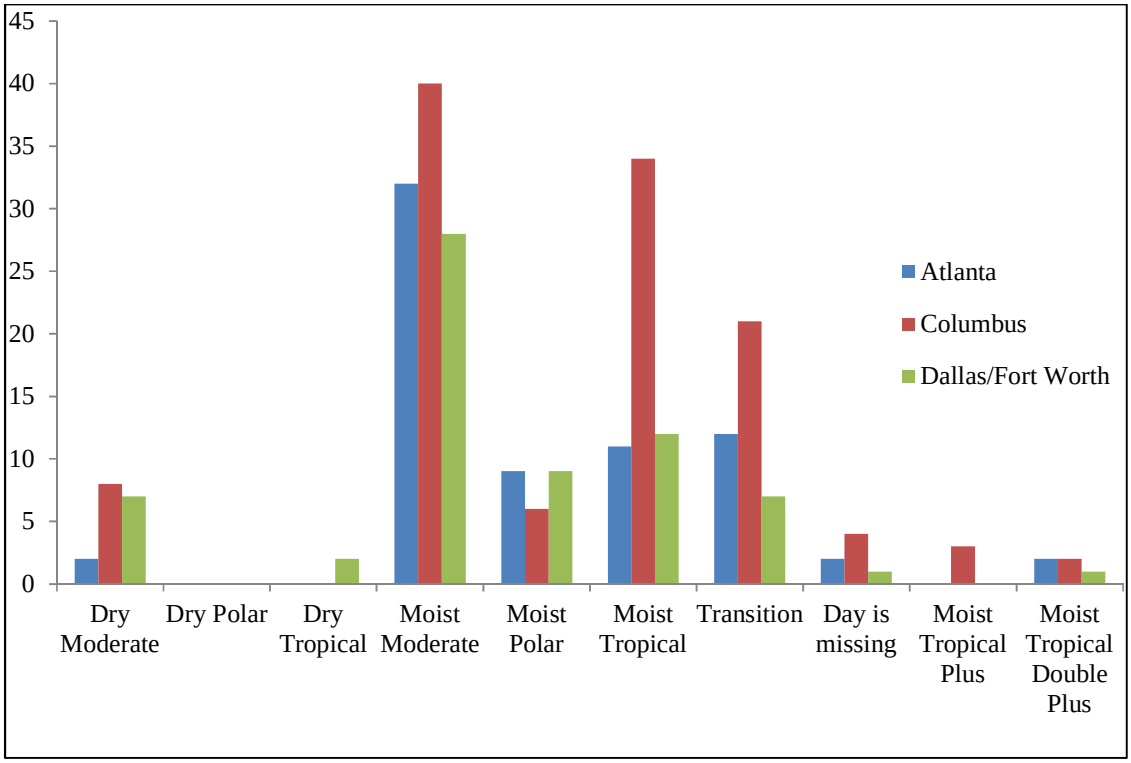

Figure 5.11. SSC classification types for non-bifurcation days (2008-2009).

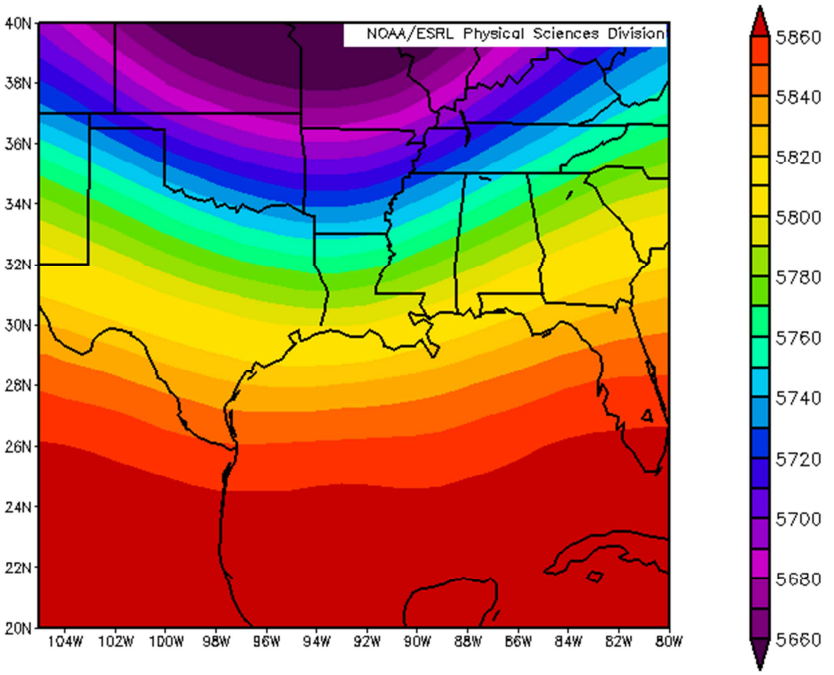

Figure 5.12. Atlanta 500 hPa composite.

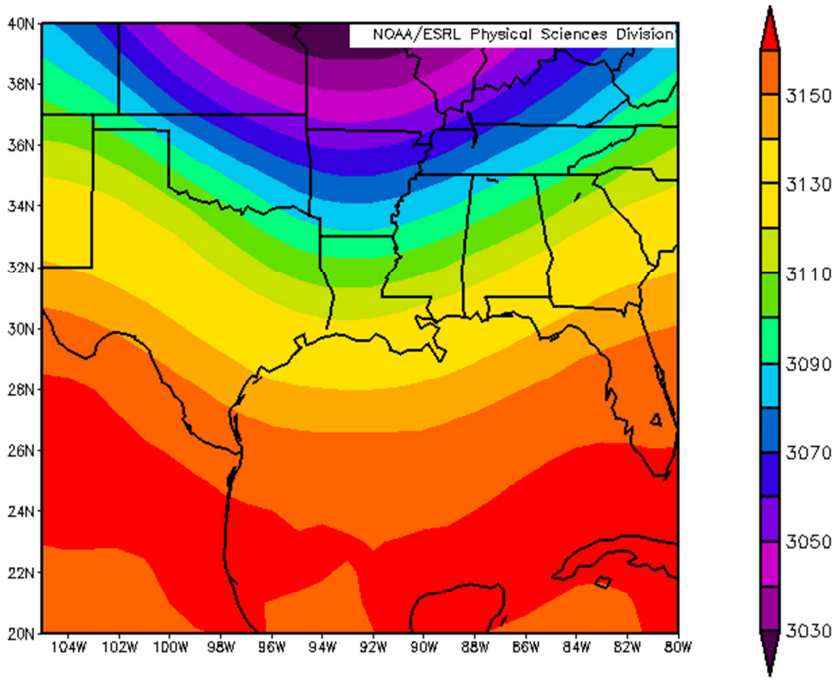

Figure 5.13. Atlanta 700 hPa composite.

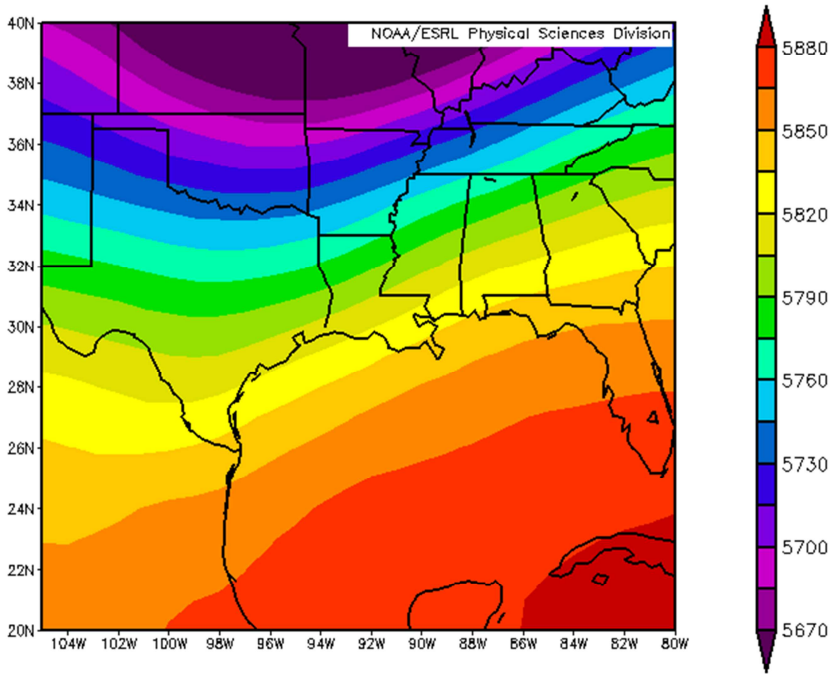

Figure 5.14. Columbus 500 hPa composite.

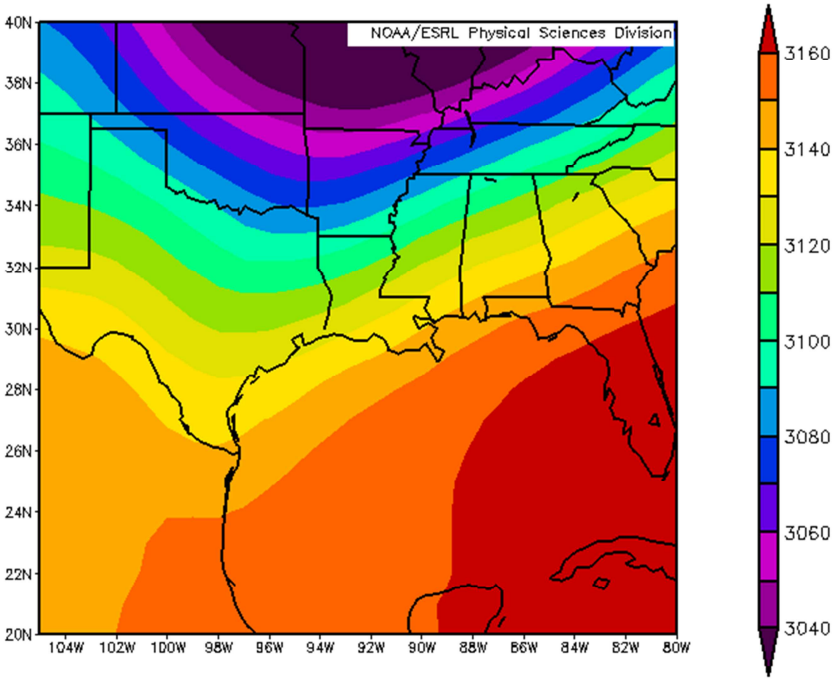

Figure 5.15. Columbus 700 hPa composite.

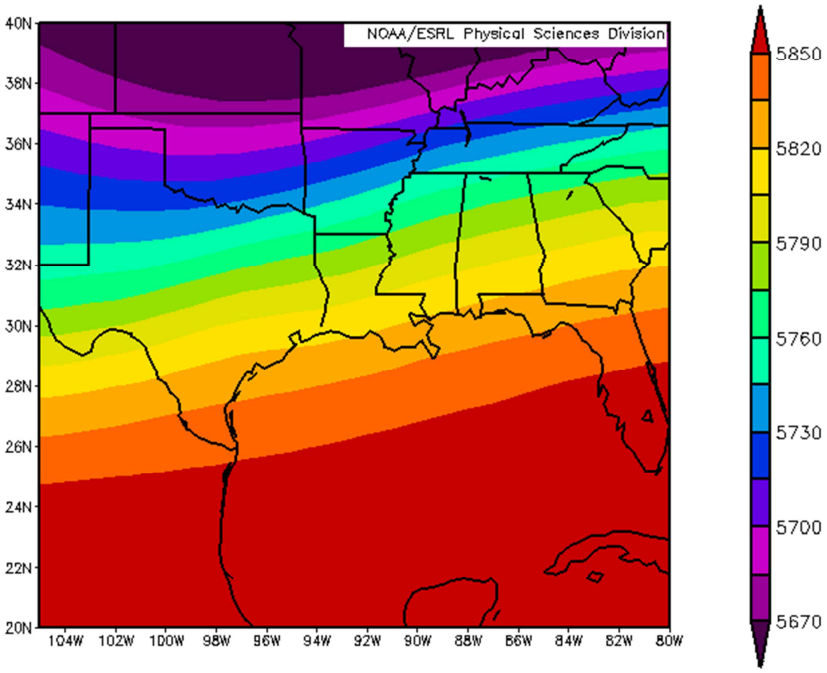

Figure 5.16. Dallas/Fort Worth 500 hPa composite.

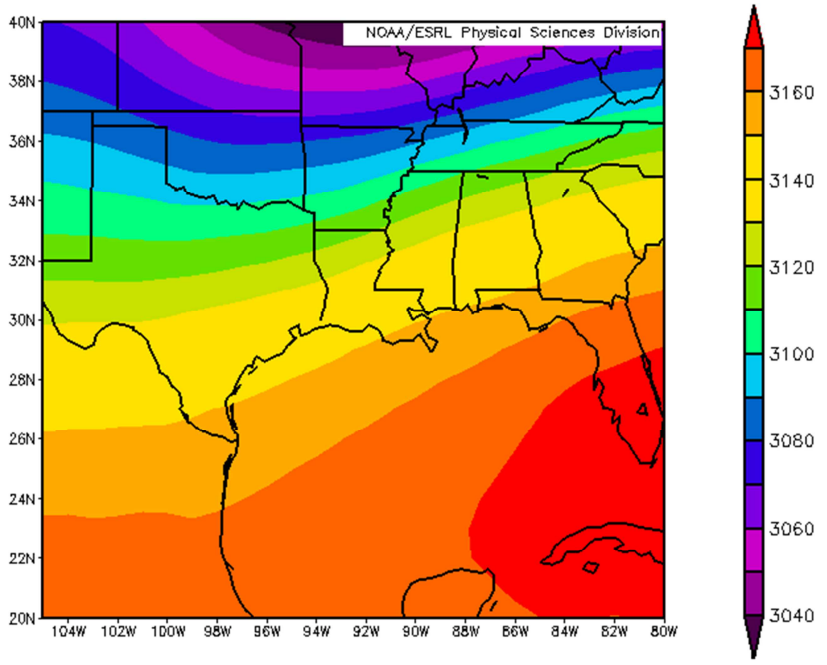

Figure 5.17. Dallas/Fort Worth 700 hPa composite.

5.5 Conclusion

Three attempts to understand the synoptic controls on bifurcation were made. The first circulation-to-environment approach -- the eigenvector-based map-pattern classification using PCA -- was very appropriate for analysis of heavy precipitation events as it showed trough-to-ridge circulation regimes and zones of strong geopotential height gradients as the dominating circulation types. The second circulation-to-environment approach -- the SSC scheme -- was inconclusive as it revealed no link between heavy precipitation bifurcation events and synoptic pattern. However, the low number of events meeting the criteria for inclusion in the analysis invites caution in the interpretation of this result. Nevertheless, it is possible that environment-to-circulation may be more appropriate for such rare, extreme events. Finally, composite 500 and 700 hPa geopotential heights during bifurcation days revealed that trough-to-ridge flow (implying upper-level support for a surface midlatitude wave cyclone) were most common among bifurcation days for Atlanta and Columbus. Dallas/Fort Worth exhibited a zonal flow, thereby displaying less upper-level support for surface frontal activity. These results suggest that upper-level support may be important, though not essential, in creating a bifurcation event. Surface roughness seems to be an important component of the phenomenon as well.

CHAPTER 6. CONCLUSION

6.1 Introduction

This study has expanded on previous work that focused on urban precipitation in the southeastern U.S. (Huff & Changnon 1973, Bornstein & Lin 2000, Shepherd et al. 2002, Burian & Shepherd 2005, Diem & Mote 2005, Diem 2006b, Mote et al. 2007, Hand & Shepherd 2009). The research generally affirms the notion that urban areas affect precipitation by altering the movement, growth, and demise of individual storm cells (Bornstein & Lin 2000). In addition, the bifurcation component of this research provided the most detailed insight to date on the mechanisms associated with urban storm bifurcation in various types of rainfall events in the southeastern United States. The derivation of an eigenvector-based map-pattern classification for this study, along with the use of the existing air-mass-based "Spatial Synoptic Classification" and compositing of atmospheric flow patterns on bifurcation days, has provided evidence that synoptic flow patterns are related to the existence or non-existence of urban bifurcation of storm events.

6.2 Precipitation Enhancement Study (Chapter 3)

6.2.1 Data and Methods

The three large and three smaller populated urban areas chosen (Atlanta, Houston, Dallas/Fort Worth, Tulsa, Memphis, and Birmingham) represent the various precipitation regimes in the southeastern U.S. and include previously studied locations to provide some precedent for the results (Keim 1996). These regimes include the prevalence of frontal systems and air-mass (convective) storms. Tropical systems are also important contributors of heavy

precipitation events in the region (Keim 1996). Data for days receiving 25 mm or greater precipitation were collected from all available stations within 100 kilometers of each city center. Three tests were employed to detect the existence of urban-enhanced precipitation: (1) "downwind *vs*. upwind" test, (2) temporal analysis, and (3) the "contour" test.

The "downwind *vs*. upwind" tests used mean 700 hPa wind direction for each day analyzed by city to determine the climatologically correct upwind and downwind sections. Two comparisons were made: (1) the "traditional test" and (2) the "90° test". For each heavy precipitation event, mean precipitation in the upwind and downwind stations was calculated. Differences in mean precipitation between the two areas were tested for statistical significance using a two-tailed Student's t-test and the Wilcoxon rank-sum test (a test equivalent to the Mann-Whitney u-test) in Matlab®. The second test used to detect precipitation enhancement, the "temporal analysis", tested for trends in the precipitation record of each study site using both the Poisson Process described in Keim & Cruise (1998) and a linear regression of the inter-arrival times between days in an annual frequency series (Keim & Cruise 1998). The "contour" test compared mean precipitation at non-urban stations to urban stations through a spatial interpolation using the inverse distance weighting (IDW) scheme. For each urban precipitation station, actual period-of-record-mean precipitation was compared to the corresponding interpolated value through the calculation of anomalies.

6.2.2 Results

For Atlanta, the traditional and 90° t-test did not reveal many significant differences between the upwind and downwind regions, either annually or in any of the four seasons. The only difference between the regions found using the u-test was at the 60 km buffer, with more precipitation received in the downwind region. The temporal test showed a high frequency of

extreme precipitation events in this region, but no significant trends were shown to occur. The contour test's spatial interpolation of non-urban stations "predicted" precipitation well at urban stations.

None of the traditional mean downwind *vs*. upwind differences were statistically significant for Birmingham using the t-test, while the u-test showed the 60 km summer and 40 km overall, summer, fall, and winter comparisons were significant. The 90° comparison showed no significant differences using the t-test while at the u-test showed the 60 km summer and 40 km overall as significant. The annual frequency series for Birmingham exhibited no trends as heavy precipitation days occurred consistently, while the contour test showed non-urban stations did not exhibit many differences with the interpolated urban precipitation.

For Dallas/Fort Worth, the "traditional" test showed significant differences at 100 km overall and winter, 80 km winter, and 60 km winter. The u-test revealed significant differences at 100 km spring and summer, 80 km spring and summer, 60 km summer, and 40 km spring and summer. The 90° t-test showed 40 km summer in addition to the same comparisons as seen in the traditional sections as significant. All u-test comparisons were found to be significant except 100 km, 80 km and 60 km summer and 40 km overall, spring, summer and fall. The annual frequency series shows a strong trend in the most extreme of precipitation days, with the highest number of events occurring in the last five years of the record, but because the data were not normally distributed, this trend may not indicate real changes occurring in the precipitation of the study region. The contour test showed a possible area of urban influence due to an under-prediction of urban precipitation by the non-urban stations.

The t-tests for Houston (traditional and 90°) showed significantly more precipitation in the downwind than upwind regions for 100 km, 80 km, and 60 km all in winter. Results for the

traditional u-test showed significant differences between upwind and downwind regions for the 100 km overall and winter, 80 km overall, spring, and winter, 60 km overall and winter, and 40 km overall and winter. The 90° u-test showed only the 100 km fall comparison to be significant. The annual frequency series showed no trends in extreme events, and the contour test did not produce any unexpected patterns based upon the interpolation of non-urban stations.

The t-test for the traditional comparisons at Memphis showed statistically significant downwind *vs*. upwind differences for 100 km overall and summer, 80 km overall, 60 km overall, spring, and winter, and for overall and all-season precipitation on heavy precipitation days at 40 km. Results from the u-tests showed all downwind *vs*. upwind comparisons as significant. Results from the 90° t-tests show overall precipitation at 100 km, 80 km, 60 km, and 40 km to be significant in addition to 40 km spring and winter. The u-test results showed significance for all comparisons except the 60 km and 40 km summer. A plot of the annual frequency series revealed no trends. The non-urban interpolation predicted the urban precipitation fairly well at all buffers as the contours of the interpolations corresponded consistently.

On heavy precipitation days in Tulsa, the only "traditional" test comparison found to be statistically significant using the t-test is 100 km overall precipitation. The u-test revealed only overall precipitation at 100 km and 80 km to be significant. Results from the 90° t-test showed significant differences between upwind and downwind heavy precipitation days for 100 km overall and 40 km overall and spring. The u-test showed significant differences for these same comparisons in addition to 100 km summer. The annual frequency series displayed no trend of the inter-arrival times. The contour test showed precipitation at some urban stations measuring higher precipitation that is not seen when interpolating precipitation at non-urban stations (for the 80 km and 60 km buffer).

Houston, Memphis, and Tulsa were the only cities to exhibit possible urban influence (urban influence seen for one out of the three tests), while Birmingham showed stronger evidence of urban influence (urban influence seen for two out of the three tests). Dallas/Fort Worth was the only city to show likely urban influence (urban influence seen for three out of the three tests) while little evidence of urban influence was found for Atlanta based upon the tests employed in this study.

6.3 Bifurcation Detection Study (Chapter 4)

6.3.1 Data and Methods

The bifurcation detection study used radar-derived precipitation estimates to identify storms during the years 2008 and 2009 which could be bifurcating. The base reflectivity of each day experiencing heavy precipitation ($\geq$ 25 mm) was analyzed spatially for evidence of bifurcation around the central business district (CBD). Storm precipitation totals for each of these bifurcation events were then used to compare precipitation in the periphery of the urban area to that of the core. If a larger amount of precipitation in the periphery is found then it is possible that bifurcation has occurred. In Test 1, the urban core included all sections within 40 km while the periphery included the sections between the 40 km and 100 km buffers. In Test 2, the urban core included all sections within 60 km while the periphery contained the sections between the 60 km and 100 km buffers. In Test 3, the urban core included all sections within 80 km while the periphery comprised the sections between the 80 km and 100 km buffers.

6.3.2 Results

Eight of the 69 events in Atlanta were thought to experience bifurcation, and the t-test results showed precipitation averages in the southeastern sectors to differ significantly from the

core. The t-test results of the non-bifurcation events showed no periphery sections to have statistically different precipitation from the core.

Nine of the 76 events in Dallas/Fort Worth bifurcated, and the t-test identified two sections, located to the west and east of the core, with significantly different precipitation from core precipitation. Periphery sections for the non-bifurcation events were located near those showing significance for the bifurcation events.

Only two of the 113 events for Columbus experienced bifurcation. No periphery sections from the bifurcation events were significant, but the t-test results of the non-bifurcation events showed many sections to have statistically significantly different precipitation from that in the core (located to the north, east, and south of the CBD).

This study suggests that bifurcation is likely occurring for Atlanta, but due to the rarity of these events, statistical testing is difficult and unlikely to disprove the existence of bifurcation. Results confirmed evidence of bifurcation in Atlanta suggested by recent literature (Dixon & Mote 2003). Little convincing evidence for bifurcation occurred for Dallas/Fort Worth, unless opposing factors masked the effects of bifurcation. Bifurcation is unlikely to exist for the Columbus study area, as only two possible events were found.

6.4 Synoptic Analysis Study

6.4.1 Data and Methods

Three attempts were made to understand the relationship between heavy precipitation days and upper-air circulation for Atlanta, Dallas/Fort Worth, and Columbus. The first attempt involved an eigenvector-based map-pattern analysis, and used daily 500 hPa geopotential heights (1971 – 2010) to identify the synoptic types most directly linked to heavy precipitation events in

the study area. The second attempt involved the use of the Spatial Synoptic Circulation (SSC) for the heavy precipitation days in 2008 – 2009, to confirm results of the eigenvalue-based map-pattern classification. The final attempt involved developing composites of 500 hPa and 700 hPa geopotential heights for days of heavy precipitation (≥ 25 mm) when bifurcation was observed at each of the three sites individually.

6.4.2 Results

The map-pattern classification produced 17 different synoptic types. The most dominant synoptic types associated with heavy precipitation days for the three cities show a nearby trough-to-ridge side of a Rossby wave and a strong geopotential height gradient which may be associated with baroclinic zones. Dallas/Fort Worth also experienced a very deep trough, likely to produce heavy precipitation events similar to the trough-to-ridge types. It is important to remember that the types consist of averages of the atmospheric circulation for heavy precipitation days, but the within-type variability could be great between each event.

The Spatial Synoptic Classification (SSC) scheme for Atlanta events showed types distributed between moist moderate (3 days), moist tropical (1 day) and the transition type (1 day). Columbus only had two moist tropical days, and Dallas/Fort Worth had three dry moderate days, one moist moderate day, one moist polar day, three moist tropical days, and one transition day. Non-bifurcating heavy precipitation (≥ 25 mm) days were more widely-distributed among nine of the ten types (no dry polar types occurred). The most frequently occurring type was moist moderate, although moist polar, moist tropical, and transition occurred frequently.

With the 500 hPa and 700 hPa composites of bifurcation days for Atlanta, a trough was found approaching the study area. Similarly, an approaching trough occurred for Columbus. The composites of Dallas/Fort Worth bifurcation days also showed a trough, but it was weaker

than that in Atlanta or Columbus with quasi-zonal flow. These results suggest that upper-level support may be important, though not essential, in creating a bifurcation event. Surface roughness seems to be an important component of the phenomenon.

6.5 Implications and Future Research

The cities in which the precipitation enhancement study showed evidence of urban influences on precipitation were: Birmingham, Dallas/Fort Worth, Memphis, and Tulsa. Possible urban influence was found for Houston. The signal of urban enhanced precipitation was weaker than expected for Atlanta. Because the results do not seem to be dependent on the size of the city, precipitation enhancement is likely to be attributed to factors other than population alone, such as the area of impervious land cover, leading to an urban heat island, or the built environment, resulting in areas of divergence (upwind) and convergence (downwind).

The bifurcation study showed that storm bifurcation is likely occurring in Atlanta, and possibly occurring in Dallas/Fort Worth but could be masked by other climatological features (competing multiple CBDs) or the location of the radar (causing possible bifurcation events to be missed). The control site, Columbus, showed only two bifurcation events but precipitation in the non-urban, periphery was shown to be statistically different from that in the CBD. It was concluded that this was the natural background signal of precipitation for the region. Limitations to the bifurcation analysis include difficulties presented by the “cone of silence”, the inability of radar to detect precipitation directly above, the small number of bifurcation days, and the need for a longer period of record for analysis.

The synoptic analysis study showed that ridge-to-trough and strong geopotential height gradients were the most influencing type for heavy precipitation days, and bifurcation days, for

Atlanta, Dallas/Fort Worth, and Columbus. However, because the number of bifurcation events uncovered in this study was very small, an environment-to-circulation approach may be a better approach to relate these events to synoptic circulation.

Future research could expand upon the results of this study in numerous ways. The precipitation enhancement study could benefit by including even more urban sites in the analysis. This would allow for more connections to be made between urban type (e.g., cities exhibiting a small or large population, large surface area, great surface roughness) and enhanced downwind precipitation. Also, an increased resolution of precipitation stations would improve the representation of the rainfall signal in the CBD, which is usually represented by a small number of stations compared to the non-urban surroundings, or by utilizing radar-based precipitation estimates. The bifurcation detection study could be improved in two ways. First, adding more years to the analysis would allow for identification of more potential events. This would improve the ability of statistical testing to "prove" the existence of bifurcation. Second, the heavy precipitation events in this study that were tested for bifurcation were based on station data. Inconsistencies in the record led to analysis of days that did not even receive precipitation. Using a combination of station and radar data to detect heavy precipitation days would "weed out" the flaws in the observation record. The synoptic characteristics study could be improved through the increase in the number of bifurcation days analyzed, allowing for more distinction between synoptic types, as it is possible that bifurcation may occur more frequently with weaker synoptic storms.

Overall, the results of this research contribute to the urban precipitation literature. By repeating and expanding on methods seen in the literature, the precipitation enhancement study showed possible urban influence in cities that have not been widely studied (Birmingham,

Memphis, and Tulsa). This study also allowed for the confirmation of results seen in Atlanta by some authors (Diem & Mote 2005, Diem 2006b, 2008) and calls into question the strength of urban enhancement detected by others (Shepherd et al. 2002, Lacke et al. 2009, Shem & Shepherd 2009). Being the first study to focus on storm bifurcation, this research contributed a methodology that can be replicated and improved for future bifurcation analyses. In addition to the contributions this research makes to the field of urban climatology, a deeper understanding of the role of urban areas on their local and regional climate has been gained. This role should be taken into consideration as cities in the southeastern United States continue to grow at such a rapid rate, possibly influencing other atmospheric features and interconnections with other components of the climate system.

REFERENCES

Arnfield AJ (2003) Two decades of urban climate research: A review of turbulence, exchanges of energy and water, and the urban heat island. International Journal of Climatology 23: 1-26

Asaeda T, Ca VT, Wake A (1996) Heat storage of pavement and its effect on the lower atmosphere. Atmospheric Environment 30: 413-427

Atkinson BW (2003) Numerical modelling of urban heat-island intensity. Boundary-Layer Meteorology 109: 285-310

Basara JB, Hall PK, Schroeder AJ, Illston BG, Nemunaitis KL (2008) Diurnal cycle of the Oklahoma City urban heat island. Journal of Geophysical Research-Atmospheres 113: 16

Bell TL, Rosenfeld D, Kim KM (2009) Weekly cycle of lightning: Evidence of storm invigoration by pollution. Geophysical Research Letters 36: 1-5

Bell TL, Rosenfeld D, Kim KM, Yoo JM, Lee MI, Hahnenberger M (2008) Midweek increase in US summer rain and storm heights suggests air pollution invigorates rainstorms. Journal of Geophysical Research-Atmospheres 113: 1-22

Bentley ML, Ashley W, Stallins JA (2010) Climatological radar delineation of urban convection for Atlanta, Georgia. International Journal of Climatology 30: 1589-1594

Bloomfield P, Davis JM (1994) Orthogonal rotation of complex principal components. International Journal of Climatology 14: 759-775

Bornstein R, Lin QL (2000) Urban heat islands and summertime convective thunderstorms in Atlanta: three case studies. Atmospheric Environment 34: 507-516

Bornstein RD, LeRoy M (1990) Urban barrier effects on convective and frontal thunderstorms. Extended Abstracts, Fourth Conf on Mesoscale Processes: 120–121

Buell CE (1975) The topography of empirical orthogonal functions. In. Proc Fourth Conference on Probability and Statistics in Atmospheric Science, American Meteorological Society

Buell CE (1979) On the physical interpretation of empirical orthogonal functions. In. Proc Sixth Conference on Probability and Statistics in Atmospheric Science, American Meteorological Society

Burian SJ, Shepherd JM (2005) Effect of urbanization on the diurnal rainfall pattern in Houston. Hydrological Processes 19: 1089-1103

Cannon AJ, Whitfield PH, Lord ER (2002) Synoptic map-pattern classification using recursive partitioning and principal component analysis. Monthly Weather Review 130: 1187-1206

Carlson TN, Arthur ST (2000) The impact of land use - land cover changes due to urbanization on surface microclimate and hydrology: a satellite perspective. Global and Planetary Change 25: 49-65

Carraca MGD, Collier CG (2007) Modelling the impact of high-rise buildings in urban areas on precipitation initiation. Meteorological Applications 14: 149-161

Carrio GG, Cotton WR (2011) Urban growth and aerosol effects on convection over Houston. Part II: Dependence of aerosol effects on instability. Atmospheric Research 102: 167-174

Carrio GG, Cotton WR, Cheng WYY (2010) Urban growth and aerosol effects on convection over Houston Part I: The August 2000 case. Atmospheric Research 96: 560-574

Changnon SA (1976) Comparison of Urban Climatic Modifications in 3 Cities. Atmospheric Environment 10: 494-494

Changnon SA (2003) Urban modification of freezing-rain events. Journal of Applied Meteorology 42: 863-870

Changnon SA, Huff FA, Semonin RG (1971) Metromex - investigation of inadvertent weather modification. Bulletin of the American Meteorological Society 52: 958-967

Changnon SA, Shealy RT, Scott RW (1991) Precipitation changes in fall, winter, and spring caused by St. Louis. Journal of Applied Meteorology 30: 126-134

Cheng YY, Byun DW (2008) Application of high resolution land use and land cover data for atmospheric modeling in the Houston-Galveston metropolitan area, Part I: Meteorological simulation results. Atmospheric Environment 42: 7795-7811

Childs PP, Raman S (2005) Observations and numerical simulations of urban heat island and sea breeze circulations over New York City. Pure and Applied Geophysics 162: 1955-1980

Chow VT (1954) The log probability law and its engineering application. Proceedings of the American Society of Civil Engineers 80: 1-25

Comrie AC (1996) An all-season synoptic climatology of air pollution in the US-Mexico border region. Professional Geographer 48: 237-251

Comrie AC (2000) Mapping a wind-modified urban heat island in Tucson, Arizona (with comments on integrating research and undergraduate learning). Bulletin of the American Meteorological Society 81: 2417-2431

Craddock JM, Flood CR (1969) Eigenvectors for representing 500-MB geopotential surface over northern hemisphere. Quarterly Journal of the Royal Meteorological Society 95: 576-593

Cuell C, Bonsal B (2009) An assessment of climatological synoptic typing by principal component analysis and kmeans clustering. Theoretical and Applied Climatology 98: 361-373

Dabberdt WF, Hales J, Zubrick S, Crook A, Krajewski W, Doran JC, Mueller C, King C, Keener RN, Bornstein R, Rodenhuis D, Kocin P, Rossetti MA, Sharrocks F, Stanley EM (2000) Forecast issues in the urban zone: Report of the 10th Prospectus Development Team of the US Weather Research Program. Bulletin of the American Meteorological Society 81: 2047-2064

Davis JM, Estis FL, Bloomfield P, Monahan JF (1991) Complex principal component analysis of sea-level pressure over the eastern USA. International Journal of Climatology 11: 27-54

Davis RE, Kalkstein LS (1990) Using a spatial synoptic climatological classification to assess changes in atmospheric-pollution concentrations. Physical Geography 11: 320-342

Dettwiller J, Changnon SA (1976) Possible urban effects on maximum daily rainfall at Paris, St. Louis and Chicago. Journal of Applied Meteorology 15: 517-519

Diaz HF (1981) Eigenvector analysis of seasonal temperature, precipitation, and synoptic-scale system frequency over the contiguous United States 2. spring, summer, fall and annual. Monthly Weather Review 109: 1285-1304

Diaz HF, Fulbright DC (1981) Eigenvector analysis of seasonal temperature, precipitation, and synoptic-scale system frequency over the contiguous United States 1. winter. Monthly Weather Review 109: 1267-1284

Diem JE (2006a) Anomalous monsoonal activity in central Arizona, USA. Geophysical Research Letters 33: L16706, 16710.11029/12006GL027259

Diem JE (2006b) Synoptic-scale controls of summer precipitation in the Southeastern United States. Journal of Climate 19: 613-621

Diem JE (2008) Detecting summer rainfall enhancement within metropolitan Atlanta, Georgia USA. International Journal of Climatology 28: 129-133

Diem JE, Brown DP (2003) Anthropogenic impacts on summer precipitation in central Arizona, USA. Professional Geographer 55: 343-355

Diem JE, Mote TL (2005) Interepochal changes in summer precipitation in the southeastern United States: Evidence of possible urban effects near Atlanta, Georgia. Journal of Applied Meteorology 44: 717-730

Diffenbaugh NS (2009) Influence of modern land cover on the climate of the United States. Climate Dynamics 33: 945-958

Dixon PG, Mote TL (2003) Patterns and causes of Atlanta's urban heat island-initiated precipitation. Journal of Applied Meteorology 42: 1273-1284

Dvorak B, Volder A (2010) Green roof vegetation for North American ecoregions: A literature review. Landscape and Urban Planning 96: 197-213

Freitas ED, Rozoff CM, Cotton WR, Dias PLS (2007) Interactions of an urban heat island and sea-breeze circulations during winter over the metropolitan area of Sao Paulo, Brazil. Boundary-Layer Meteorology 122: 43-65

Gero AF, Pitman AJ, Narisma GT, Jacobson C, Pielke RA (2006) The impact of land cover change on storms in the Sydney Basin, Australia. Global and Planetary Change 54: 57-78

Givati A, Rosenfeld D (2004) Quantifying precipitation suppression due to air pollution. Journal of Applied Meteorology 43: 1038-1056

Givoni B (1994) Urban design for hot humid regions. Renewable Energy 5: 1047-1053

Gomez F, Gil L, Jabaloyes J (2004) Experimental investigation on the thermal comfort in the city: relationship with the green areas, interaction with the urban microclimate. Building and Environment 39: 1077-1086

Greene JS, Kalkstein LS, Ye H, Smoyer K (1999) Relationships between synoptic climatology and atmospheric pollution at 4 US cities. Theoretical and Applied Climatology 62: 163-174

Grimmond CSB, King TS, Roth M, Oke TR (1998) Aerodynamic roughness of urban areas derived from wind observations. Boundary-Layer Meteorology 89: 1-24

Grimmond CSB, Souch C, Hubble MD (1996) Influence of tree cover on summertime surface energy balance fluxes, San Gabriel Valley, Los Angeles. Climate Research 6: 45-57

Hamada S, Ohta T (2010) Seasonal variations in the cooling effect of urban green areas on surrounding urban areas. Urban Forestry & Urban Greening 9: 15-24

Hand LM, Shepherd JM (2009) An Investigation of warm-season spatial rainfall variability in Oklahoma City: Possible linkages to urbanization and prevailing wind. Journal of Applied Meteorology and Climatology 48: 251-269

Hawkins TW, Brazel AJ, Stefanov WL, Bigler W, Saffell EM (2004) The role of rural variability in urban heat island determination for Phoenix, Arizona. Journal of Applied Meteorology 43: 476-486

Hicks BB, Callahan WJ, Hoekzema MA (2010) On the Heat Islands of Washington, DC, and New York City, NY. Boundary-Layer Meteorology 135: 291-300

Hidalgo J, Pigeon G, Masson V (2008) Urban-breeze circulation during the CAPITOUL experiment: observational data analysis approach. Meteorology and Atmospheric Physics 102: 223-241

Hirano Y, Yasuoka Y, Ichinose T (2004) Urban climate simulation by incorporating satellite-derived vegetation cover distribution into a mesoscale meteorological model. Theoretical and Applied Climatology 79: 175-184

Hobbs PV, Radke LF, Shumway SE (1970) Cloud condensation nuclei from industrial sources and their apparent influence on precipitation in Washington state. Journal of the Atmospheric Sciences 27: 81-89

Huff FA, Changnon SA (1973) Precipitation modification by major urban areas. Bulletin of the American Meteorological Society 54: 1220-1232

Huff FA, Vogel JL (1978) Urban, topographic and diurnal effects on rainfall in St. Louis region. Journal of Applied Meteorology 17: 565-577

Huff FA, Vogel JL (1979) Urban, topographic and diurnal effects on rainfall in the St. Louis region - Reply. Journal of Applied Meteorology 18: 375-378

Illinois State Water Survey (1974) Metromex - Overview of Illinois State Water Survey projects. Bulletin of the American Meteorological Society 55: 89-90

Imhoff ML, Zhang P, Wolfe RE, Bounoua L (2010) Remote sensing of the urban heat island effect across biomes in the continental USA. Remote Sensing of Environment 114: 504-513

Jauregui E, Romales E (1996) Urban effects on convective precipitation in Mexico City. Atmospheric Environment 30: 3383-3389

Jirak IL, Cotton WR (2006) Effect of air pollution on precipitation along the front range of the Rocky Mountains. Journal of Applied Meteorology and Climatology 45: 236-245

Kalkstein LS, Nichols MC, Barthel CD, Greene JS (1996) A new spatial synoptic classification: Application to air-mass analysis. International Journal of Climatology 16: 983-1004

Kalkstein LS, Tan GR, Skindlov JA (1987) An evaluation of 3 clustering procedures for use in synoptic climatological classification. Journal of Climate and Applied Meteorology 26: 717-730

Kalnay E, Kanamitsu M, Kistler R, Collins W, Deaven D, Gandin L, Iredell M, Saha S, White G, Woollen J, Zhu Y, Chelliah M, Ebisuzaki W, Higgins W, Janowiak J, Mo KC, Ropelewski C, Wang J, Leetmaa A, Reynolds R, Jenne R, Joseph D (1996) The NCEP/NCAR 40-year reanalysis project. Bulletin of the American Meteorological Society 77: 437-471

Karl TRM, Jerry M.; Peterson, Thomas C.; (2009) Global Climate Change Impacts in the United States. Cambridge University Press

Kassomenos P, Vardoulakis S, Borge R, Lumbreras J, Papaloukas C, Karakitsios S (2010) Comparison of statistical clustering techniques for the classification of modelled atmospheric trajectories. Theoretical and Applied Climatology 102: 1-12

Keim BD (1996) Spatial, synoptic, and seasonal patterns of heavy rainfall in the southeastern United States. Physical Geography 17: 313-328

Keim BD (1997) Preliminary analysis of the temporal patterns of heavy rainfall across the southeastern United States. Professional Geographer 49: 94-104

Keim BD, Cruise JF (1998) A technique to measure trends in the frequency of discrete random events. Journal of Climate 11: 848-855

Keim BD, Muller RA (2009) Hurricanes of the Gulf of Mexico. Louisiana State University Press

Kishtawal C, Niyogi D, Lei M, Shepherd M, Entin J (2010) A novel radar-based analysis of urban-induced convergence: A possible explanation of the downwind urban rainfall anomaly. Geophysical Research Letters: 1-15

Kurtzman D, Scanlon BR (2007) El Niño-Southern Oscillation and Pacific Decadal Oscillation impacts on precipitation in the southern and central United States: Evaluation of spatial distribution and predictions. Water Resources Research 43: 1-12

Lacke MC, Mote TL, Shepherd JM (2009) Aerosols and associated precipitation patterns in Atlanta. Atmospheric Environment 43: 4359-4373

Lamptey B (2010) An analytical framework for estimating the urban effect on climate. International Journal of Climatology 30: 72-88

Li GH, Wang Y, Lee KH, Diao YW, Zhang RY (2009) Impacts of aerosols on the development and precipitation of a mesoscale squall line. Journal of Geophysical Research-Atmospheres 114: 1-18

Loose T, Bornstein RD (1977) Observations of mesoscale effects on frontal movement through an urban area. Monthly Weather Review 105: 563-571

Matzarakis A, Endler C (2010) Climate change and thermal bioclimate in cities: impacts and options for adaptation in Freiburg, Germany. International Journal of Biometeorology 53: 479-483

McCarthy MP, Best MJ, Betts RA (2010) Climate change in cities due to global warming and urban effects. Geophysical Research Letters 37: 5

Mesinger F, DiMego G, Kalnay E, Mitchell K, Shafran PC, Ebisuzaki W, Jovic D, Woollen J, Rogers E, Berbery EH, Ek MB, Fan Y, Grumbine R, Higgins W, Li H, Lin Y, Manikin G, Parrish D, Shi W (2006) North American regional reanalysis. Bulletin of the American Meteorological Society 87: 343-+

Mo KC, Schemm JE (2008) Relationships between ENSO and drought over the southeastern United States. Geophysical Research Letters 35: 1-5

Mote TL, Lacke MC, Shepherd JM (2007) Radar signatures of the urban effect on precipitation distribution: A case study for Atlanta, Georgia. Geophysical Research Letters 34: 1-4

NASA and the Japan Aerospace Exploration Agency (JAXA) Tropical Rainfall Measuring Mission (TRMM). http://trmm.gsfc.nasa.gov/

Ntelekos AA, Smith JA, Krajewski WF (2007) Climatological analyses of thunderstorms and flash floods in the Baltimore metropolitan region. Journal of Hydrometeorology 8: 88-101

Oke TR (1973) City size and urban heat island. Atmospheric Environment 7: 769-779

Oke TR (1987) Boundary Layer Climates. London: Methuen

Orville RE, Huffines G, Nielsen-Gammon J, Zhang RY, Ely B, Steiger S, Phillips S, Allen S, Read W (2001) Enhancement of cloud-to-ground lightning over Houston, Texas. Geophysical Research Letters 28: 2597-2600

Rajasekar U, Weng QH (2009) Urban heat island monitoring and analysis using a non-parametric model: A case study of Indianapolis. Isprs Journal of Photogrammetry and Remote Sensing 64: 86-96

Ramanathan V, Crutzen PJ, Kiehl JT, Rosenfeld D (2001) Atmosphere - Aerosols, climate, and the hydrological cycle. Science 294: 2119-2124

Rose LS, Stallins JA, Bentley ML (2008) Concurrent Cloud-to-Ground Lightning and Precipitation Enhancement in the Atlanta, Georgia (United States), Urban Region. Earth Interactions 12: 1-30

Rosenfeld AH, Akbari H, Bretz S, Fishman BL, Kurn DM, Sailor D, Taha H (1995) Mitigation of urban heat islands - materials, utility programs, updates. Energy and Buildings 22: 255-265

Rosenfeld D, Givati A (2006) Evidence of orographic precipitation suppression by air pollution-induced aerosols in the western United States. Journal of Applied Meteorology and Climatology 45: 893-911

Rosenfeld D, Lohmann U, Raga GB, O'Dowd CD, Kulmala M, Fuzzi S, Reissell A, Andreae MO (2008a) Flood or drought: How do aerosols affect precipitation? Science 321: 1309-1313

Rosenfeld D, Woodley WL, Axisa D, Freud E, Hudson JG, Givati A (2008b) Aircraft measurements of the impacts of pollution aerosols on clouds and precipitation over the Sierra Nevada. Journal of Geophysical Research-Atmospheres 113: 1-23

Seager R, Tzanova A, Nakamura J (2009) Drought in the southeastern United States: causes, variability over the last millennium, and the potential for future hydroclimate change. Journal of Climate 22: 5021-5045

Shashua-Bar L, Hoffman ME (2000) Vegetation as a climatic component in the design of an urban street - An empirical model for predicting the cooling effect of urban green areas with trees. Energy and Buildings 31: 221-235

Shem W, Shepherd M (2009) On the impact of urbanization on summertime thunderstorms in Atlanta: Two numerical model case studies. Atmospheric Research 92: 172-189

Shepherd JM (2005) A review of current investigations of urban-induced rainfall and recommendations for the future. Earth Interactions 9: 1-27

Shepherd JM (2006) Evidence of urban-induced precipitation variability in arid climate regimes. Journal of Arid Environments 67: 607-628

Shepherd JM, Carter M, Manyin M, Messen D, Burian S (2010) The impact of urbanization on current and future coastal precipitation: a case study for Houston. Environment and Planning B-Planning & Design 37: 284-304

Shepherd JM, Pierce H, Negri AJ (2002) Rainfall modification by major urban areas: Observations from spaceborne rain radar on the TRMM satellite. Journal of Applied Meteorology 41: 689-701

Sheridan SC (2002) The redevelopment of a weather-type classification scheme for North America. International Journal of Climatology 22: 51-68

Skinner WR, Flannigan MD, Stocks BJ, Martell DL, Wotton BM, Todd JB, Mason JA, Logan KA, Bosch EM (2002) A 500 hPa synoptic wildland fire climatology for large Canadian forest fires, 1959-1996. Theoretical and Applied Climatology 71: 157-169

Souch C, Grimmond S (2006) Applied climatology: urban climate. Progress in Physical Geography 30: 270-279

Svoma BM, Balling RC (2009) An anthropogenic signal in Phoenix, Arizona winter precipitation. Theoretical and Applied Climatology 98: 315-321

Svoma BM, Brazel A (2010) Urban effects on the diurnal temperature cycle in Phoenix, Arizona. Climate Research 41: 21-29

Our City. The City of Tulsa (2012). http://www.cityoftulsa.org/our-city/our-city-overview.aspx

Thielen J, Wobrock W, Gadian A, Mestayer PG, Creutin JD (2000) The possible influence of urban surfaces on rainfall development: a sensitivity study in 2D in the meso-gamma-scale. Atmospheric Research 54: 15-39

Trainer M, Ridley BA, Buhr MP, Kok G, Walega J, Hubler G, Parrish DD, Fehsenfeld FC (1995) Regional ozone and urban plumes in the southeastern United States - Birmingham, a case study. Journal of Geophysical Research-Atmospheres 100: 18823-18834

U.S.A. Census Bureau: Population Division (2010), 2010 Census Demographic Profile Summary File.

United States Geological Survey (USGS) National Elevation Dataset (NED). http://seamless.usgs.gov/about_elevation.php

van den Heever SC, Cotton WR (2007) Urban aerosol impacts on downwind convective storms. Journal of Applied Meteorology and Climatology 46: 828-850

Vanos J, Warland J, Gillespie T, Kenny N (2010) Review of the physiology of human thermal comfort while exercising in urban landscapes and implications for bioclimatic design. International Journal of Biometeorology 54: 319-334

Voogt JA, Oke TR (2003) Thermal remote sensing of urban climates. Remote Sensing of Environment 86: 370-384

Wikimedia Commons Columbus, MS. http://en.wikipedia.org/wiki/Columbus,_Mississippi

Tulsa, Oklahoma: Geography. Wikipedia (2012). http://en.wikipedia.org/wiki/Tulsa,_Oklahoma#Geography

Xie HM, Huang Z, Wang JS (2006) The impact of urban street layout on local atmospheric environment. Building and Environment 41: 1352-1363

Yarnal B (1993) Synoptic climatology in environmental analysis. Belhaven Press, London

Yarnal B, Comrie AC, Frakes B, Brown DP (2001) Developments and prospects in synoptic climatology. International Journal of Climatology 21: 1923-1950

Zhang DL, Shou YX, Dickerson RR (2009) Upstream urbanization exacerbates urban heat island effects. Geophysical Research Letters 36: 1-5

Zhou J, Chen YH, Wang JF, Zhan WF (2011) Maximum Nighttime Urban Heat Island (UHI) Intensity Simulation by Integrating Remotely Sensed Data and Meteorological Observations. Ieee Journal of Selected Topics in Applied Earth Observations and Remote Sensing 4: 138-146

Zhou Y, Shepherd JM (2009) Atlanta's urban heat island under extreme heat conditions and potential mitigation strategies. Natural Hazards 52: 639-668

APPENDIX A: “SYNOPTIC TYPER” CLASSIFICATIONS

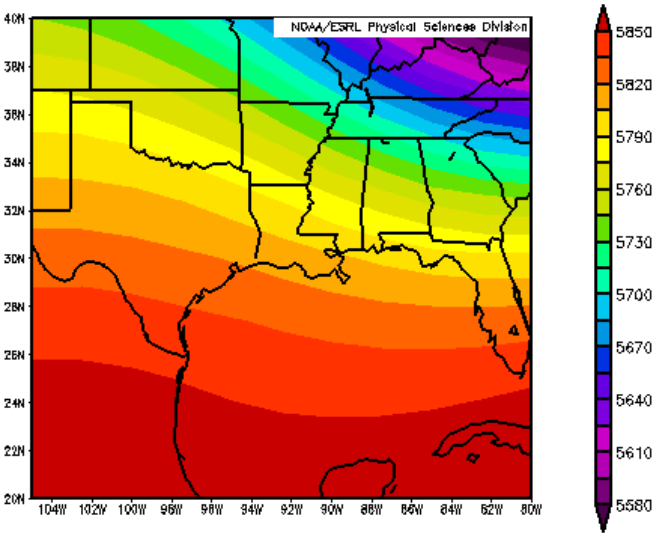

Figure A.1. Synoptic Type 1 for all days (1971-2010).

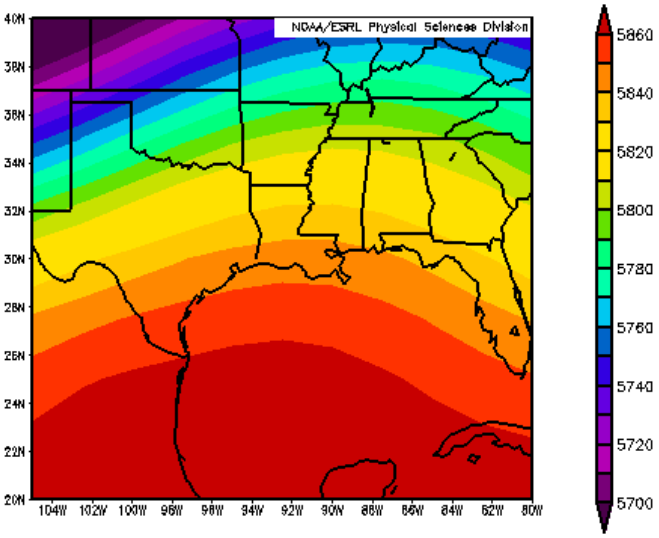

Figure A.2. Synoptic Type 2 for all days (1971-2010).

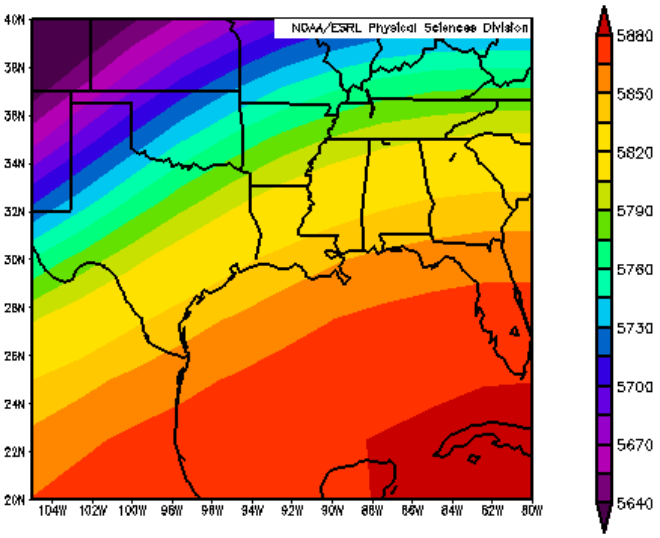

Figure A.3. Synoptic Type 3 for all days (1971-2010).

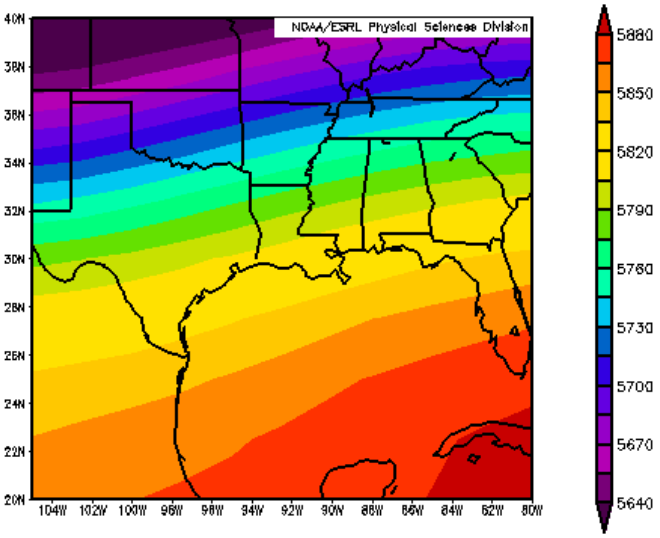

Figure A.4. Synoptic Type 4 for all days (1971-2010).

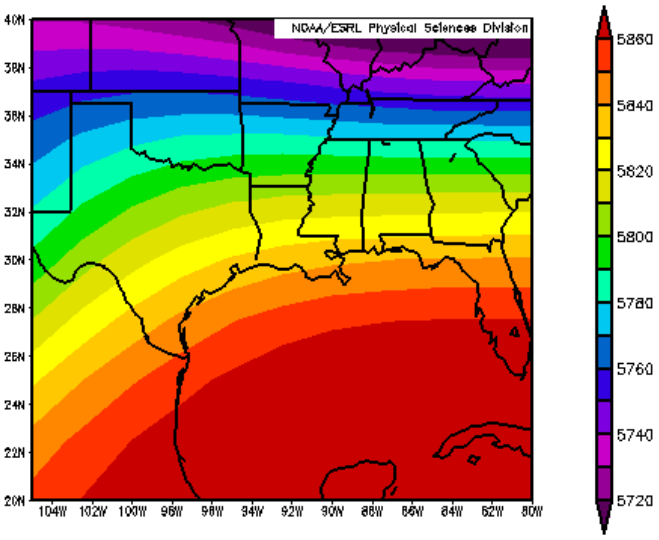

Figure A.5. Synoptic Type 5 for all days (1971-2010).

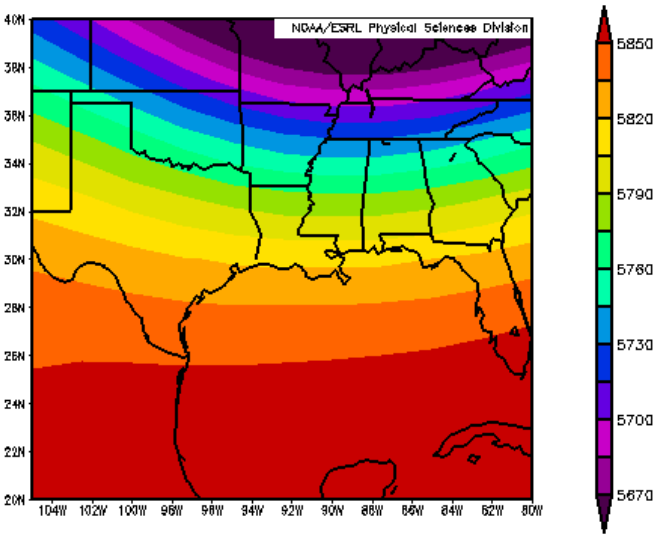

Figure A.6. Synoptic Type 6 for all days (1971-2010).

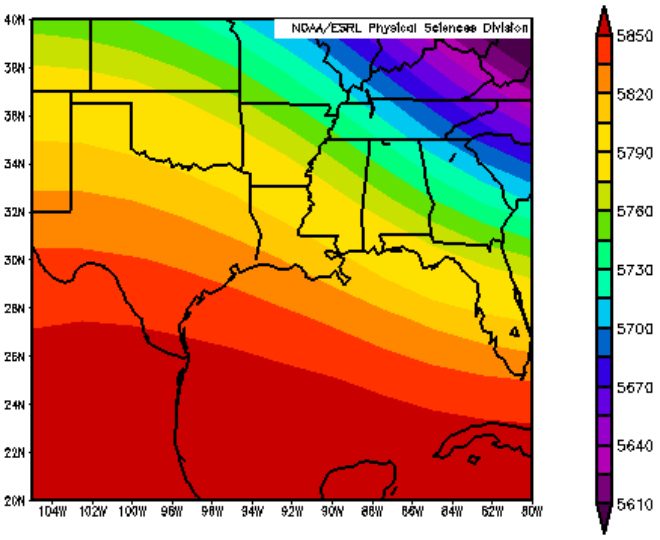

Figure A.7. Synoptic Type 7 for all days (1971-2010).

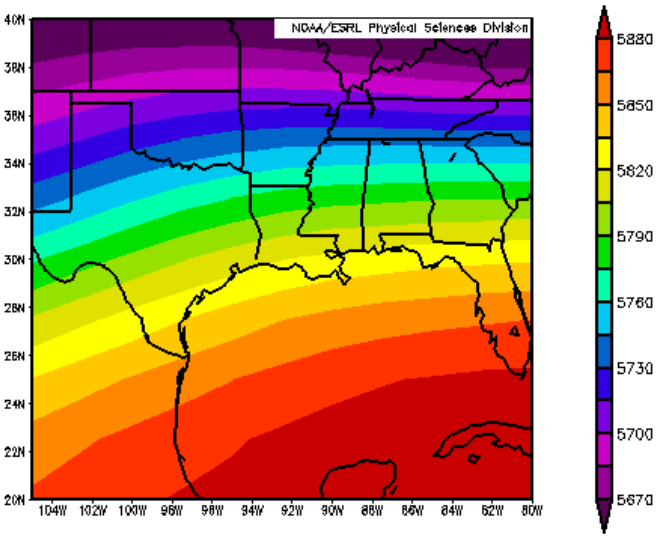

Figure A.8. Synoptic Type 8 for all days (1971-2010).

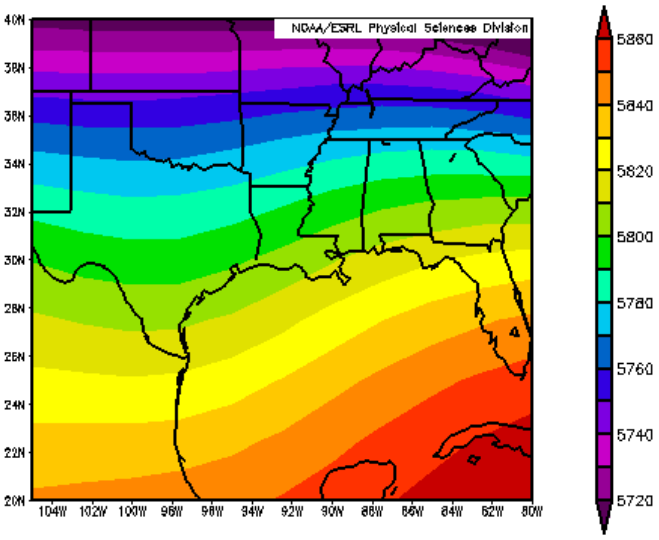

Figure A.9. Synoptic Type 9 for all days (1971-2010).

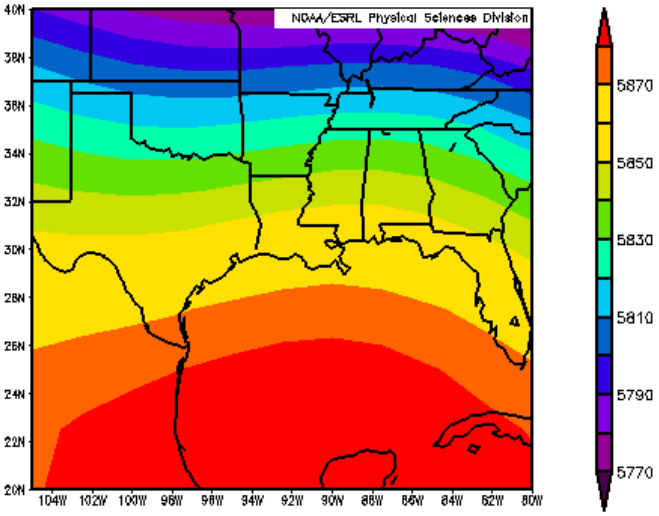

Figure A.10. Synoptic Type 10 for all days (1971-2010).

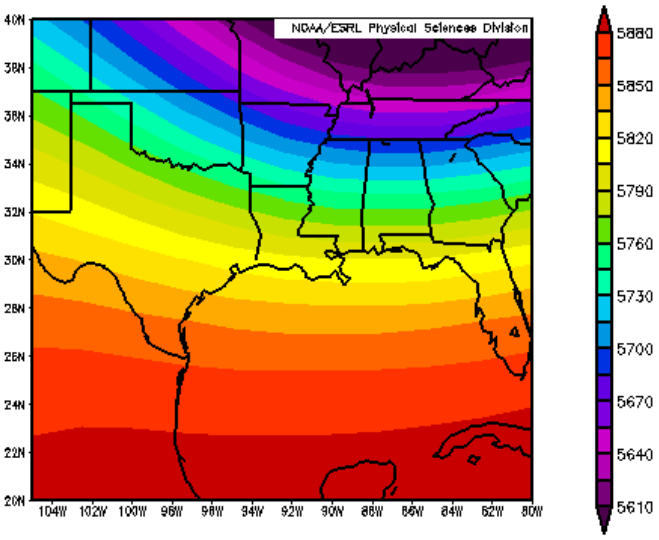

Figure A.11. Synoptic Type 11 for all days (1971-2010).

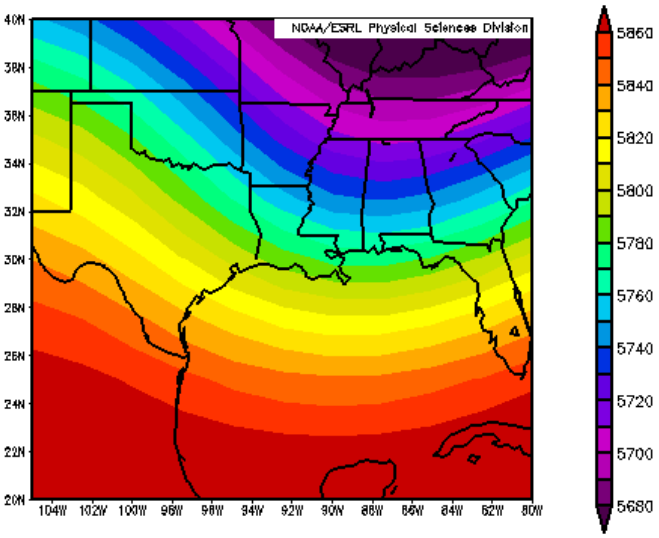

Figure A.12. Synoptic Type 12 for all days (1971-2010).

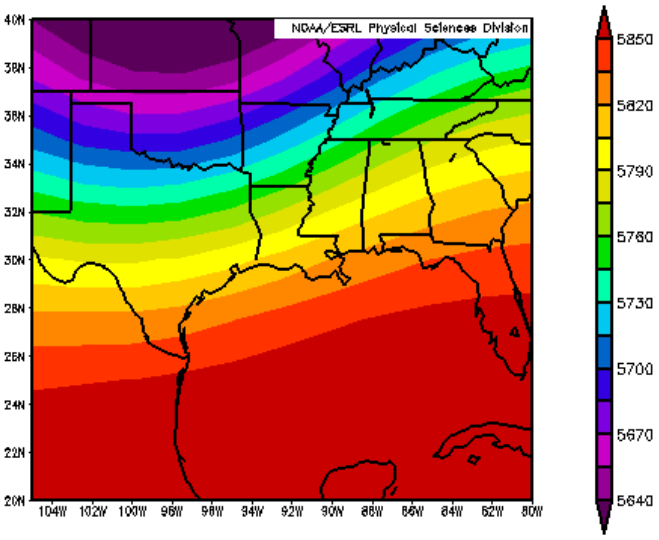

Figure A.13. Synoptic Type 13 for all days (1971-2010).

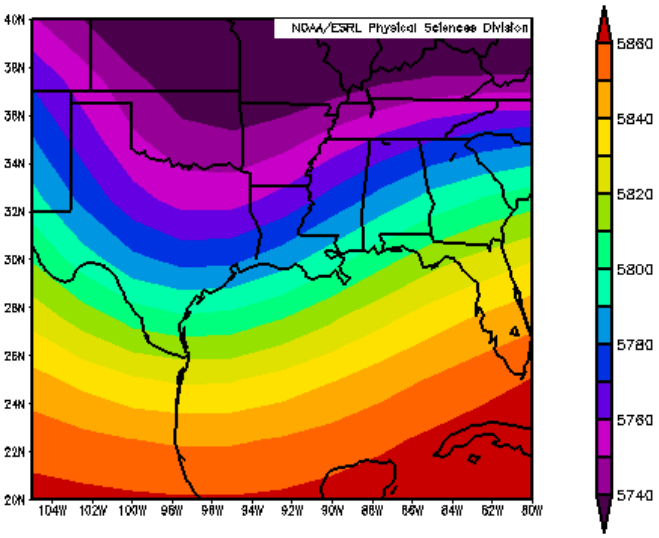

Figure A.14. Synoptic Type 14 for all days (1971-2010).

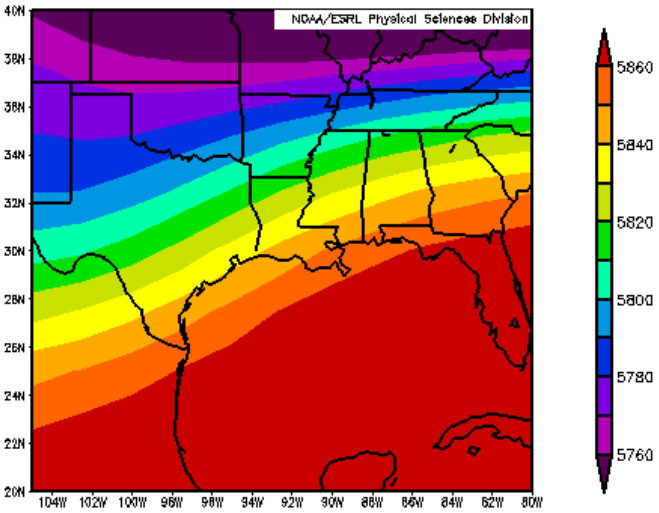

Figure A.15. Synoptic Type 15 for all days (1971-2010).

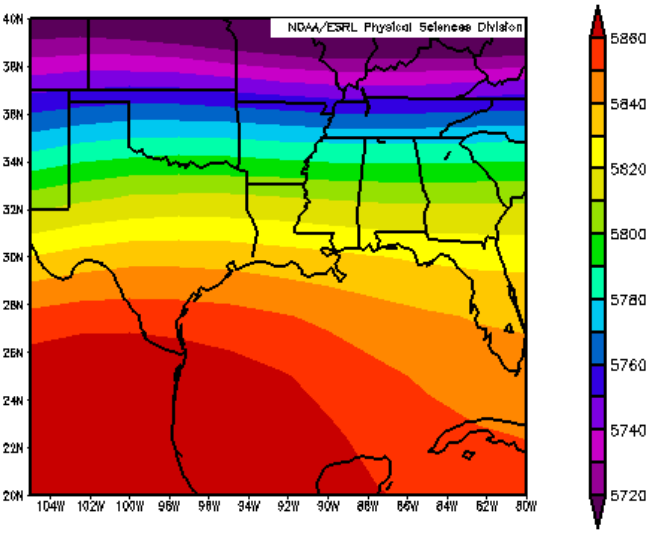

Figure A.16. Synoptic Type 16 for all days (1971-2010).

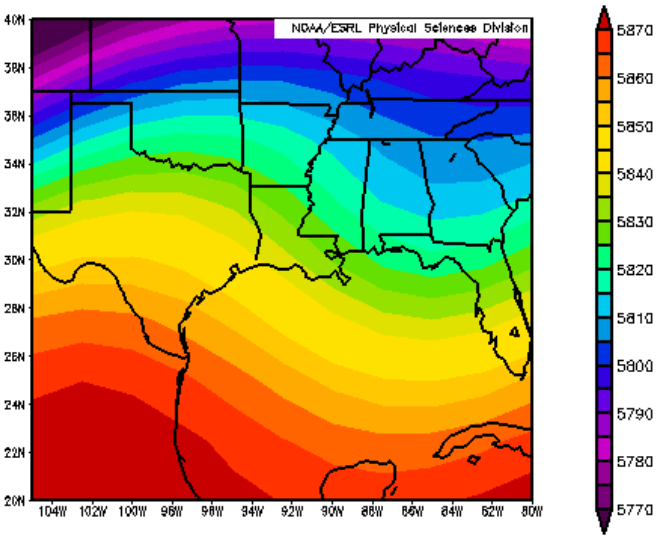

Figure A.17. Synoptic Type 17 for all days (1971-2010).

APPENDIX B: BIFURCATION DETECTION TEST RESULTS

Table B.1. T-test results for bifurcation days for Test 1 for Atlanta.

	Paired Sections	**t**	**d.f.**	**p-value**
Pair 1	core - s100_16	1.139	7	0.292
Pair 2	core - s100_15	1.354	7	0.218
Pair 3	core - s100_14	0.560	7	0.593
Pair 4	core - s100_13	0.599	7	0.568
Pair 5	core - s100_12	0.493	7	0.637
Pair 6	core - s100_11	-0.021	7	0.984
Pair 7	core - s100_10	-0.424	7	0.684
Pair 8	core - s100_9	0.062	7	0.953
Pair 9	core - s100_8	-0.331	7	0.750
Pair 10	core - s100_7	1.115	7	0.302
Pair 11	core - s100_6	0.036	7	0.973
Pair 12	core - s100_5	0.221	7	0.831
Pair 13	core - s100_4	-0.047	7	0.964
Pair 14	core - s100_3	-0.947	7	0.375
Pair 15	core - s100_2	-1.851	7	0.107
Pair 16	core - s100_1	0.047	7	0.964
Pair 17	core - s80_16	0.916	7	0.390
Pair 18	core - s80_15	2.556	7	0.038
Pair 19	core - s80_14	1.815	7	0.112
Pair 20	core - s80_13	1.256	7	0.249
Pair 21	core - s80_12	1.033	7	0.336
Pair 22	core - s80_11	0.680	7	0.518
Pair 23	core - s80_10	-0.226	7	0.828
Pair 24	core - s80_9	-0.106	7	0.919
Pair 25	core - s80_8	-1.313	7	0.230
Pair 26	core - s80_7	0.925	7	0.386
Pair 27	core - s80_6	-0.892	7	0.402
Pair 28	core - s80_5	-1.207	7	0.267
Pair 29	core - s80_4	-1.090	7	0.312
Pair 30	core - s80_3	-1.052	7	0.328
Pair 31	core - s80_2	-1.119	7	0.300
Pair 32	core - s80_1	-0.080	7	0.938
Pair 33	core - s60_16	0.908	7	0.394
Pair 34	core - s60_15	1.906	7	0.098
Pair 35	core - s60_14	2.326	7	0.053
Pair 36	core - s60_13	2.726	7	0.030

Table B.1. continued.

Pair 37	core - s60_12	3.409	7	0.011
Pair 38	core - s60_11	2.522	7	0.040
Pair 39	core - s60_10	-0.025	7	0.981
Pair 40	core - s60_9	-0.188	7	0.856
Pair 41	core - s60_8	-0.984	7	0.358
Pair 42	core - s60_7	-0.101	7	0.923
Pair 43	core - s60_6	0.886	7	0.405
Pair 44	core - s60_5	0.845	7	0.426
Pair 45	core - s60_4	0.482	7	0.645
Pair 46	core - s60_3	0.066	7	0.949
Pair 47	core - s60_2	-0.859	7	0.419
Pair 48	core - s60_1	-0.580	7	0.580

Table B.2. T-test results for bifurcation days for Test 2 for Atlanta.

	Paired Sections	**t**	**d.f.**	**p-value**
Pair 1	core - s100_16	0.843	7	0.427
Pair 2	core - s100_15	1.146	7	0.289
Pair 3	core - s100_14	0.384	7	0.712
Pair 4	core - s100_13	0.427	7	0.682
Pair 5	core - s100_12	0.324	7	0.755
Pair 6	core - s100_11	-0.185	7	0.859
Pair 7	core - s100_10	-0.723	7	0.493
Pair 8	core - s100_9	-0.234	7	0.822
Pair 9	core - s100_8	-0.731	7	0.489
Pair 10	core - s100_7	0.807	7	0.446
Pair 11	core - s100_6	-0.157	7	0.880
Pair 12	core - s100_5	-0.099	7	0.924
Pair 13	core - s100_4	-0.329	7	0.752
Pair 14	core - s100_3	-1.321	7	0.228
Pair 15	core - s100_2	-2.435	7	0.045
Pair 16	core - s100_1	-0.335	7	0.747
Pair 17	core - s80_16	0.548	7	0.601
Pair 18	core - s80_15	2.385	7	0.049
Pair 19	core - s80_14	1.644	7	0.144
Pair 20	core - s80_13	1.077	7	0.317
Pair 21	core - s80_12	0.857	7	0.420
Pair 22	core - s80_11	0.474	7	0.650
Pair 23	core - s80_10	-0.536	7	0.609
Pair 24	core - s80_9	-0.357	7	0.732
Pair 25	core - s80_8	-1.609	7	0.152
Pair 26	core - s80_7	0.297	7	0.775
Pair 27	core - s80_6	-1.377	7	0.211
Pair 28	core - s80_5	-1.486	7	0.181
Pair 29	core - s80_4	-1.389	7	0.207
Pair 30	core - s80_3	-1.394	7	0.206
Pair 31	core - s80_2	-1.915	7	0.097
Pair 32	core - s80_1	-0.453	7	0.664

Table B.3. T-test results for bifurcation days for Test 3 for Atlanta.

	Paired Sections	**t**	**d.f.**	**p-value**
Pair 1	core - s100_16	0.892	7	0.402
Pair 2	core - s100_15	1.253	7	0.250
Pair 3	core - s100_14	0.457	7	0.661
Pair 4	core - s100_13	0.509	7	0.626
Pair 5	core - s100_12	0.397	7	0.703
Pair 6	core - s100_11	-0.173	7	0.867
Pair 7	core - s100_10	-0.753	7	0.476
Pair 8	core - s100_9	-0.209	7	0.840
Pair 9	core - s100_8	-0.659	7	0.531
Pair 10	core - s100_7	0.863	7	0.417
Pair 11	core - s100_6	-0.135	7	0.896
Pair 12	core - s100_5	-0.049	7	0.962
Pair 13	core - s100_4	-0.329	7	0.751
Pair 14	core - s100_3	-1.382	7	0.209
Pair 15	core - s100_2	-2.737	7	0.029
Pair 16	core - s100_1	-0.280	7	0.788

Table B.4. T-test results for non-bifurcation days for Test 1 for Atlanta.

	Paired Sections	**t**	**d.f.**	**p-value**
Pair 1	core - s100_16	-1.743	60	0.086
Pair 2	core - s100_15	0.968	60	0.337
Pair 3	core - s100_14	-0.978	60	0.332
Pair 4	core - s100_13	-0.989	60	0.327
Pair 5	core - s100_12	-1.031	60	0.307
Pair 6	core - s100_11	-0.998	60	0.322
Pair 7	core - s100_10	-1.045	60	0.300
Pair 8	core - s100_9	-1.005	60	0.319
Pair 9	core - s100_8	-0.954	60	0.344
Pair 10	core - s100_7	-0.914	60	0.364
Pair 11	core - s100_6	1.103	60	0.274
Pair 12	core - s100_5	0.971	60	0.335
Pair 13	core - s100_4	0.975	60	0.333
Pair 14	core - s100_3	0.972	60	0.335
Pair 15	core - s100_2	0.892	60	0.376
Pair 16	core - s100_1	0.787	60	0.435
Pair 17	core - s80_16	0.884	60	0.380
Pair 18	core - s80_15	0.967	60	0.338
Pair 19	core - s80_14	0.901	60	0.371
Pair 20	core - s80_13	1.002	60	0.320
Pair 21	core - s80_12	-0.936	60	0.353
Pair 22	core - s80_11	-0.981	60	0.330
Pair 23	core - s80_10	-1.028	60	0.308
Pair 24	core - s80_9	-1.002	60	0.320
Pair 25	core - s80_8	-0.938	60	0.352
Pair 26	core - s80_7	-0.851	60	0.398
Pair 27	core - s80_6	1.415	60	0.162
Pair 28	core - s80_5	1.077	60	0.286
Pair 29	core - s80_4	0.993	60	0.325
Pair 30	core - s80_3	0.979	60	0.332
Pair 31	core - s80_2	0.859	60	0.394
Pair 32	core - s80_1	0.664	60	0.510
Pair 33	core - s60_16	0.977	60	0.332
Pair 34	core - s60_15	0.992	60	0.325
Pair 35	core - s60_14	0.987	60	0.327
Pair 36	core - s60_13	1.017	60	0.313
Pair 37	core - s60_12	-0.733	60	0.466
Pair 38	core - s60_11	-0.952	60	0.345
Pair 39	core - s60_10	-1.041	60	0.302

Table B.4. continued.

Pair 40	core - s60_9	-1.019	60	0.312
Pair 41	core - s60_8	-0.625	60	0.535
Pair 42	core - s60_7	-0.662	60	0.510
Pair 43	core - s60_6	-0.445	60	0.658
Pair 44	core - s60_5	1.243	60	0.219
Pair 45	core - s60_4	1.056	60	0.295
Pair 46	core - s60_3	1.065	60	0.291
Pair 47	core - s60_2	-1.233	60	0.222
Pair 48	core - s60_1	-1.072	60	0.288

Table B.5. T-test results for non-bifurcation days for Test 2 for Atlanta.

	Paired Sections	**t**	**d.f.**	**p-value**
Pair 1	core - s100_16	-1.655	60	0.103
Pair 2	core - s100_15	0.951	60	0.345
Pair 3	core - s100_14	-1.084	60	0.283
Pair 4	core - s100_13	-1.018	60	0.313
Pair 5	core - s100_12	-1.046	60	0.300
Pair 6	core - s100_11	-1.004	60	0.319
Pair 7	core - s100_10	-1.059	60	0.294
Pair 8	core - s100_9	-1.019	60	0.313
Pair 9	core - s100_8	-0.969	60	0.337
Pair 10	core - s100_7	-0.967	60	0.337
Pair 11	core - s100_6	1.071	60	0.288
Pair 12	core - s100_5	0.952	60	0.345
Pair 13	core - s100_4	0.960	60	0.341
Pair 14	core - s100_3	0.961	60	0.340
Pair 15	core - s100_2	0.859	60	0.394
Pair 16	core - s100_1	0.692	60	0.491
Pair 17	core - s80_16	0.827	60	0.412
Pair 18	core - s80_15	0.955	60	0.343
Pair 19	core - s80_14	0.851	60	0.398
Pair 20	core - s80_13	0.973	60	0.334
Pair 21	core - s80_12	-0.971	60	0.335
Pair 22	core - s80_11	-0.989	60	0.326
Pair 23	core - s80_10	-1.044	60	0.300
Pair 24	core - s80_9	-1.014	60	0.315
Pair 25	core - s80_8	-0.956	60	0.343
Pair 26	core - s80_7	-0.895	60	0.375
Pair 27	core - s80_6	1.151	60	0.254
Pair 28	core - s80_5	1.052	60	0.297
Pair 29	core - s80_4	0.979	60	0.331
Pair 30	core - s80_3	0.967	60	0.338
Pair 31	core - s80_2	0.769	60	0.445
Pair 32	core - s80_1	0.458	60	0.649

Table B.6. T-test results for non-bifurcation days for Test 3 Atlanta.

	Paired Sections	**t**	**d.f.**	**p-value**
Pair 1	core - s100_16	-1.615	60	0.112
Pair 2	core - s100_15	0.957	60	0.343
Pair 3	core - s100_14	-1.060	60	0.293
Pair 4	core - s100_13	-1.009	60	0.317
Pair 5	core - s100_12	-1.040	60	0.302
Pair 6	core - s100_11	-1.002	60	0.320
Pair 7	core - s100_10	-1.054	60	0.296
Pair 8	core - s100_9	-1.014	60	0.315
Pair 9	core - s100_8	-0.964	60	0.339
Pair 10	core - s100_7	-0.954	60	0.344
Pair 11	core - s100_6	1.088	60	0.281
Pair 12	core - s100_5	0.959	60	0.342
Pair 13	core - s100_4	0.965	60	0.338
Pair 14	core - s100_3	0.965	60	0.338
Pair 15	core - s100_2	0.868	60	0.389
Pair 16	core - s100_1	0.711	60	0.480

Table B.7. T-test results for bifurcation days for Test 1 for Dallas/Fort Worth.

	Paired Sections	**t**	**d.f.**	**p-value**
Pair 1	core - s100_16	-0.069	8	0.947
Pair 2	core - s100_15	1.422	8	0.193
Pair 3	core - s100_14	1.733	8	0.121
Pair 4	core - s100_13	0.992	8	0.350
Pair 5	core - s100_12	0.975	8	0.358
Pair 6	core - s100_11	1.426	8	0.192
Pair 7	core - s100_10	2.311	8	0.050
Pair 8	core - s100_9	0.650	8	0.534
Pair 9	core - s100_8	-0.413	8	0.691
Pair 10	core - s100_7	-0.829	8	0.431
Pair 11	core - s100_6	-1.007	8	0.344
Pair 12	core - s100_5	-0.940	8	0.375
Pair 13	core - s100_4	-1.098	8	0.304
Pair 14	core - s100_3	-1.286	8	0.234
Pair 15	core - s100_2	-2.659	8	0.029
Pair 16	core - s100_1	-2.009	8	0.079
Pair 17	core - s80_16	-0.211	8	0.838
Pair 18	core - s80_15	0.529	8	0.611
Pair 19	core - s80_14	1.247	8	0.248
Pair 20	core - s80_13	0.815	8	0.439
Pair 21	core - s80_12	0.712	8	0.497
Pair 22	core - s80_11	1.750	8	0.118
Pair 23	core - s80_10	2.314	8	0.049
Pair 24	core - s80_9	1.156	8	0.281
Pair 25	core - s80_8	-0.535	8	0.607
Pair 26	core - s80_7	-0.659	8	0.528
Pair 27	core - s80_6	-1.115	8	0.297
Pair 28	core - s80_5	-1.161	8	0.279
Pair 29	core - s80_4	-0.951	8	0.370
Pair 30	core - s80_3	-1.272	8	0.239
Pair 31	core - s80_2	-2.735	8	0.026
Pair 32	core - s80_1	-1.545	8	0.161
Pair 33	core - s60_16	-0.298	8	0.773
Pair 34	core - s60_15	0.498	8	0.632
Pair 35	core - s60_14	0.920	8	0.384
Pair 36	core - s60_13	1.457	8	0.183
Pair 37	core - s60_12	2.278	8	0.052
Pair 38	core - s60_11	2.143	8	0.065
Pair 39	core - s60_10	2.030	8	0.077

Table B.7. continued.

Pair 40	core - s60_9	1.130	8	0.291
Pair 41	core - s60_8	-0.518	8	0.619
Pair 42	core - s60_7	-0.740	8	0.480
Pair 43	core - s60_6	-0.546	8	0.600
Pair 44	core - s60_5	-0.546	8	0.600
Pair 45	core - s60_4	-0.720	8	0.492
Pair 46	core - s60_3	-1.849	8	0.102
Pair 47	core - s60_2	-2.345	8	0.047
Pair 48	core - s60_1	-0.710	8	0.498

Table B.8. T-test results for bifurcation days for Test 2 for Dallas/Fort Worth.

	Paired Sections	**t**	**d.f.**	**p-value**
Pair 1	core - s100_16	-0.033	8	0.974
Pair 2	core - s100_15	1.657	8	0.136
Pair 3	core - s100_14	1.917	8	0.092
Pair 4	core - s100_13	1.060	8	0.320
Pair 5	core - s100_12	1.065	8	0.318
Pair 6	core - s100_11	1.574	8	0.154
Pair 7	core - s100_10	2.683	8	0.028
Pair 8	core - s100_9	0.632	8	0.545
Pair 9	core - s100_8	-0.392	8	0.705
Pair 10	core - s100_7	-0.856	8	0.417
Pair 11	core - s100_6	-1.057	8	0.322
Pair 12	core - s100_5	-1.006	8	0.344
Pair 13	core - s100_4	-1.205	8	0.263
Pair 14	core - s100_3	-1.410	8	0.196
Pair 15	core - s100_2	-2.710	8	0.027
Pair 16	core - s100_1	-1.918	8	0.091
Pair 17	core - s80_16	-0.187	8	0.856
Pair 18	core - s80_15	0.694	8	0.507
Pair 19	core - s80_14	1.636	8	0.140
Pair 20	core - s80_13	0.962	8	0.364
Pair 21	core - s80_12	0.818	8	0.437
Pair 22	core - s80_11	2.039	8	0.076
Pair 23	core - s80_10	2.799	8	0.023
Pair 24	core - s80_9	1.119	8	0.295
Pair 25	core - s80_8	-0.530	8	0.610
Pair 26	core - s80_7	-0.675	8	0.519
Pair 27	core - s80_6	-1.156	8	0.281
Pair 28	core - s80_5	-1.229	8	0.254
Pair 29	core - s80_4	-1.042	8	0.328
Pair 30	core - s80_3	-1.441	8	0.188
Pair 31	core - s80_2	-2.684	8	0.028
Pair 32	core - s80_1	-1.456	8	0.183

Table B.9. T-test results for bifurcation days for Test 3 for Dallas/Fort Worth.

	Paired Sections	**t**	**d.f.**	**p-value**
Pair 1	core - s100_16	0.125	8	0.904
Pair 2	core - s100_15	1.892	8	0.095
Pair 3	core - s100_14	2.075	8	0.072
Pair 4	core - s100_13	1.168	8	0.277
Pair 5	core - s100_12	1.200	8	0.264
Pair 6	core - s100_11	1.739	8	0.120
Pair 7	core - s100_10	3.015	8	0.017
Pair 8	core - s100_9	0.769	8	0.464
Pair 9	core - s100_8	-0.255	8	0.806
Pair 10	core - s100_7	-0.816	8	0.438
Pair 11	core - s100_6	-1.042	8	0.328
Pair 12	core - s100_5	-0.993	8	0.350
Pair 13	core - s100_4	-1.231	8	0.253
Pair 14	core - s100_3	-1.436	8	0.189
Pair 15	core - s100_2	-2.600	8	0.032
Pair 16	core - s100_1	-1.689	8	0.130

Table B.10. T-test results for non-bifurcation days for Test 1 for Dallas/Fort Worth.

	Paired Sections	**t**	**d.f.**	**p-value**
Pair 1	core - s100_16	-0.831	66	0.409
Pair 2	core - s100_15	-0.412	66	0.681
Pair 3	core - s100_14	0.395	66	0.694
Pair 4	core - s100_13	0.427	66	0.670
Pair 5	core - s100_12	0.602	66	0.549
Pair 6	core - s100_11	0.960	66	0.340
Pair 7	core - s100_10	1.756	66	0.084
Pair 8	core - s100_9	1.664	66	0.101
Pair 9	core - s100_8	1.518	66	0.134
Pair 10	core - s100_7	1.696	66	0.095
Pair 11	core - s100_6	1.231	66	0.223
Pair 12	core - s100_5	1.003	66	0.319
Pair 13	core - s100_4	0.309	66	0.758
Pair 14	core - s100_3	-0.353	66	0.725
Pair 15	core - s100_2	-0.420	66	0.676
Pair 16	core - s100_1	-0.577	66	0.566
Pair 17	core - s80_16	-1.055	66	0.295
Pair 18	core - s80_15	-0.008	66	0.994
Pair 19	core - s80_14	0.419	66	0.676
Pair 20	core - s80_13	-0.302	66	0.763
Pair 21	core - s80_12	-0.265	66	0.792
Pair 22	core - s80_11	1.188	66	0.239
Pair 23	core - s80_10	1.918	66	0.059
Pair 24	core - s80_9	1.297	66	0.199
Pair 25	core - s80_8	1.146	66	0.256
Pair 26	core - s80_7	1.792	66	0.078
Pair 27	core - s80_6	1.401	66	0.166
Pair 28	core - s80_5	1.337	66	0.186
Pair 29	core - s80_4	0.251	66	0.803
Pair 30	core - s80_3	-0.236	66	0.814
Pair 31	core - s80_2	-0.793	66	0.431
Pair 32	core - s80_1	-1.621	66	0.110
Pair 33	core - s60_16	-1.507	66	0.137
Pair 34	core - s60_15	-0.270	66	0.788
Pair 35	core - s60_14	0.092	66	0.927
Pair 36	core - s60_13	0.378	66	0.706
Pair 37	core - s80_12	-0.265	66	0.792
Pair 38	core - s60_11	1.233	66	0.222
Pair 39	core - s60_11	1.233	66	0.222

Table B.10. continued.

Pair 40	core - s60_10	1.739	66	0.087
Pair 41	core - s60_9	0.621	66	0.537
Pair 42	core - s60_8	-0.186	66	0.853
Pair 43	core - s60_7	0.937	66	0.352
Pair 44	core - s60_6	1.220	66	0.227
Pair 45	core - s60_5	0.814	66	0.419
Pair 46	core - s60_4	0.387	66	0.700
Pair 47	core - s60_3	0.302	66	0.764
Pair 48	core - s60_2	-1.459	66	0.149
Pair 49	core - s60_1	-2.311	66	0.024

Table B.11. T-test results for non-bifurcation days for Test 2 for Dallas/Fort Worth.

	Paired Sections	**t**	**d.f.**	**p-value**
Pair 1	core - s100_16	-0.895	66	0.374
Pair 2	core - s100_15	-0.508	66	0.613
Pair 3	core - s100_14	0.383	66	0.703
Pair 4	core - s100_13	0.422	66	0.674
Pair 5	core - s100_12	0.620	66	0.538
Pair 6	core - s100_11	1.023	66	0.310
Pair 7	core - s100_10	1.959	66	0.054
Pair 8	core - s100_9	1.929	66	0.058
Pair 9	core - s100_8	1.740	66	0.086
Pair 10	core - s100_7	1.916	66	0.060
Pair 11	core - s100_6	1.352	66	0.181
Pair 12	core - s100_5	1.055	66	0.295
Pair 13	core - s100_4	0.296	66	0.768
Pair 14	core - s100_3	-0.430	66	0.668
Pair 15	core - s100_2	-0.529	66	0.599
Pair 16	core - s100_1	-0.755	66	0.453
Pair 17	core - s80_16	-1.018	66	0.312
Pair 18	core - s80_15	-0.094	66	0.926
Pair 19	core - s80_14	0.416	66	0.678
Pair 20	core - s80_13	-0.403	66	0.689
Pair 21	core - s80_12	-0.357	66	0.722
Pair 22	core - s80_11	1.314	66	0.193
Pair 23	core - s80_10	2.156	66	0.035
Pair 24	core - s80_9	1.480	66	0.144
Pair 25	core - s80_8	1.271	66	0.208
Pair 26	core - s80_7	2.083	66	0.041
Pair 27	core - s80_6	1.585	66	0.118
Pair 28	core - s80_5	1.513	66	0.135
Pair 29	core - s80_4	0.232	66	0.817
Pair 30	core - s80_3	-0.327	66	0.744
Pair 31	core - s80_2	-0.976	66	0.333
Pair 32	core - s80_1	-1.933	66	0.058

Table B.12. T-test results for non-bifurcation days for Test 3 for Dallas/Fort Worth.

	Paired Sections	**t**	**d.f.**	**p-value**
Pair 1	core - s100_16	-1.009	66	0.317
Pair 2	core - s100_15	-0.667	66	0.507
Pair 3	core - s100_14	0.289	66	0.774
Pair 4	core - s100_13	0.341	66	0.734
Pair 5	core - s100_12	0.559	66	0.578
Pair 6	core - s100_11	0.992	66	0.325
Pair 7	core - s100_10	2.006	66	0.049
Pair 8	core - s100_9	1.992	66	0.051
Pair 9	core - s100_8	1.747	66	0.085
Pair 10	core - s100_7	1.957	66	0.055
Pair 11	core - s100_6	1.374	66	0.174
Pair 12	core - s100_5	1.037	66	0.304
Pair 13	core - s100_4	0.229	66	0.820
Pair 14	core - s100_3	-0.549	66	0.585
Pair 15	core - s100_2	-0.691	66	0.492
Pair 16	core - s100_1	-1.014	66	0.314

Table B.13. T-test results for bifurcation days for Test 1 for Columbus.

	Paired Sections	**t**	**d.f.**	**p-value**
Pair 1	core - s100_16	1.003	1	0.499
Pair 2	core - s100_15	1.003	1	0.499
Pair 3	core - s100_14	1.003	1	0.499
Pair 4	core - s100_13	1.004	1	0.499
Pair 5	core - s100_12	1.065	1	0.480
Pair 6	core - s100_11	-0.996	1	0.501
Pair 7	core - s100_10	-0.995	1	0.502
Pair 8	core - s100_9	-0.997	1	0.501
Pair 9	core - s100_8	-0.997	1	0.501
Pair 10	core - s100_7	-1.049	1	0.485
Pair 11	core - s100_6	-1.231	1	0.434
Pair 12	core - s100_5	-1.200	1	0.442
Pair 13	core - s100_4	-1.050	1	0.485
Pair 14	core - s100_3	-1.027	1	0.492
Pair 15	core - s100_2	1.007	1	0.498
Pair 16	core - s100_1	1.003	1	0.499
Pair 17	core - s80_16	1.003	1	0.499
Pair 18	core - s80_15	1.003	1	0.499
Pair 19	core - s80_14	1.004	1	0.499
Pair 20	core - s80_13	1.013	1	0.496
Pair 21	core - s80_12	-0.987	1	0.504
Pair 22	core - s80_11	-0.994	1	0.502
Pair 23	core - s80_10	-0.992	1	0.502
Pair 24	core - s80_9	-0.996	1	0.501
Pair 25	core - s80_8	-0.996	1	0.501
Pair 26	core - s80_7	-1.051	1	0.484
Pair 27	core - s80_6	-1.054	1	0.483
Pair 28	core - s80_5	-1.044	1	0.486
Pair 29	core - s80_4	-1.025	1	0.492
Pair 30	core - s80_3	0.714	1	0.605
Pair 31	core - s80_2	1.005	1	0.498
Pair 32	core - s80_1	1.004	1	0.499
Pair 33	core - s60_16	1.003	1	0.499
Pair 34	core - s60_15	1.004	1	0.499
Pair 35	core - s60_14	1.006	1	0.498
Pair 36	core - s60_13	1.042	1	0.487
Pair 37	core - s60_12	-0.978	1	0.507
Pair 38	core - s60_11	-0.978	1	0.507
Pair 39	core - s60_10	-0.987	1	0.504

Table B.13. continued.

Pair 40	core - s60_9	-0.996	1	0.501
Pair 41	core - s60_8	-0.997	1	0.501
Pair 42	core - s60_7	-1.063	1	0.481
Pair 43	core - s60_6	-0.994	1	0.502
Pair 44	core - s60_5	-1.055	1	0.483
Pair 45	core - s60_4	0.806	1	0.568
Pair 46	core - s60_3	0.952	1	0.516
Pair 47	core - s60_2	1.005	1	0.499
Pair 48	core - s60_1	1.004	1	0.499

Table B.14. T-test results for bifurcation days for Test 2 for Columbus.

	Paired Sections	**t**	**d.f.**	**p-value**
Pair 1	core - s100_16	1.006	1	0.498
Pair 2	core - s100_15	1.006	1	0.498
Pair 3	core - s100_14	1.006	1	0.498
Pair 4	core - s100_13	1.008	1	0.498
Pair 5	core - s100_12	1.250	1	0.430
Pair 6	core - s100_11	-0.991	1	0.503
Pair 7	core - s100_10	-0.991	1	0.503
Pair 8	core - s100_9	-0.993	1	0.502
Pair 9	core - s100_8	-0.994	1	0.502
Pair 10	core - s100_7	-1.044	1	0.486
Pair 11	core - s100_6	-1.202	1	0.442
Pair 12	core - s100_5	-1.183	1	0.447
Pair 13	core - s100_4	-1.045	1	0.486
Pair 14	core - s100_3	-1.017	1	0.495
Pair 15	core - s100_2	1.015	1	0.495
Pair 16	core - s100_1	1.006	1	0.498
Pair 17	core - s80_16	1.006	1	0.498
Pair 18	core - s80_15	1.007	1	0.498
Pair 19	core - s80_14	1.008	1	0.497
Pair 20	core - s80_13	1.029	1	0.491
Pair 21	core - s80_12	-0.976	1	0.508
Pair 22	core - s80_11	-0.989	1	0.504
Pair 23	core - s80_10	-0.986	1	0.505
Pair 24	core - s80_9	-0.993	1	0.502
Pair 25	core - s80_8	-0.993	1	0.502
Pair 26	core - s80_7	-1.045	1	0.486
Pair 27	core - s80_6	-1.051	1	0.484
Pair 28	core - s80_5	-1.041	1	0.487
Pair 29	core - s80_4	-1.021	1	0.493
Pair 30	core - s80_3	0.538	1	0.686
Pair 31	core - s80_2	1.010	1	0.497
Pair 32	core - s80_1	1.008	1	0.498

Table B.15. T-test results for bifurcation days for Test 3 for Columbus.

	Paired Sections	**t**	**d.f.**	**p-value**
Pair 1	core - s100_16	1.006	1	0.498
Pair 2	core - s100_15	1.005	1	0.498
Pair 3	core - s100_14	1.005	1	0.498
Pair 4	core - s100_13	1.007	1	0.498
Pair 5	core - s100_12	1.075	1	0.477
Pair 6	core - s100_11	-0.991	1	0.503
Pair 7	core - s100_10	-0.990	1	0.503
Pair 8	core - s100_9	-0.993	1	0.502
Pair 9	core - s100_8	-0.993	1	0.502
Pair 10	core - s100_7	-1.047	1	0.485
Pair 11	core - s100_6	-1.252	1	0.429
Pair 12	core - s100_5	-1.209	1	0.440
Pair 13	core - s100_4	-1.048	1	0.485
Pair 14	core - s100_3	-1.020	1	0.494
Pair 15	core - s100_2	1.013	1	0.496
Pair 16	core - s100_1	1.006	1	0.498

Table B.16. T-test results for non-bifurcation days for Test 1 for Columbus.

	Paired Sections	**t**	**d.f.**	**p-value**
Pair 1	core - s100_16	6.547	112	0.000
Pair 2	core - s100_15	3.834	112	0.000
Pair 3	core - s100_14	2.925	112	0.004
Pair 4	core - s100_13	0.171	112	0.865
Pair 5	core - s100_12	0.230	112	0.819
Pair 6	core - s100_11	-0.399	112	0.690
Pair 7	core - s100_10	-0.989	112	0.325
Pair 8	core - s100_9	-1.601	112	0.112
Pair 9	core - s100_8	-0.995	112	0.322
Pair 10	core - s100_7	1.229	112	0.222
Pair 11	core - s100_6	1.581	112	0.117
Pair 12	core - s100_5	2.564	112	0.012
Pair 13	core - s100_4	4.262	112	0.000
Pair 14	core - s100_3	2.115	112	0.037
Pair 15	core - s100_2	0.527	112	0.599
Pair 16	core - s100_1	4.933	112	0.000
Pair 17	core - s80_16	8.204	112	0.000
Pair 18	core - s80_15	4.305	112	0.000
Pair 19	core - s80_14	2.889	112	0.005
Pair 20	core - s80_13	-0.002	112	0.998
Pair 21	core - s80_12	-0.283	112	0.778
Pair 22	core - s80_11	-0.783	112	0.435
Pair 23	core - s80_10	-0.887	112	0.377
Pair 24	core - s80_9	-2.500	112	0.014
Pair 25	core - s80_8	-1.275	112	0.205
Pair 26	core - s80_7	0.558	112	0.578
Pair 27	core - s80_6	1.264	112	0.209
Pair 28	core - s80_5	2.131	112	0.035
Pair 29	core - s80_4	3.821	112	0.000
Pair 30	core - s80_3	1.218	112	0.226
Pair 31	core - s80_2	4.779	112	0.000
Pair 32	core - s80_1	4.411	112	0.000
Pair 33	core - s60_16	6.884	112	0.000
Pair 34	core - s60_15	5.370	112	0.000
Pair 35	core - s60_14	1.697	112	0.092
Pair 36	core - s60_13	-0.503	112	0.616
Pair 37	core - s60_12	-0.229	112	0.820
Pair 38	core - s60_11	0.039	112	0.969
Pair 39	core - s60_10	-0.850	112	0.397

Table B.16. continued.

Pair 40	core - s60_9	-3.822	112	0.000
Pair 41	core - s60_8	-1.133	112	0.260
Pair 42	core - s60_7	0.356	112	0.723
Pair 43	core - s60_6	0.741	112	0.460
Pair 44	core - s60_5	1.275	112	0.205
Pair 45	core - s60_4	3.871	112	0.000
Pair 46	core - s60_3	5.282	112	0.000
Pair 47	core - s60_2	7.908	112	0.000
Pair 48	core - s60_1	7.626	112	0.000

Table B.17. T-test results for non-bifurcation days for Test 2 for Columbus.

	Paired Sections	**t**	**d.f.**	**p-value**
Pair 1	core - s100_16	6.563	112	0.000
Pair 2	core - s100_15	3.581	112	0.001
Pair 3	core - s100_14	2.624	112	0.010
Pair 4	core - s100_13	-0.381	112	0.704
Pair 5	core - s100_12	-0.301	112	0.764
Pair 6	core - s100_11	-1.028	112	0.306
Pair 7	core - s100_10	-1.724	112	0.087
Pair 8	core - s100_9	-2.544	112	0.012
Pair 9	core - s100_8	-1.774	112	0.079
Pair 10	core - s100_7	0.457	112	0.648
Pair 11	core - s100_6	0.952	112	0.343
Pair 12	core - s100_5	2.006	112	0.047
Pair 13	core - s100_4	3.861	112	0.000
Pair 14	core - s100_3	1.439	112	0.153
Pair 15	core - s100_2	-0.297	112	0.767
Pair 16	core - s100_1	4.760	112	0.000
Pair 17	core - s80_16	8.393	112	0.000
Pair 18	core - s80_15	3.934	112	0.000
Pair 19	core - s80_14	2.556	112	0.012
Pair 20	core - s80_13	-0.590	112	0.557
Pair 21	core - s80_12	-0.954	112	0.342
Pair 22	core - s80_11	-1.569	112	0.119
Pair 23	core - s80_10	-1.704	112	0.091
Pair 24	core - s80_9	-3.650	112	0.000
Pair 25	core - s80_8	-2.025	112	0.045
Pair 26	core - s80_7	-0.294	112	0.769
Pair 27	core - s80_6	0.443	112	0.659
Pair 28	core - s80_5	1.406	112	0.162
Pair 29	core - s80_4	3.321	112	0.001
Pair 30	core - s80_3	0.444	112	0.658
Pair 31	core - s80_2	4.422	112	0.000
Pair 32	core - s80_1	4.031	112	0.000

Table B.18. T-test results for non-bifurcation days for Test 3 for Columbus.

	Paired Sections	**t**	**d.f.**	**p-value**
Pair 1	core - s100_16	6.796	112	0.000
Pair 2	core - s100_15	3.665	112	0.000
Pair 3	core - s100_14	2.641	112	0.009
Pair 4	core - s100_13	-0.596	112	0.552
Pair 5	core - s100_12	-0.503	112	0.616
Pair 6	core - s100_11	-1.300	112	0.196
Pair 7	core - s100_10	-2.073	112	0.040
Pair 8	core - s100_9	-2.969	112	0.004
Pair 9	core - s100_8	-1.998	112	0.048
Pair 10	core - s100_7	0.201	112	0.841
Pair 11	core - s100_6	0.761	112	0.449
Pair 12	core - s100_5	1.876	112	0.063
Pair 13	core - s100_4	3.864	112	0.000
Pair 14	core - s100_3	1.228	112	0.222
Pair 15	core - s100_2	-0.607	112	0.545
Pair 16	core - s100_1	4.847	112	0.000

VITA

Anna Marie Treviño, born in 1984 in San Antonio, Texas, is currently pursuing her Doctor of Philosophy in Geography, with a minor in Disaster Science Management, at Louisiana State University. She received her Master of Science in Geography from Texas A&M University in August 2008 and her Bachelor of Science in Environmental Geoscience at Texas A&M University in August 2006.

Her intended career field is climatology, allowing her to use and expand her skills and interests in environmental and spatial analytic research. Anna has obtained experience in both research and teaching during her time at Louisiana State University. Projects in which she worked on include *Interpolating Peak Gust and Maximum Sustained Wind Speeds from European Storms* under the supervision of Carol Friedland in 2011, *Developing a Climate Characterization for the Local and Regional Scale* at the National Climatic Data Center under the supervision of Derek Arndt in 2010, and her contribution to the *Southern Climate Impacts Planning Program* under the supervision of Robert Rohli and David Brown from 2008 – 2012. Anna instructed GEOG 2050, *Physical Geography: the Atmosphere*, at Louisiana State University in 2009.

Awards received by Anna include the Graduate School Dissertation Year Fellowship, provided by Louisiana State University from 2011 – 2012, the Earth System Science Interdisciplinary Center (ESSIC) Travel Award in 2011, the William Haag Alumni Award in 2011, the Evelyn L. Pruitt Travel Award in 2011, and the Ellinor H. Behre Prize in Science Writing in 2011.

Anna married her husband, Lucas Treviño, in 2008, and gave birth to their first child, Lillian Victoria Treviño, in March 2012. They currently reside in Baton Rouge, Louisiana.